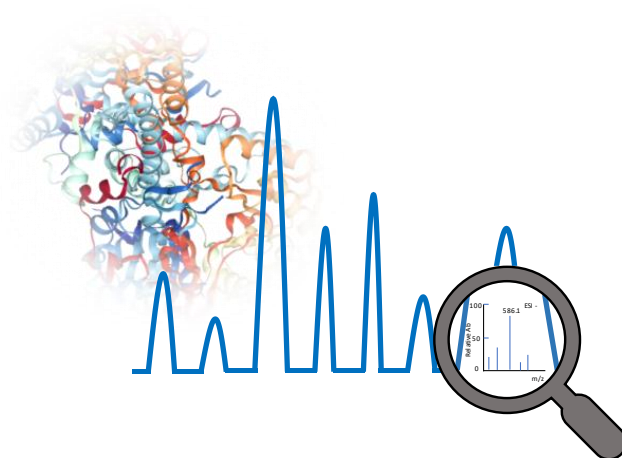


Università degli Studi del Piemonte Orientale
“Amedeo Avogadro”

Department of Pharmaceutical Sciences

Ph.D. in Chemistry & Biology
XXXI cycle 2015-2018

**LC-MS applications in Pharmaceutical Analysis,
Bioanalysis and Proteomics**



Michele Bianchi

Supervised by Prof. Erika Del Grosso

PhD program co-ordinator Prof. Guido Lingua

Università degli Studi del Piemonte Orientale
“Amedeo Avogadro”

Department of Pharmaceutical Sciences

Ph.D. in Chemistry & Biology
XXXI cycle 2015-2018

**LC-MS applications in Pharmaceutical Analysis,
Bioanalysis and Proteomics**

Michele Bianchi

Supervised by Prof. Erika Del Grosso

PhD program co-ordinator: Prof. Guido Lingua



UNIVERSITÀ DEL PIEMONTE ORIENTALE
DOTTORATO DI RICERCA
IN CHEMISTRY & BIOLOGY

Via Duomo, 6
13100 – Vercelli (ITALY)

DECLARATION AND AUTHORISATION TO ANTIPLAGIARISM DETECTION

The undersigned ... Michele Bianchi student of the Chemistry & Biology
Ph.D course (~~XXX~~ Cycle)

declares:

- to be aware that the University has adopted a web-based service to detect plagiarism through a software system called “Turnit.in”,
- his/her Ph.D. thesis was submitted to Turnit.in scan and reasonably it resulted an original document, which correctly cites the literature;

acknowledges:

- his/her Ph.D. thesis can be verified by his/her Ph.D. tutor and/or Ph.D Coordinator in order to confirm its originality.

Date: 11/11/18 Signature: Michele Bianchi

To my family

Contents

Chapter 1	11
1. Introduction	12
1.1 Liquid Chromatography	12
1.2 Mass Spectrometry (MS)	18
1.3 Liquid Chromatography tandem Mass Spectrometry	23
1.4 LC-MS applications	26
Chapter 2	48
2. Outline of the thesis	49
Chapter 3	51
3. Troxerutin, a mixture of O-hydroxyethyl derivatives of the natural flavonoid rutin: Chemical stability and analytical aspects	52
Chapter 4	92
4. Synthesis and Degradation of Adenosine 5'-Tetraphosphate by Nicotinamide and Nicotinate Phosphoribosyltransferases	93
Chapter 5	129
5. Proneurogenic effects of trazodone in murine and human neural progenitors	130
Chapter 6	150
6. Study of Nicotinamide Phosphoribosyltransferase (NAMPT) phosphorylation sites in melanoma cells	151
Chapter 7	179
7. Discussion	180
Chapter 8	187
8. List of Publications	188
Acknowledgements	190

Chapter 1

1. Introduction

Liquid Chromatography tandem Mass Spectrometry (LC-MS) is a powerful tool available for scientists. According to pubmed publications data collected from <https://www.ncbi.nlm.nih.gov/pubmed/> using Liquid Chromatography Mass Spectrometry or LC-MS as input search, more than 130,000 results came out. Furthermore, the publications trend is keeping rising overcoming more than 8,400 papers per year in the last five years. These data are the demonstration that LC-MS is increasing in terms of popularity in the scientific world. LC-MS is widespread in many scientific applications starting from chemistry to biology and much more.

On these basis, in this introduction we will address the following topics:

- (1) From the born of chromatography to development of modern UHPLC system.
- (2) Mass spectrometer analyzers.
- (3) The coupling of liquid chromatography to mass spectrometry systems.
- (4) The main LC-MS applications in pharmaceutical analysis, bioanalysis and proteomics.

1.1 Liquid Chromatography

1.1.1 Liquid Chromatography (LC)

The first paper published about chromatography was published by A. J. P. Martin and R. L. M. Synge on Biochemical Journal in 1941. In this paper, the concepts of chromatography and theoretical plates were described and applied, and it allowed them to win the Nobel prize in chemistry in 1952¹. Nevertheless, the inventor of chromatography is recognized as Mikhail S. Tswett, a Russian botanist who worked on the separation of plant pigments at the beginning of 1900². The first High Performed Liquid Chromatography (HPLC) apparatus was described by C. G. Horváth e S. R. Lipsky and B. A. Preiss with two papers published on Nature and Analytical Chemistry in 1966 and 1967^{3,4}, respectively. From those days to now, considerable progress has been made until the born of modern UHPLC.

The aim of Chromatography is to separate single components in a mixture relying on the adsorption and desorption equilibrium of each compounds between the liquid (mobile) phase and the solid (stationary) phase⁵.

So, two adjacent compounds can be defined separated if their peaks result resolved and spaced at the peak bases. To evaluate and to improve the chromatographic resolution, van Deemter et al.⁶ proposed the following equation 1(1):

$$H = 2\lambda d_p + \frac{2\gamma D_m}{u} + \frac{\omega(d_p \text{ or } d_c)^2 u}{D_m} + \frac{Rd_f^2 u}{D_s} \quad 1 (1)$$

1 (1) where:

H is plate height, λ is particle shape (with regard to the packing), d_p is particle diameter, γ , ω , and R are constants, D_m is the diffusion coefficient of the mobile phase, d_c is the capillary diameter, d_f is the film thickness, D_s is the diffusion coefficient of the stationary phase, u is the linear velocity.

Equation 1 (1) can be simplified as following in 1 (2):

$$H = A + \frac{B}{u} + Cu \quad 1 (2)$$

1 (2) where:

A is the Eddy diffusion, determined by the possible pathway of the mixture compounds which can go across the porous of the stationary phase causing peak broadening.

B is the longitudinal diffusion of two adjacent compounds during the chromatographic elution. C is the resistance to mass transfer, which means all the possible chemical interaction between the mobile and stationary phases.

The van Deemter equation can be represented in the following plot (figure 1):

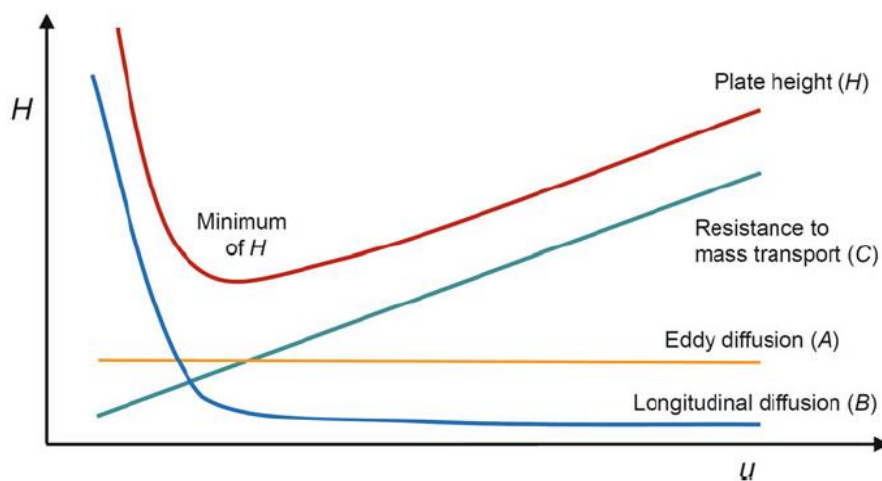


Figure 1. Van Deemter equations and plot of plate height(modified from Gross et al⁷)

From van Deemter work, it is possible to determine the optimum flow rate to achieve the lowest height of H , allowing the best efficient chromatographic resolution for each chromatographic system.

There are a lot of parameters that can be studied and optimized to improve a chromatographic separation, such as the peaks retention time, the selectivity, the robustness and column efficiency.

1.1.2 High Performance Liquid Chromatography (HPLC) sections and method development

HPLC systems are constituted by mobile phase reservoirs, degasser, pumps, automated injector and autosampler, LC column, detector and PC as shown in figure 2.

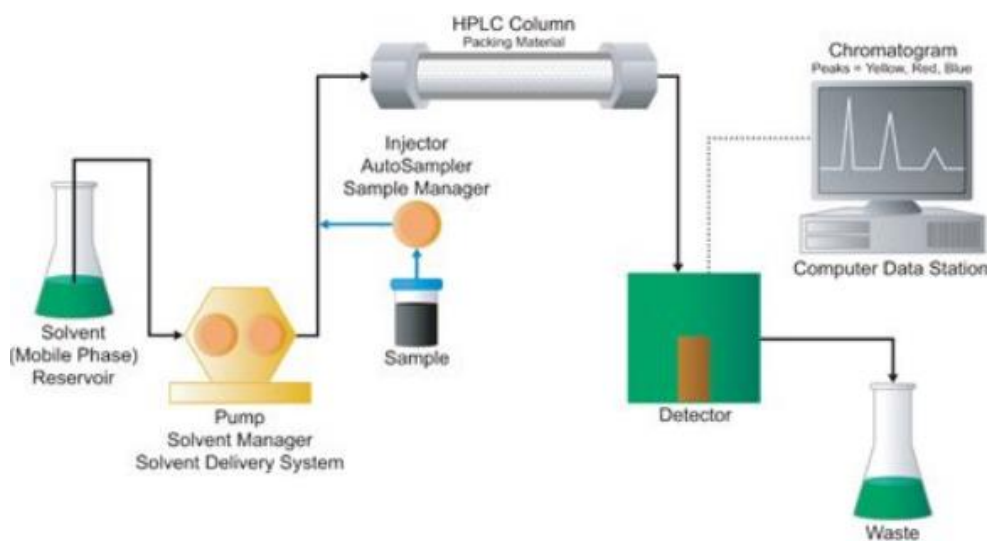


Figure 2. Schematic design of an HPLC system (figure from waters, <http://www.waters.com>)

All the HPLC compartments are always object of research to provide to the scientists instruments with robustness, sensitivity, accuracy and precision performance updated and improved.

Mobile phases, stationary phases, injection volume and detector setting values are the main parameters to be optimized during the method development.

In both reversed phase LC and hydrophilic LC mobile phases are constituted by a lipophylic (*e.g.* methanol and acetonitrile) and polar (*e.g.* water, saline buffers) solvents with or without pH modifiers (*e.g.* formic or acetic acid and sodium hydroxide). A pH modifier can gain importance in LC tandem mass spectrometry system in modifying the compounds ionization before the MS analysis.

Stationary phases which characterized a chromatographic column are the key factors during the method development. Available on the market, there are essentially three kinds of column which differ each others for the structural features of the column packaging. They are: the monoliths of second generation, the silica fully porous particles and the silica core shell particles.

Focusing on the last two and more common kind of columns, both of them can have the silica functionalized with different chemical moieties (*e.g.* C18, C8, C4, C1, HILIC, cyano, phenyl, fluoro-phenyl, amino, amide and phenyl-hexyl) to allow different compounds partitions between mobile and stationary phases, with the possibility of taking advantages in term of resolution. Different silica functionalizations make different chemical interactions (*e.g.* hydrophobic, hydrogen binding, electrostatic, steric and π - π interaction) between column and analytes.

Nevertheless, fully porous and core shell particles differ for the structure of the microsphere. For the first one, microspheres are made of a porous fully silica particle while for the core shell, the core is made by a solid silica sphere covered by a porous silica shell.

For the fully porous, 100% of the surface can interact with the analytes, while in core shell this surface is limited for the shell, decreasing the number of theoretical plates. At the same time, a lot of advantages are provided by core shell particles compared to equal diameter fully porous one: increased permeability, reduced pore volume, reduced porosity, reduced van Deemter, A, B and C terms (the last one for macromolecules *e.g.* peptides) and the thermal conductivity is increased. All of these positive features made of the core shell a good alternative to fully the porous particles as column packing material for HPLC systems^{8,9,10,11,12,13,14}.

Despite these core shell advantages listed before, fully porous particles are still the golden standard in terms of column efficiency, resolution, productivity and robustness^{12,15}. The real disadvantage of fully porous particles, which limit their use, is constituted by the huge backpressure generated, especially from the sub-2 μ m

particles. High backpressure forces these particles to Ultra-HPLC (UHPLC) instruments⁸.

1.1.3 Ultra High Performance Liquid Chromatography (UHPLC)

In the last line of the previous paragraph, it has been introduced the concept of UHPLC. The main difference between an UHPLC and HPLC analysis is in the backpressure managed by pumps. UHPLC pumps can work also over 1000 bar of pressure vs the 300 - 400 bar on HPLC instruments^{16,17}. The impact of UHPLC with the use of sub-2 μ m particles size column was huge in different application fields¹⁸. To simplify the introduction of UHPLC system in laboratories, especially the pharmaceuticals of quality control, different protocols for transferring the HPLC methods on UHPLC were developed¹⁶.

Finally, UHPLC operating with low micro and nanoflow rates are surely the last frontier in the liquid chromatography, especially for the analysis of large molecules^{19,20}.

1.2 Mass Spectrometry (MS)

Nowadays mass spectrometry is an indispensable tool, especially in R&D in so many disciplines. The first MS was built by J. J. Thomson (Nobel Prize for physics in 1906 for electron discovery) who collected also the first MS spectra in 1909⁷. From that day, we assisted to an outstanding growth of MS analyzers. At the state of the art, the most common MS are: the quadrupole, time of flight (TOF), magnetic sector (B), linear ion trap (LIT), QIT (quadrupole ion trap), Fourier transform ion cyclotron resonance (FT-ICR) and the orbitrap.

Quadrupole, QIT and orbitrap are discussed in the next paragraphs.

1.2.1 quadrupole (*q*)

The quadrupole mass analyzer consists of four cylindrical (or even better hyperbolic) rod electrodes set perfectly parallel each other. As shown in figure 3, the rods have a z-direction and are mounted in a x, y plane configuration.

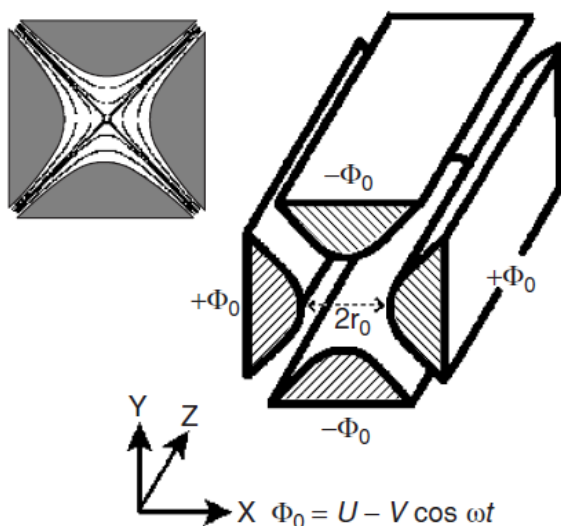


Figure 3. Quadrupole geometry with hyperbolic rods and applied potentials²¹. Usually, quadrupoles have rods of 10-15 mm of diameter and a length of 15-25 cm. The radiofrequency is in the order of 1-4 MHz with voltages between 100-1000 V, providing also 100 ion oscillations per ion passage

The quadrupole principle of working is based on the use of an oscillating electric field to separate ions and so to stabilize ion trajectories at fixed m/z ratio.

The pairs of opposite bars are each held at the same potential (Φ) which is composed of a DC and an AC component. Ions travel along the z axis and they are subjected to the influence of the electric field made by a quadrupolar alternative electric field superimposed to a constant electric field. This mechanism allows the m/z selection of ions of interest, excluding others that move out on x and y axis.

This principle of action is explained from motions equation²¹.

A way to evaluate the capability of a MS is the calculation of its resolving power or resolution (R). R is the ability of the MS analyzers to resolve to adjacent peaks and it is expressed by the following formula according to the peak width definition 1 (3)²²:

$$R = \frac{m}{\Delta m} = \frac{m/z}{\Delta(m/z)} \quad 1 (3)$$

1 (3) where:

R is the resolving power, m is the m/z of the peak ion, and Δm is peak width at the 0.5 peak height.

The resolution power of the quadrupole is unitary. It means that at 200 m/z , the resolving power is 200⁷. So, quadrupole is not considered a high-resolution analyzer. Nevertheless, considering the ability of the quadrupole as mass selector, it is common to see quadrupole series instruments applied for quantitative analysis (i.e. QqQ) or hybrid instruments such as Q-TOF, Q-FT-ICR or Q-LIT-orbitrap.

1.2.2 quadrupole ion trap (QIT)

A quadrupole ion trap (QIT) is based on the same principles of the quadrupole, even if the geometries of the analyzers differ. The QIT is constituted by two end caps that are hyperbolic electrodes, along with a ring electrode replaces the remaining two

rods of the quadrupole (figure 4). An open section between the r, y and z axis, is the inlet entrance for the ions. All components of the trap are structured to generate DC and RF potential between them. Due to these potentials, it is possible to set stable trajectories for ions in a set m/z range or of a fixed m/z , removing ions by leaving them to collide on the trap components or by axial ejection by instable trajectories. Another difference is made by the electric field generated in the trap. In fact, there is a three-dimension electric field, allowing 3D trajectories⁷.

The motion equations of ions in the QIT are similar to the ones of quadrupole analyzer proposed by Mathieu and completed by Paul (Nobel Prize for physics in 1989 for his work in developing MS analyzers²³).

According to Cooks et al.²⁴, Ion traps resolution could reach 10000 at m/z 1000. It means that at 200 m/z , R is 2000, that it is not considered high resolution.

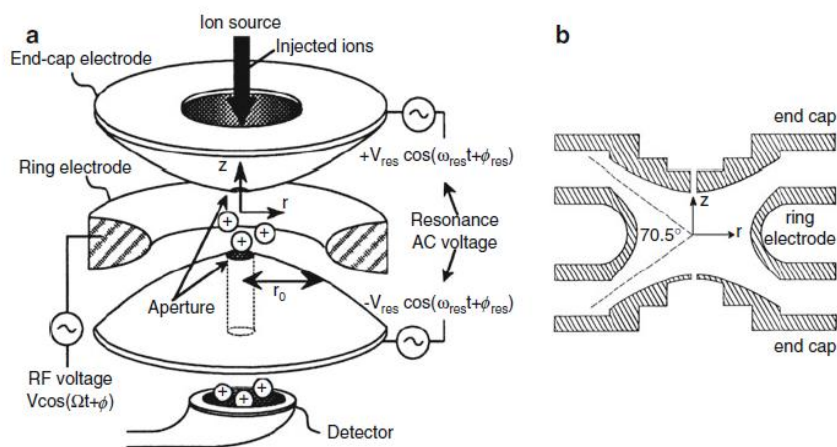


Figure 4. QIT scheme (a) and its r and y section (b)²⁵

1.2.3 Orbitrap

Orbitrap mass analyzer was described for the first time by Makarov in 2000²⁶, basing on Kingdon trap projects made in 1920s²⁷. The first MS equipped with an orbitrap as first MS analyzer was introduced on the market by Thermo Fisher Scientific in 2005²⁸. The orbitrap is constituted by two parts: an external electrode with a shape

of barrel cut in two equal parts with a small interval, and a central electrode with a spindle shape. The maximum dimensions of the electrodes are 20 mm and 8 mm, respectively (figure 5).

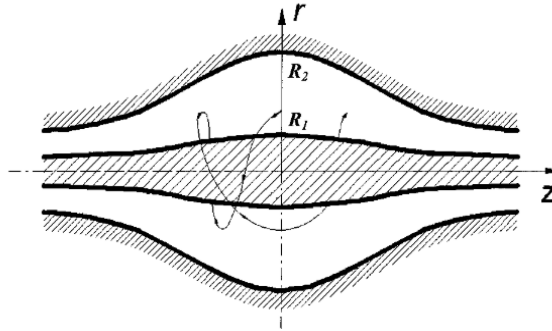


Figure 5. Orbitrap scheme design as proposed by Makarov²⁶

The orbitrap mechanism of action is resumed. Ions are injected from the ion source and trapped in the linear ion trap. Ions of interest can be isolated and fragmented in the linear ion trap, and even scanned out and detected by an independent set of detectors.

To obtain high accuracy measurements, the ions are axially ejected from the linear trap into the c-trap where they are captured again and thermalized by collisions with nitrogen gas. Then, they are squeezed into a smaller cloud within the c-trap ready for injection into the orbitrap.

When ions are into the orbitrap, the voltage on the central electrode increases and it forces the ion packages circling around the central electrode.

Finally, ions come into the orbitrap lightly off axis and keep oscillating along the central electrode, until their stabilization 1 (4). The frequency of the harmonic axial oscillation (ω_z) is inversely proportional to the square root of m/z ratio of the ions (figure 6).

$$\omega_z = \sqrt{k \left(\frac{q}{m_i} \right)} \quad 1 (4)$$

1 (4) where:

w_z is the frequency of the harmonic axial oscillation, k is q is the ion charge and m is the ion mass.

Afterwards, the image current is recorded on the outer split electrodes. The signals are amplified and transformed into a frequency spectrum by the fast Fourier Transform which is finally converted into a mass spectrum²⁸.

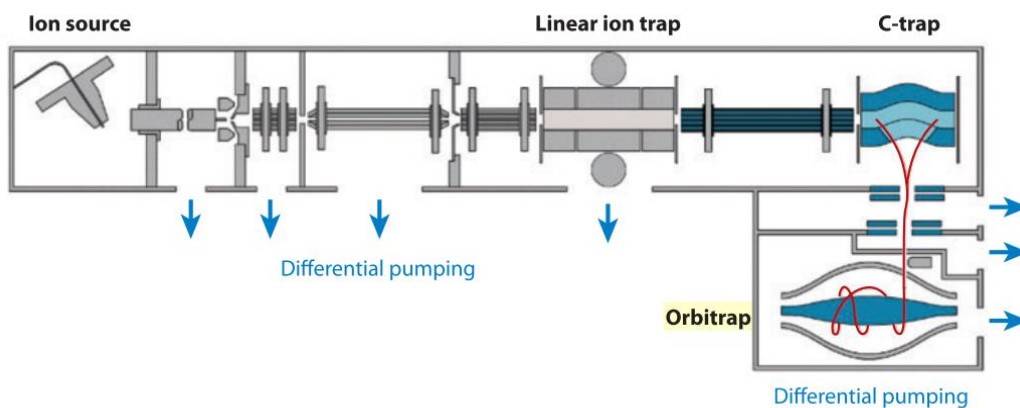


Figure 6. Orbitrap design scheme²⁹

The last orbitrap MS instrument released on the market from Thermo Fisher Scientific is the Orbitrap Fusion Lumos, an hybrid instrument which can reach a R (FWHM) value of 500,000 at 200 m/z (www.thermofisher.com).

1.3 Liquid Chromatography tandem Mass Spectrometry

The first concept of electrospray ionization (ESI) was first described by Dole et al. and Taylor in the 1960s^{30,31}. Only in the late 1980s, Mann et al^{32,33} applied this technique with success on molecules with a M.W. in the range of 100 - 2000 Da.

Today, ESI is one of the most common ionization mode in LC-MS instruments. It is an ionization type belonging to class of atmospheric pressure ionization (API) methods, as the atmospheric pressure chemical ionization (APCI) and atmospheric pressure photoionization (APPI). ESI is the golden standard choice for liquid chromatography tandem mass spectrometry analysis, for either small and large molecules⁷.

ESI together with matrix-assisted laser desorption/ionization (MALDI)³⁴, another ionization mode, allowed the application of MS techniques also in biology for studies of large biomolecules. J. B. Fenn and K. Tanaka received the Nobel Prize in chemistry in 2002 for the development of soft ionization methods for mass spectrometric analyses of biological macromolecules^{35,36}.

1.3.1 ESI working concept

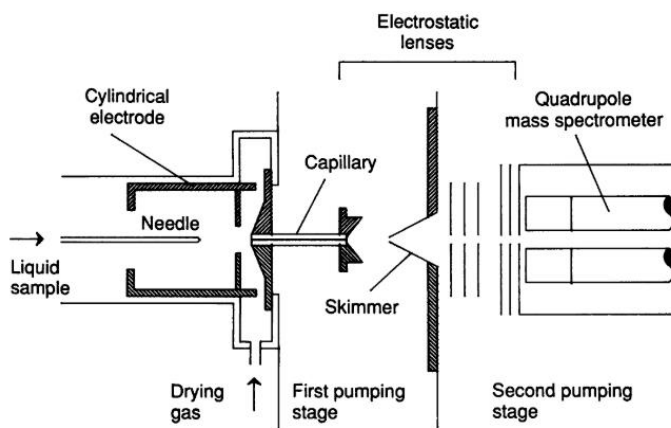


Figure 7. ESI schematic design³³

In ESI, the sample solution coming from a capillary tube at 1-20 $\mu\text{l min}^{-1}$ of flow rate is ionized by applying an electric field at atmospheric pressure. The potential is applied by a cylindrical electrode which surrounds the capillary tube, to guarantee an ionization at 3-6 kV. At this point, there is a charge accumulation on the liquid surface at the end of the capillary, which will be broken to form highly charged droplets once left in the space. Then, the droplets aerosol just formed pass into a countercurrent stream of hot inert nitrogen gas at low flow rates, as a heat source for supplying the complete solvent evaporation.

A small portion of the sprayed material comes into the aperture of a transfer capillary (4-8 cm length with an internal diameter of 0.2 mm) at 10^2 Pa of pressure. A minor portion passes through the orifice of a skimmer (a cone-shaped electrode named Taylor cone, with a small aperture at its end) into the high vacuum behind (10^{-3} and 10^{-4} Pa). Finally, desolvation of the ions is completed and they are focused into a mass analyzer. A general scheme of the ESI is reported in figure 7.

The potentials applied to the electrode, capillary, skimmer, and lenses behind provide an effective transfer of ions through the interface. These parameters are optimized depending of chemical features of the molecules to be ionized.

The ions obtained from large molecules carry a greater number of charges if several ionizable sites are present (multicharged ions). Typically, a protein has one charge per thousand Da approximately. Small molecules with a M.W. lower than a thousand Da, will produce mainly monocharged ions. ESI can also be used in the case of molecules without any ionizable site through the formation of sodium, potassium, ammonium, formate, acetate or other adducts. However, ions have to be already present in sample solution before the electrospray ionization.

1.3.2 ESI application to different LC flow rates

Nowadays, ESI is suitable of working at different flow rate from 50-200 $\mu\text{l min}^{-1}$ for chemical and bioanalytical LC-MS applications to 200-400 nl min^{-1} for proteomics applications.

For micro flow rate, the ESI has been assisted with the use of a nebulizer or sheath gas flow that provides a pneumatic assistance during the spray capillary process^{37,38}. This improvement allows the use of higher sample solution flow rate reducing the surface tension of the solvent and providing its complete evaporation.

At the same time, working with nano flow rate requires a nano ionization source and a nanoESI is essential for the optimal ionization of highly polar solutions. Both these two factors are common in the analysis of peptides in proteomics LC-MS based works. The nanoESI has been described by Wilm and Mann³⁹, modifying the capillary spray structure of the electrospray. The spray needle is replaced with a borosilicate glass capillary with a narrow tip terminal of few μm of i.d. Lower droplets size are produced, and the sample consumption is reduced^{39,40}. The spray voltage applied to the counter electrode is less than 1.5 kV. A micromanipulator working in three dimensions and a camera are necessary to set a correct distance of about 1 mm between the capillary and the entrance in the source.

1.4 LC-MS applications

1.4.1 Pharmaceutical Analysis

LC-MS technique is widespread in pharmaceutical analysis. There are a lot of applications in which LC-MS is involved, among them: determination of pesticides^{41,42}, dose formulation analysis⁴³, ADME studies⁴⁴, impurity profiling⁴⁵, toxicity studies^{46,47}, quality assurance and quality control methods⁴⁸, therapeutic drug monitoring⁴⁹ and forced degradation studies^{14,50,51}. In this paragraph, the forced degradation studies and the identification of the stability indicator of a drug will be discussed. This research field is regulated by the International Conference of Harmonization (ICH) guidelines Q1(A)R2 stability testing of new drug substances and products⁵². These guidelines report an overview on how to perform a validated stability study in case of drugs to be used for humans. Nevertheless, the experimental conditions are not detailed described, and the chemist has to set them up depending on the features of individual drug substances.

The stress testing conditions aim to identify degradation products arising from drug substances, to establish a degradation pathway and to study the intrinsic stability of the compounds evaluated. The forced conditions studied usually include natural, acidic, alkaline, oxidative, the presence of a radical initiator and photodegradation in both daylight and UV light. Time points are dependent to concentrations involved to each stress reactions and they are fixed from few hours to 48 hours until 14 days for daylight photodegradation exposure. Also, the temperature is a key feature to be examined and it is set for all conditions between room temperature and 50°C.

After planning the protocol with the stress testing condition, it is common to develop an LC-MS method for the identification of the drug substances and of the degradation products that could be developed during the experimental conditions.

A linear gradient covering all the percentages of the organic mobile phase is the golden standard strategy during the LC-MS method optimization. It is an important

aspect to be evaluated, considering that the nature on the possible degradation products is unknown in the early stages of the stability testing. Other LC-MS parameters are set on drug substances.

Once a product degradation product is identified, full MS, MS2 and MS3 spectra are studied to propose a structure and so for the identification. Orthogonal techniques to mass spectrometry are necessary such the nuclear magnetic resonance (NMR) and the infrared spectroscopy (IR) for the complete characterization.

The following step is the production of the degradation compounds in order to have them pure to compare the results obtained during stress studies. This is essential to confirm and to validate the degradation pathway of drug substances.

Examining degradation products under stress conditions is useful also in developing and validating suitable analytical procedures for stability studies of drug products. In fact, the degradation compounds identified could be formed during the life of a pharmaceutical products.

At the same time, ICH Q2 (R1) guidelines are followed to validate an analytical method suitable for stability analyses in pharmaceutical field⁵³. The parameters investigated for the method validation are: the selectivity, robustness, lower limit of detection (LOD) and lower limit of quantification (LOQ), linearity, intraday and interday precision and accuracy¹⁴.

1.4.2 Bioanalysis

Bioanalyses are described as the identification or quantification of analytes in biological samples (*e.g.* tissue culture, blood, plasma, serum, urine, feces and saliva) coming from different species. Analytes are either large (*e.g.* proteins and peptides) and small molecules (*e.g.* metabolites and drugs). The applications are numerous: molecular biology, clinical and preclinical, pharmacokinetic, pharmacodynamic and toxicology studies. Different apparatus can be employed for performing bioanalysis. In this paragraph, it will be discussed bioanalysis carried out with LC-MS instruments.

1.4.2.1 Sample preparation techniques

Sample preparations are different approaches performed before the LC-MS analysis, to clean and to purify the biological samples from salts and other molecules which could interfere with the ionization and detection of the analytes. Considering that the biological samples are complex mixtures made of proteins, lipids, small polar compounds, the extraction of the analytes of interest is a key step in bioanalysis. The main methodologies are the following:

(1) Protein precipitation (PPT): it consists in the adding of organic solvents (*e.g.* acetonitrile, methanol or acetone), pH modulator (trichloroacetic and perchloric acids) and metal ions (*e.g.* zinc salts). PPT is one of the most common techniques^{14,54}, quick, easy to do, not expensive, with high ion suppression and good sensitivity. It is suitable for the extraction of both polar and hydrophobic compounds.

(2) Liquid liquid extraction (LLE): it is used for liquid biological samples (*e.g.* plasma⁵⁵, serum⁵⁶ and urine⁵⁷) which are mixed with organic solvents. This technique is common for acidic or basic drugs. Often, LLE and PPT are coupled with an evaporation step to concentrate the analytes before the LC-MS analysis. The LLE 96-well plates automation has been a key upgrade of this technique, solving the mixing issues^{58,59}.

(3) Solid phase extraction (SPE)⁶⁰: it is often the first choice in the analytical labs due its high reproducibility and efficiency. SPE consists in the loading of the sample upon few centimeters of sorbent cartridge. It is functionalized in different ways offering numerous types of interactions between the stationary phase and the analytes to be extracted. Washing and an elution steps are required during the extraction process. SPE negative points are the time consuming either during the method development and the sample handling in routine analysis. Positive aspects are the preconcentration of the biological samples and the automation with online methods which guarantee a reliable, robustness and time saving in this step of the analysis⁶¹.

Moreover, it is a recent trend, the miniaturization of some sample preparation methodologies such as the SPE. This approach allows low sample consumption, less volume of solvents is required with same effectiveness of the “classic” methods^{62,63}.

1.4.2.2 LC-MS bioanalytical method parameters

Some LC-MS method parameters must be evaluated and measured during the method development phase. Handling biological matrices mean working with a lot of biological interferences that could vary the detection of the compounds of interests. Hence, the evaluation of the LC-MS parameters guarantees the quality and the robustness of the bioanalysis. The parameters are: selectivity, linearity, precision, accuracy, matrix effect, recovery, stability and sensitivity⁶⁴.

(1) The selectivity is the ability of the bioanalytical method to measure and differentiate the analytes in the presence of components that may be expected to be present. These could include metabolites, impurities, degradants, or matrix components. It is evaluated by injecting a matrix blank sample coming from different sources. The aim is to exclude interferences peaks with analytes at lower limit of quantification (LLOQ) concentration. To do that, the signal to noise (S/N) ratio is a

useful system suitability parameter. The S/N ratio is calculated as follows as described on U. S. Pharmacopeia (621):

$$S/N \text{ ratio} = 2H/h \quad 1(5)$$

1 (5) where:

H is the height of the peak measured from the peak apex to a baseline extrapolated over a distance ≥ 5 times the peak width at its half-height; and h is the difference between the largest and smallest noise values observed over a distance ≥ 5 times the width at the half-height of the peak.

(2) The linearity is evaluated for quantitative methods with the internal or the external calibration method, depending on the diluting solutions (matrix or solvents, respectively) used for preparing the calibration points. 6-8 points are suggested for rough calibration curves included a blank sample (with n=5 of repeatability). A calibration curve has to be prepared fresh before each batch analysis.

(3) The precision is the closeness of agreement between a series of measurements obtained from multiple sampling of the same homogenous sample under the prescribed conditions. It is evaluated at least on three levels (LLOQ, MQ and HQ), n=5. Precision is evaluated intrabatch and interbatch.

(4) The accuracy is the degree of closeness of the determined value to the nominal or known true value under prescribed conditions. This is sometimes termed trueness. It is evaluated on three different levels (LLOQ, MQ and HQ), n=5. It is calculated with following formula.

$$Accuracy = \frac{\text{Observed conc} - \text{Nominal conc}}{\text{Nominal conc}} \times 100 \quad 1(6)$$

(5) The matrix effect is the direct or indirect alteration or interference in response due to the presence of unintended analytes (for analysis) or other interfering substances in the sample. While, the recovery is the extraction efficiency of an

analytical process, reported as a percentage of the known amount of an analyte carried through the sample extraction and processing steps of the method.

To measure the matrix effect (ME) and the recovery (RE), three samples are prepared:

- A: analyte in solvent;
- B: analyte added to the matrix after the extraction procedure;
- C: analyte added to the matrix before the extraction procedure.

% ME is calculated as:

$$\% ME = \frac{B}{A} \times 100 \quad 1(7)$$

Moreover, matrix effect could be evaluated also with a qualitative method when a blank matrix (without analytes) is available⁶⁵.

% RE is calculated as:

$$\% RE = \frac{C}{B} \times 100 \quad 1(8)$$

(6) The stability could be evaluated with four different assays: freeze and thaw stability, short term temp stability (between 4-24 h), long term stability (between 20 to 60 days), stock solution stability and post preparative stability.

(7) The sensitivity is evaluated as: limit of detection (LOD, the lowest concentration of an analyte that the bioanalytical procedure can reliably differentiate from background noise) and the lower limit of quantification (LLOQ, the lowest amount of an analyte in a sample that can be quantitatively determined with suitable precision and accuracy).

In general, CV values are retained satisfactory when $\leq 15\%$ or $\leq 20\%$ for LLOQ. While for % ME and % RE there are not reported values, but it is suggested to reach percentages closest to 100%.

1.4.3 Proteomics

1.4.3.1 Introduction

Proteomics as word was born in the middle of nineties as the fusion of protein and genomics^{66,67}. The proteomics general aim is the identification and characterization of the whole proteome of all the organisms⁶⁸. Moreover, to understand the protein sequencing, protein post translational modifications (PTMs), protein localization, protein quantification and protein-protein interactions are even more challenging than a genome identification^{69,70}. By the years, proteomics grew up becoming a new discipline across chemistry and biology. The proteomics backbone is constituted by the mass spectrometry (MS), sample preparation and bioinformatic data analysis. Each of these aspects must be accurately planned in order to achieve the results required.

1.4.3.2 Proteomics approaches

An LC-MS based proteomic analysis may be performed on biological samples constituted by intact proteins or enzymatically digested proteins into peptides. So, depending on the approach chosen, the strategies available are essentially three: top down, bottom-up and shotgun.

The first one, top down proteomics means that proteins are analyzed as intact entities without any proteolysis. The main advantages of this approach are determined in the study of PTMs, in the sequence coverage and in protein quantitation. However, there are some limitations, such as the limited fragmentation of intact protein in the gas phase, protein front-end separation is challenging, and it is applicable only for pure protein or small protein mixtures. All these disadvantages, make this approach quite far from the routine analysis.

Secondly, bottom up proteomics is the characterization of proteins after their enzymatically digestion into peptides prior the MS analysis. While, Yates lab.⁷¹ coined the term shotgun proteomics referring to bottom up proteomics performed on

complex protein mixture. With the shotgun proteomics all the disadvantages of the top down proteomics are overcome. However, peptides identification is a key point and it is achieved by the overlapping of the peptides MS2 spectra generated from the LC-MS analysis with the ones generated from the *in silico* digestion of the appropriate protein database. Furthermore, the peptide identified is assigned to the protein (if single so uniquely associate to only one protein) or proteins which shared that peptide. The identification is regulated by search criteria and scoring schemes and it is usually followed by the filtering of the results evaluating the false discovery rate^{29,69,72,73,74}.

The following paragraphs will be focused on shotgun proteomics.

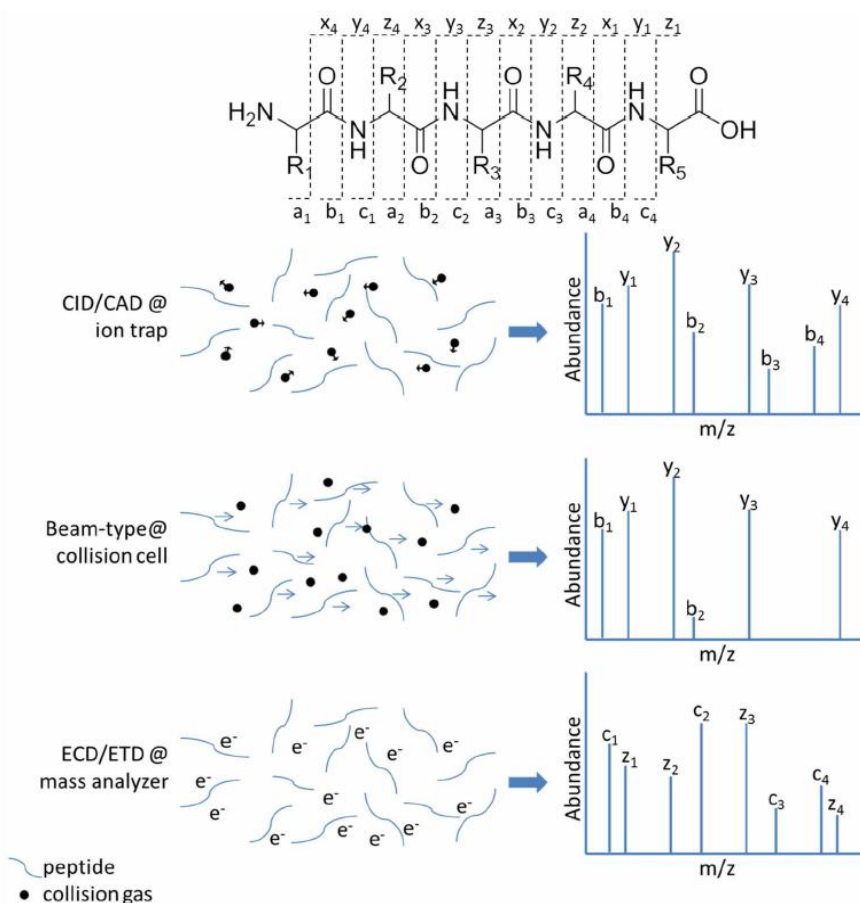
1.4.3.3 Ionization, fragmentation and acquisition mode

In shotgun proteomics, two types of soft ionization techniques are commonly used, able to perform the ionization of peptides. They are the nanoelectrospray (nESI) and the matrix-assisted laser desorption/ionization (MALDI)^{75,76}. In general, nESI is used for peptides in solution, so it is coupled with UHPLC instruments working with nano- or low-micro flow rates, while MALDI is involved for gel based matrix or tissue samples.

After the sample ionization, another key point is the fragmentation mode, essential to generate MS2 spectra of peptide ionized. The first one to be developed and applied for peptides fragmentation was the collision induced dissociation (CID). In low energy CID, b- and y- fragment ions are generated (backbone C-N bond broken), due to multiple collisions with rare gas atoms to the ion peptide positively charged. A modification of CID technique is the higher-energy collisional dissociation (HCD). It is specific for orbitrap and hybrid instruments and it takes place external to the ion trap (*e.g.* HCD cell)⁷⁷. HCD is considered one of the most used fragmentation methods due to its applicability also for PTMs studies. Another technique was introduced by MacLafferty lab in 1998^{78,79} and it is called electron-capture

dissociation (ECD). It consists in the capture of a thermal electron by peptides positively charged inducing a N-C α backbone fragmentation generating c- and z-type fragment ions. It allows to produce more product ions in the peptide MS2 than CID and HCD, getting a better sequence coverage and a good PTMs identification in comparison with CID and HCD. Finally, one more fragmentation methods is represented by the electron-transfer dissociation (ETD), developed by Hunt lab. in 2004⁸⁰. It is similar to the previous one in producing essentially c- and z- type fragment ions. In fact, ETD induces fragmentation of large, multiply-charged cations by transferring electrons to them from radical anions with low electron affinity. It provides fragmentations with femtomole of peptides due to the fast and efficient mechanism of generating MS2 product ions. With this technique, there is the increasing of sequence coverage. PTMs are left intact during the fragmentation making this fragmentation technique the golden standard for these analyses. Unlucky, ECD and ETD are relegated essentially on ions trap, FTICR and hybrid expensive instruments (figure 8).

In conclusion, the CID/HCD fragmentation mode are the most common and the most used in proteomics LC-MS based analysis.

Figure 8. MS fragmentation techniques applied in proteomics⁶⁹

While, another theme faced in the last period is about the acquisition mode in proteomics analysis. There essentially two acquisition modes: the data dependent acquisition (DDA) and the data independent acquisition (DIA)⁸¹. DDA consists in the acquiring a full MS spectrum of the peptides (MS1), followed by the collection of as many fragmentation spectra (MS2) as possible, within a cycle time of about 1 second (time window is variable). It is common to find methods with the selection of the top 12 MS1 peptide ions fragmented to design the MS2 spectra per cycle. While, DIA is constituted by sequential windows of acquisition made usually of 25 m/z units, in which all the MS1 ions identified are selected, fragmented and acquired

by the MS detector. DIA MS2 spectra are really complex and specific deconvolution and identification software are required for the data analysis^{81,82,83}.

Another acquisition technique used in proteomics even if not widespread in this field is the single reaction monitoring mode (SRM). It is common in triple quadrupoles instruments (QqQ) or in ion traps for quantitative analysis. SRM finds proteomics applications in ion traps and orbitrap instruments for quantitative analysis of targeted peptides.

Theoretically, DIA should include both the advantages of DDA and SRM modes⁸².

1.4.3.4 Mass Spectrometry instruments for proteomics

To perform LC-MS based proteomics analysis is essential to have a high-resolution mass spectrometer. Mass analyzers that can provide high resolution analysis are: FTICR, TOF and Orbitrap trend by mass spectrometers producers to configure hybrid instruments to improve mass accuracy, sensitivity and resolution. The main configurations found in proteomics are: LTQ-Orbitrap, Qq-Orbitrap, LTQ-FTICR, QqQ-FTICR, Q-TOF and IT-TOF²⁹.

1.4.3.5 Starting material and sample preparation for shotgun proteomics

For shotgun proteomics analysis, the starting material could be different and coming from various origin. Usually, the principle biological matrices are analysed such as biological fluids, cells and tissue. The development of working protocols is a key point of the proteomics. Focusing on the analysis of the intracellular content, some sample preparations steps and tips are maintained. So, proteins were extracted after cells culture and then lysed. Afterwards, proteins extracted were firstly reduced to break disulphide bonds, and then alkylated to reduce the sulfhydryl free moieties. The last steps are the proteins digestion into peptides and the sample desalting before the injection in the LC-MS^{84,85,86}.

1.4.3.6 Bioinformatics

As previously mentioned in 1.4.3.2 section, bioinformatics tools are gaining popularity and are still under development to make data analysis reproducible, easy to do and accurate. Since the publication of SEQUEST in 1994⁸⁷, a software for the protein identification from peptides mixture, numerous other algorithms were published (^{88,89,90}). However, the integration of software packages into pipelines helped the scientists to standardize and simplify the proteomics analysis workflow. Nowadays, there are various pipeline, by which: Proteomics Pipeline (IP2, <http://integratedproteomics.com/>), pFind Studio (<http://pfind.ict.ac.cn/>)^{91,92}, ProteomeDiscoverer (www.thermoscientific.com), MaxQuant (<http://maxquant.org/>)⁹³. A representative pathway of data acquisition and bioinformatic data analysis pathway is reported in figure 9.

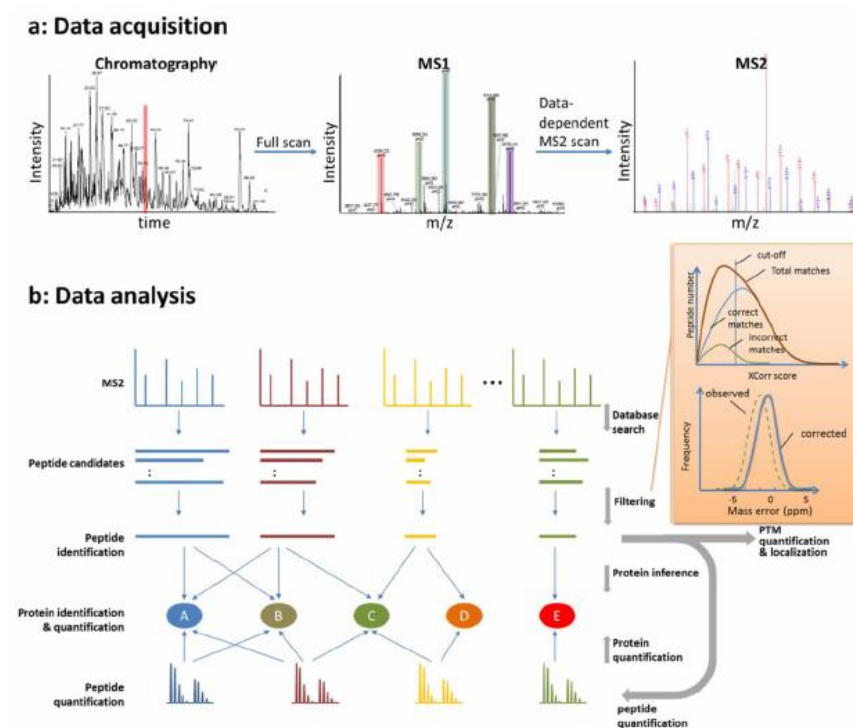


Figure 9. Representative LC-MS/MS data acquisition and bioinformatic data analysis pipeline for protein identification and quantification in shotgun proteomics⁶⁹

References:

1. Martin, A. J. P. & Synge, R. L. M. A new form of chromatogram employing two liquid phases. *Biochem. J. London* 1906 **35**, 1358–1368 (1941).
2. Ettre, L. S. & Sakodynskii, K. I. M.S. Tswett and the discovery of chromatography. I: Early work (1899-1903). *Chromatographia* **35**, 223–231 (1993).
3. J. C. Horvath, J. C. & Lipsky, S. R. Use of liquid ion exchange chromatography for the separation of organic compounds. *Nature* **211**, 748 (1966).
4. Horvath, C. G., Preiss, B. A. & Lipsky, S. R. Fast Liquid Chromatography: An Investigation of Operating Parameters and the Separation of Nucleotides on Pellicular Ion Exchangers. *Anal. Chem.* **39**, 1422–1428 (1967).
5. Fanali, S., Haddad, P. R., Poole, C. F., Schoenmakers, P. & Lloyd, D. *Liquid Chromatography: Fundamentals and Instrumentation*. Elsevier, Amsterdam, (2013).
6. van Deemter, J. J., Zuiderweg, F. J. & Klinkenberg, A. Longitudinal diffusion and resistance to mass transfer as causes of nonideality in chromatography. *Chem. Eng. Sci.* **5**, 271–289 (1956).
7. Gross, J. H. *Mass Spectrometry*. Springer (2017).
8. Fekete, S., Oláh, E. & Fekete, J. Fast liquid chromatography: The domination of core-shell and very fine particles. *J. Chromatogr. A* **1228**, 57–71 (2012).
9. González-Ruiz, V., Olives, A. I. & Martín, M. A. Core-shell particles lead the way to renewing high-performance liquid chromatography. *TrAC- Trends Anal. Chem.* **64**, 17–28 (2015).
10. Ali, I., Al-Othman, Z. A. & Al-Za'abi, M. Superficially porous particles columns for super fast HPLC separations. *Biomed. Chromatogr.* **26**, 1001–1008 (2012).
11. Fekete, S., Veuthey, J. L. & Guillarme, D. Comparison of the most recent

- chromatographic approaches applied for fast and high resolution separations: Theory and practice. *J. Chromatogr. A* **1408**, 1–14 (2015).
12. Salisbury, J. J. Fused-core particles: A practical alternative to sub-2 micron particles. *J. Chromatogr. Sci.* **46**, 883–886 (2008).
 13. Gritti, F. *et al.* Performance of columns packed with the new shell particles, Kinetex-C18. *J. Chromatogr. A* **1217**, 1589–1603 (2010).
 14. Bianchi, M., Canavesi, R., Aprile, S., Grosa, G. & Del Grosso, E. Troxerutin, a mixture of O-hydroxyethyl derivatives of the natural flavonoid rutin: Chemical stability and analytical aspects. *J. Pharm. Biomed. Anal.* **150**, 248–257 (2018).
 15. Yang, P., McCabe, T. & Pursch, M. Practical comparison of LC columns packed with different superficially porous particles for the separation of small molecules and medium size natural products. *J. Sep. Sci.* **34**, 2975–2982 (2011).
 16. Guillarme, D., Ruta, J., Rudaz, S. & Veuthey, J. L. New trends in fast and high-resolution liquid chromatography: A critical comparison of existing approaches. *Anal. Bioanal. Chem.* **397**, 1069–1082 (2010).
 17. Fekete, S., Schappler, J., Veuthey, J. L. & Guillarme, D. Current and future trends in UHPLC. *TrAC - Trends Anal. Chem.* **63**, 2–13 (2014).
 18. Chawla, G. & Ranjan, C. Principle, Instrumentation, and Applications of UPLC: A Novel Technique of Liquid Chromatography. *Open Chem. J.* **3**, 1–16 (2016).
 19. Drake, J. M. *et al.* Phosphoproteome Integration Reveals Patient- Specific Networks in Prostate Cancer. *Cell* **166**, 1041–1054 (2016).
 20. Nitarska, J. *et al.* Article A Functional Switch of NuRD Chromatin Remodeling Complex Subunits Regulates Mouse Cortical Article A Functional Switch of NuRD Chromatin Remodeling Complex Subunits Regulates Mouse Cortical Development. *CellReports* **17**, 1683–1698 (2016).

21. Hoffmann, E. D. & Stroobant, V. *Mass Spectrometry-Principles and Applications. Mass spectrometry reviews* (Wiley, 2007).
22. Balogh, M. Debating Resolution and Mass Accuracy in Mass Spectrometry. *Spectroscopy* **19**, 34–40 (2004).
23. Paul, W., Reinhard, H. P. & von Zahn U. Das elektrische massenfilter als massenspektrometer und isotopentrenner, *Z. Phys.* **152** 143–182 (1958).
24. Plass, W. R., Li, H. & Cooks, R. G. Theory, Simulation and Measurement of Chemical Mass Shifts in RF Quadrupole Ion Traps. *Int. J. Mass Spectrom.* **228**, 237–267 (2003).
25. Yoshinari, K. Theoretical and numerical analysis of the behavior of ions injected into a quadrupole ion trap mass spectrometer. **223**, 215–223 (2000).
26. Makarov, A. Electrostatic axially harmonic orbital trapping: A high-performance technique of mass analysis. *Anal. Chem.* **72**, 1156–1162 (2000).
27. Kingdon, K. H. A Method for Neutralizing the Electron Space Charge by Positive Ionization at Very Low Pressures. *Phys. Rev.* **21**, 408–418 (1923).
28. Hu, Q. *et al.* The Orbitrap: A new mass spectrometer. *J. Mass Spectrom.* **40**, 430–443 (2005).
29. Yates, J. R., Ruse, C. I. & Nakorchevsky, A. Proteomics by Mass Spectrometry: Approaches, Advances, and Applications. *Annu. Rev. Biomed. Eng.* **11**, 49–79 (2009).
30. Taylor, G. Disintegration of Water Drops in an Electric Field. *Proc. R. Soc. A Math. Phys. Eng. Sci.* **280**, 383–397 (1964).
31. Dole, M. *et al.* Molecular beams of macroions. *J. Chem. Phys.* **49**, 2240–2249 (1968).
32. Mann, M., Meng, C. K. & Fenn, J. B. Interpreting Mass Spectra of Multiply Charged Ions. *Anal. Chem.* **61**, 1702–1708 (1989).
33. Fenn, J. B., Mann, M., Meng, C. K., Wong, S. F. & Whitehouse, C. M. Electrospray ionization for mass spectrometry of large biomolecules. *Science*

- 246**, 64–71 (1989).
34. Tanaka, K. *et al.* Protein and polymer analyses up to m/z 100 000 by laser ionization time-of-flight mass spectrometry. *Rapid Commun. Mass Spectrom.* **2**, 151–153 (1988).
 35. Fenn, J. B. Electrospray wings for molecular elephants (Nobel lecture). *Angew. Chemie-Int. Ed.* **42**, 3871–3894 (2003).
 36. Tanaka, K. The Origin of Macromolecule Ionization by Laser Irradiation (Nobel Lecture). *Angew. Chemie Int. Ed.* **42**, 3860–3870 (2003).
 37. Bruins, A. P., Covey, T. R. & Henion, J. D. Ion spray interface for combined liquid chromatography/atmospheric pressure ionization mass spectrometry. *Anal. Chem.* **59**, 2642–2646 (1987).
 38. Ikononou, M. G., Blades, A. T. & Kebarle, P. Electrospray-Ion Spray: A Comparison of Mechanisms and Performance. *Anal. Chem.* **63**, 1989–1998 (1991).
 39. Wilm, M. S. & Mann, M. Electrospray and Taylor-Cone theory, Dole's beam of macromolecules at last? *Int. J. Mass Spectrom. Ion Process.* **136**, 167–180 (1994).
 40. Gibson, G. A. A., Mugo, S. M. & Oleschuk, R. D. Nanoelectrospray emitters: trends and perspective. *Mass Spectrom. Rev.* **28**, 918–936 (2009).
 41. Moreno-González, D., Alcántara-Durán, J., Addona, S. M. & Beneito-Cambra, M. Multi-residue pesticide analysis in virgin olive oil by nanoflow liquid chromatography high resolution mass spectrometry. *J. Chromatogr. A* **1562**, 27–35 (2018).
 42. Casado, J., Santillo, D. & Johnston, P. Multi-residue analysis of pesticides in surface water by liquid chromatography quadrupole-Orbitrap high resolution tandem mass spectrometry. *Anal. Chim. Acta* **1024**, 1–17 (2018).
 43. Chen, Y. A. & Hsu, K. Y. Development of a LC-MS/MS-based method for determining metolazone concentrations in human plasma: Application to a

- pharmacokinetic study. *J. Food Drug Anal.* **21**, 154–159 (2013).
44. Jian, W., Shou, W., Edom, R. W., Weng, N. & Zhu, M. *Mass Spectrometry Handbook: LC-MS in Drug Metabolism and Industry Perspective.* (2012).
 45. Canavesi, R., Aprile S., Giovenzana G.B., Di Sotto A., Di Giacomo S., Del Grosso E. & Grosa G. New insights in oxybutynin chemical stability: Identification in transdermal patches of a new impurity arising from oxybutynin N-oxide rearrangement. *Eur. J. Pharma Sci.* **84**, 123–131 (2016).
 46. Ojanperä, I., Kolmonen, M. & Pelander, A. Current use of high-resolution mass spectrometry in drug screening relevant to clinical and forensic toxicology and doping control. *Anal. Bioanal. Chem.* **403**, 1203–1220 (2012).
 47. Nordgren, H. K., Holmgren, P., Liljeberg, P., Eriksson, N. & Beck, O. Application of Direct Urine LC-MS-MS Analysis for Screening of Novel Substances in Drug Abusers. *J. Anal. Toxicol.* **29**, 234–239 (2005).
 48. Hugo, J. *et al.* Forced degradation of L-(+)-bornesitol, a bioactive marker of *Hancornia speciosa*: Development and validation of stability indicating UHPLC-MS method and effect of degraded products on ACE inhibition. *J. Chromatogr. B Anal. Technol. Biomed. Life Sci.* **1093–1094**, 31–38 (2018).
 49. Adaway, J. E. & Keevil, B. G. Therapeutic drug monitoring and LC-MS/MS. *J. Chromatogr. B Anal. Technol. Biomed. Life Sci.* **883–884**, 33–49 (2012).
 50. Del Grosso, E., Aprile, S. & Grosa, G. Forced degradation study of thiocolchicoside: Characterization of its degradation products. *J. Pharm. Biomed. Anal.* **61**, 215–223 (2012).
 51. Canavesi, R., Aprile, S., Varese, E. & Grosa, G. Development and validation of a stability-indicating LC-UV method for the determination of pantethine and its degradation product based on a forced degradation study. *J. Pharm. Biomed. Anal.* **97**, 141–150 (2014).

52. ICH Guidelines Q1A (R2), Stability Testing of New Drug Substances and Products: Text and Methodology, *International Conference on Harmonisation* (2005).
53. ICH Q2A (R1), Validation of Analytical Procedures: Text and Methodology, *International Conference on Harmonisation*, (2005).
54. Bortolotto, V., Mancini F., Mangano G., Salem R., Xia E., Del Grosso E., Bianchi M., Canonico P.L., Polenzani L. & Grilli M. Proneurogenic Effects of Trazodone in Murine and Human Neural Progenitor Cells. *ACS Chem. Neurosci.* **8**, 2027–2038 (2017).
55. Gu, G. *et al.* Validation of an LC-MS/MS method for simultaneous quantification of venlafaxine and its five metabolites in rat plasma and its application in a pharmacokinetic study. *J. Chromatogr. B Anal. Technol. Biomed. Life Sci.* **1087–1088**, 29–35 (2018).
56. Abdallaha, I. A., Hammell, D. C., Stinchcomb, A. L. & Hassan, H. E. A fully validated LC-MS/MS method for simultaneous determination of nicotine and its metabolite cotinine in human serum and its application to a pharmacokinetic study after using nicotine transdermal delivery systems with standard heat application in adul. *J. Chromatogr. B Anal. Technol. Biomed. Life Sci.* **1020**, 67–77 (2016).
57. Thevis, M., Thomas, A. & Schänzer, W. Current role of LC-MS(/MS) in doping control. *Anal. Bioanal. Chem.* **401**, 405–420 (2011).
58. Song, Q. & Naidong, W. Analysis of omeprazole and 5-OH omeprazole in human plasma using hydrophilic interaction chromatography with tandem mass spectrometry (HILIC-MS/MS) - Eliminating evaporation and reconstitution steps in 96-well liquid/liquid extraction. *J. Chromatogr. B Anal. Technol. Biomed. Life Sci.* **830**, 135–142 (2006).
59. Xue, Y. J., Liu, J. & Unger, S. A 96-well single-pot liquid-liquid extraction, hydrophilic interaction liquid chromatography-mass spectrometry method for

- the determination of muraglitazar in human plasma. *J. Pharm. Biomed. Anal.* **41**, 979–988 (2006).
60. Paíga, P. *et al.* Development of a SPE-UHPLC-MS/MS methodology for the determination of non-steroidal anti-inflammatory and analgesic pharmaceuticals in seawater. *J. Pharm. Biomed. Anal.* **106**, 61–70 (2015).
61. Pensi, D. *et al.* First UHPLC–MS/MS method coupled with automated online SPE for quantification both of tacrolimus and everolimus in peripheral blood mononuclear cells and its application on samples from co-treated pediatric patients. *J. Mass Spectrom.* **52**, 187–195 (2017).
62. Rahman, M. *et al.* HybridSPE: A novel technique to reduce phospholipid-based matrix effect in LC-ESI-MS Bioanalysis. *J. Pharm. Bioallied Sci.* **4**, 267 (2012).
63. Eerkes, A., Shou, W. Z. & Naidong, W. Liquid/liquid extraction using 96-well plate format in conjunction with hydrophilic interaction liquid chromatography-tandem mass spectrometry method for the analysis of fluconazole in human plasma. *J. Pharm. Biomed. Anal.* **31**, 917–928 (2003).
64. Food and Drug Administration. *Guidance for Industry: Bioanalytical Method Validation*. U.S. Department of Health and Human Services (2001).
65. Matuszewski, B. K., Constanzer, M. L. & Chavez-Eng, C. M. Strategies for the assessment of matrix effect in quantitative bioanalytical methods based on HPLC-MS/MS. *Anal. Chem.* **75**, 3019–3030 (2003).
66. Wilkins, M. R. *et al.* From proteins to proteomes: Large scale protein identification by two-dimensional electrophoresis and amino acid analysis. *Nat. Biotechnology* **14**, 61–65 (1996).
67. James, P. Protein identification in the post-genome era: The rapid rise of proteomics. *Q. Rev. Biophys.* **30**, 279–331 (1997).
68. Aebersold, R. & Mann, M. Mass spectrometry-based proteomics. *Nature* **402**, 198–207 (2003).

69. Zhang Yaoyang, Fonslow Bryan R., Shan Bing, Baek, Moon-Chang & Yates, J. R. III. Protein Analysis by Shotgun/Bottom-up Proteomics. *Chem Rev* **113**, 2343–2394 (2013).
70. Bensimon, A., Heck, A. J. R. & Aebersold, R. Mass Spectrometry–Based Proteomics and Network Biology. *Annu. Rev. Biochem.* **81**, 379–405 (2012).
71. Yates, J. R. III Mass spectrometry and the age of the proteome. *J. Mass Spectrom.* **33**, 1–19 (1998).
72. Yates, J. R. III Mass Spectral Analysis in Proteomics. *Annu. Rev. Biophys. Biomol. Struct.* **33**, 297–316 (2004).
73. Kall, L., Canterbury, J. D., Weston, J., Noble, W. S. & MacCoss, M. J. Semi-supervised learning for peptide identification from shotgun proteomics datasets. *Nat. Methods* 923–925 (2007). doi:2007
74. Spivak, M., Weston, J., Bottou, L., Käll, L. & Noble, W. S. Improvements to the Percolator algorithm for peptide identification from shotgun proteomics data sets. *J. Proteome Res.* **8**, 3737–3745 (2009).
75. Wilm, M. & Mann, M. Analytical properties of the nanoelectrospray ion source. *Anal. Chem.* **68**, 1–8 (1996).
76. Hillenkamp, F. & Karas, M. Mass spectrometry of peptides and proteins by matrix-assisted ultraviolet laser desorption/ionization. *Methods Enzymol.* **193**, 280–295 (1990).
77. Olsen, J. V *et al.* Higher-energy C-trap dissociation for peptide modification analysis. *Nat. Methods* **4**, 709–712 (2007).
78. Zubarev, R. A. *et al.* Electron Capture Dissociation for Structural Characterization of Multiply Charged Protein Cations than the conventional MS / MS methods. *Anal. Chem.* **72**, 563–573 (2000).
79. Zubarev, R. Protein primary structure using orthogonal fragmentation techniques in Fourier transform mass spectrometry. *Expert Rev. Proteomics* **3**, 251–261 (2006).

80. Syka, J. E. P., Coon, J. J., Schroeder, M. J., Shabanowitz, J. & Hunt, D. F. Peptide and protein sequence analysis by electron transfer dissociation mass spectrometry. *Proc. Natl. Acad. Sci.* **101**, 9528–9533 (2004).
81. Aebersold, R. & Mann, M. Mass-spectrometric exploration of proteome structure and function. *Nature* **537**, 347–355 (2016).
82. Doerr, A. DIA mass spectrometry. *Nat. Methods* **12**, 35 (2014).
83. Gillet, L. C. *et al.* Targeted Data Extraction of the MS/MS Spectra Generated by Data-independent Acquisition: A New Concept for Consistent and Accurate Proteome Analysis. *Mol. Cell. Proteomics* **11**, O111.016717 (2012).
84. Giansanti, P., Tsiatsiani, L., Low, T. Y. & Heck, A. J. R. Six alternative proteases for mass spectrometry-based proteomics beyond trypsin. *Nat. Protoc.* **11**, 993–1006 (2016).
85. Liu, Q. *et al.* Molecular basis for blue light-dependent phosphorylation of Arabidopsis cryptochrome 2. *Nat. Commun.* **8**, 1–12 (2017).
86. Kelstrup, C. D., Young, C., Lavalley, R., Nielsen, M. L. & Olsen, J. V. Optimized fast and sensitive acquisition methods for shotgun proteomics on a quadrupole orbitrap mass spectrometer. *J. Proteome Res.* **11**, 3487–3497 (2012).
87. Eng, J. K., McCormack, A. L. & Yates, J. R. III. An approach to correlate tandem mass spectral data of peptides with amino acid sequences in a protein database. *J. Am. Mass Spectrom.* **5**, 976–989 (1994).
88. Kim, S. & Pevzner, P. A. MS-GF+ makes progress towards a universal database search tool for proteomics. *Nat. Commun.* **5**, 1–10 (2014).
89. Craig, R. & Beavis, R. C. TANDEM: Matching proteins with tandem mass spectra. *Bioinformatics* **20**, 1466–1467 (2004).
90. Mueller, L. N. *et al.* SuperHirn - A novel tool for high resolution LC-MS-based peptide/protein profiling. *Proteomics* **7**, 3470–3480 (2007).
91. Yang, B. *et al.* Identification of cross-linked peptides from complex samples.

- Nat. Methods* **9**, 904–909 (2012).
92. Lu, S. *et al.* Mapping native disulfide bonds at a proteome scale. *Nat. Methods* **11**, 1–8 (2015).
93. Cox, J. & Mann, M. MaxQuant enables high peptide identification rates, individualized p.p.b.-range mass accuracies and proteome-wide protein quantification. *Nat. Biotech.* **26**, 1367–1372 (2008).

Chapter 2

2. Outline of the thesis

Especially in the last 25 years, a lot of efforts and investments were made in R&D to develop new LC-MS components and instruments. The huge adaptability of the technique and the unlimited applications of the LC-MS, pushed the scientists in the pathway of breaking limits and achieving new records.

In this context, the main aim of the thesis was to show the versatility of LC-MS in the chemistry and biology research. LC-MS was applied in medicinal chemistry for degradation studies of active compounds, in quantitative bioanalysis of small molecules in plasma, intracellular and extracellular compartments and in proteomics to study post translational modifications.

To perform all of these LC-MS analyses different instruments were used, suitable to achieve the results required.

The liquid chromatography instrument used were HPLC and UHPLC systems equipped with quaternary pumps operating with micro- and nano-flow rates. Mass Spectrometry ion source was constituted by the electrospray ion source (ESI) or by the nano-ESI. Moreover, MS detectors were constituted by a linear ion trap, or an hybrid instrument constituted by a quadrupole, linear trap and orbitrap.

The instruments were working in both positive and negative ionizations mode with different scans type: full MS, MS2, MS3, SRM (Single reaction monitoring), MRM (Multiple Reaction Monitoring) and DDA (Data Dependent acquisition) mode. Fragmentations method involved were CID (Collision Induced Dissociation) and HCD (Higher-energy Collisional Dissociation).

In these three working years, the LC-MS tool was applied to the following projects:

(1) Investigation of troxerutin (TRX) degradation pathway, degradation products characterization and identification of TRX stability indicator.

- (2) Development of a bioanalytical LC-MS method for the quantification of adenosine 5'-tetraphosphate (Ap₄) and other five analytes related to Nicotinamide phosphoribosyltransferase (NAMPT) metabolism in different biological matrices.
- (3) Development of a quantitative LC-MS bioanalytical method for the quantitation of serotonin extracellular levels of murine neural progenitor cells.
- (4) Identification, quantification and investigation of post-translational modifications (PTMs) on Nicotinamide phosphoribosyltransferase (NAMPT) in murine melanoma B16 cells.

Chapter 3

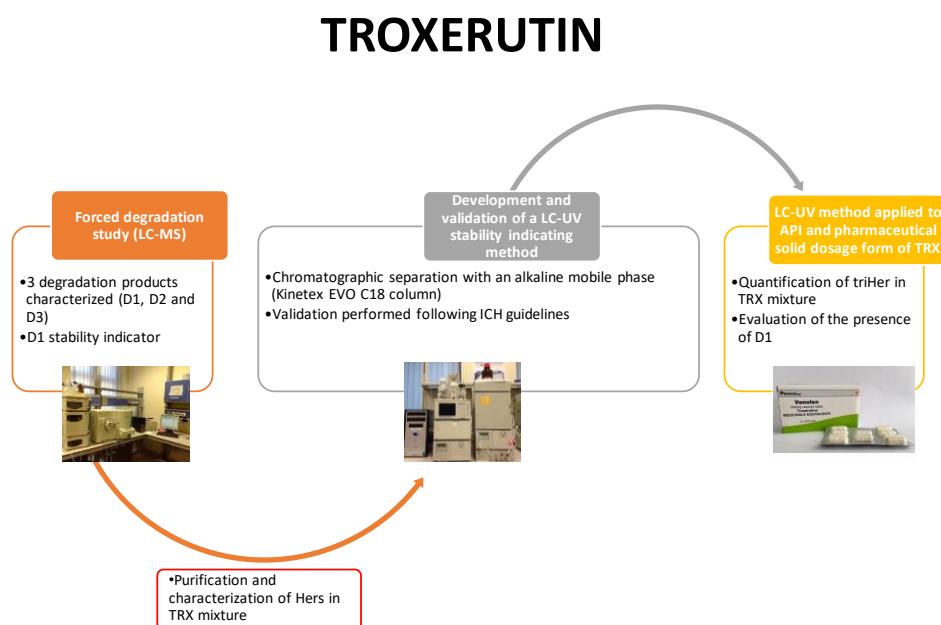
3. Troxerutin, a mixture of O-hydroxyethyl derivatives of the natural flavonoid rutin: Chemical stability and analytical aspects

Michele Bianchi, Rossana Canavesi, Silvio Aprile, Giorgio Grosa,
Erika Del Grosso*

Laboratory of Pharmaceutical Analysis, Department of Pharmaceutical Sciences,
Università del Piemonte Orientale, Largo Donegani 2, 28100 Novara, Italy

*Corresponding Author

Graphical Abstract:



Abstract:

Troloxerutin (TRX) is a mixture of semisynthetic hydroxyethylrutosides (Hers) arising from hydroxyethylation of rutin, a natural occurring flavonoid. TRX is commonly used for its anti-oxidant and anti-inflammatory properties in chronic venous insufficiency and other vascular disorders. In recent studies, the protective effects of TRX in Alzheimer's disease, colon carcinogenesis and hepatocellular carcinoma are emerged. However, the chemical stability of TRX has never been studied. Hence, the aims of the work were to study the TRX chemical stability through a forced degradation study and to develop and validate a new stability indicating LC-UV method for determination of TRX. In order to perform the study, TRX stability was tested in various stress conditions analysing the degradation samples by LC-MS. Three degradation products (DPs; D1, D2 and D3, 3',4',7-Tri-O-(β -hydroxyethyl)quercetin, 3',4',5,7-Tetra-O-(β -hydroxyethyl)quercetin and 3',4'-Di-O-(β -hydroxyethyl)quercetin respectively) arising from degradation in acidic conditions were identified and synthesized: among them, D1 resulted the stability indicator for hydrolytic degradation. Furthermore, a stability-indicating LC-UV method for simultaneous determination of triHer (3',4',7-Tri-O-(β -hydroxyethyl)rutin, the principal component of the mixture) and D1 was developed and validated. The LC-UV method consisted in a gradient elution on a Phenomenex Kinetex EVO C18 (150 \times 3 mm, 5 μ m) with acetonitrile and ammonium bicarbonate buffer (10 mM, pH 9.2). The method was linear for triHer (20–60 μ g mL⁻¹) and D1 (5.1–35 μ g mL⁻¹). The intraday and inter-day precision were determined and expressed as RSDs: all the values were \leq 2% for both triHer and D1. The method demonstrated also to be accurate and robust and the average recoveries were 98.8 and 97.9% for triHer and D1, respectively. Moreover, the method resulted selective and specific for all of the components present in the degradation pattern of TRX (diHer (3',4'-Di-O-(β -hydroxyethyl)rutin), triHer, tetraHer (3',4',5,7-Tetra-O-(β -

hydroxyethyl)rutin), D3, D1 and D2) and it was successfully applied for the stability studies of both drug substances and drug products.

1. Introduction:

Troxerutin (TRX) is a mixture of semisynthetic O-hydroxyethylrutosides (Hers), arising from hydroxyethylation of rutin¹, a natural occurring flavonoid mainly extracted from *Dimorphandra gardneriana*² and *Sophora japonica*³. As reported in the European Pharmacopoeia⁴, TRX contains minimum 80% of tris(hydroxyethyl)rutin as the principal component, while tetrakis(hydroxyethyl)rutin, bis(hydroxyethyl)rutin and mono(hydroxyethyl)rutin are also described as related components present in minor amount. In therapy, TRX is currently used against sign and symptoms of chronic venous insufficiency and other vascular disorders such as hemorrhoids, microangiopathy and diabetic retinopathy, also displaying effectiveness and safety in elderly patients and pregnant women. TRX acts mainly on the microvascular endothelium by means of its anti-oxidant and anti-inflammatory properties reducing hyperpermeability, edema and improving microvascular perfusion and microcirculation⁵⁻⁸. Furthermore, recent studies proposed TRX as a promising agent with neuroprotective effects on cognitive deficits⁹, in Alzheimer's disease¹⁰ and in Parkinson's disease¹¹. Besides a number of other beneficial effects have been highlighted, such as the chemoprevention in colon carcinogenesis¹², hepato-cellular carcinoma¹³ and as adjuvant with 5-Fluorouracil in gastric cancer¹⁴, a potential role against neuropathic pain¹⁵, cardioprotective and antifibrogenic effects^{16,17}, its use as adjuvant in radiotherapy to protect normal tissues¹⁸ and in the reduction of the severity of myocardial ischemia-reperfusion injury¹⁹. As a matter of fact, despite the lots of recent published *in vitro* and *in vivo* studies establishing new potential biological properties of this drug, TRX is always reported as triHer single isomer (3',4',7-tris(hydroxyethyl)rutin), without considering the presence, in the mixture, of the other Hers²⁰⁻²³. At the best of our

knowledge, the literature reports very few papers dealing with the characterization of TRX related compounds, whose number can theoretically reach fifteen^{24,25}; moreover, none deals with the chemical stability of TRX. This is probably due to the fact that TRX composition depends on the synthetic strategy and on the difficulties in the chromatographic separation of this mixture²⁶. In this complex scenario, the aims of the present study were first to establish the intrinsic chemical stability of a batch of TRX through a forced degradation study in parallel with the characterization both of the principal pure isolable Hers and their degradation products (DPs); secondly to develop and validate a new LC-UV stability indicating method for the simultaneous quantification of TRX as its major component triHer and its stability indicator, D1.

2. Experimental:

2.1. Reagents and chemicals

Acetonitrile (HPLC grade), ammonium bicarbonate, 25% ammonia solution, sodium hydroxide, dimethyl sulfoxide, 30% w/w hydrogen peroxide solution, hydrochloric acid, sodium borohydride, 4,4'-azobis(4-cyanopentanoic acid), methanol, tetrahydrofuran, ethyl acetate, isopropanol, acetic acid, pyridine-d₅, dichloromethane, potassium bromide, ascorbic acid, titanium dioxide, gum arabic, corn starch, talc, polyvinylpyrrolidone (PVP), colloidal silica, magnesium stearate, calcium carbonate, kaolin, orange yellow (E110), indigotine (E132), sucrose, sodium chloride were purchased from Sigma-Aldrich (Milano, Italy); silica gel 60 (0.040-0.063 mm) purchased from Merck (Darmstadt, Germany). Water (HPLC grade) was obtained from Milli-Q RO system. Carbazochrome (lot n° CA-073-03) was obtained as gift sample from Pharmafar S.r.l. (Torino, Italy). Batches of Troxerutin (TRX, batches n°: 335539190, 33553C024, 33553T164), were kindly gifted by Acarpia (Torino, Italy). Venolen[®] capsules (batch n° 120054), Fleboside[®] ampoules (batch n° A107)

and Fleboside[®] coated tablets (batch n^o A0711) were purchased from local pharmacy.

2.2. Purification of Hers from TRX, synthesis of DPs and spectroscopic characterization

2.2.1. Purification of Hers from TRX

TRX was purified by silica gel column chromatography. The mobile phase consisted in a mixture of ethyl acetate-isopropanol-water-acetic acid (7:2:1:0.5, v/v/v/v) up to complete elution of diHer and triHer, then with ethyl acetate-isopropanol-water-acetic acid (5:4:1:0.5, v/v/v/v) to complete elution of tetraHer. The purification of 6 g of TRX gave: diHer (0.117 g, 2% yield, HPLC purity (254 nm): 63%, ESI-MS m/z 699 $[M+H]^+$ calculated for $C_{31}H_{38}O_{18}$), triHer (1.635 g, 28% yield, HPLC purity (254 nm): 94%, ESI-MS m/z 743 $[M+H]^+$ calculated for $C_{33}H_{42}O_{19}$), and tetra-Her (0.555 g, 9% yield, HPLC purity (254 nm): 88%, ESI-MS m/z 787 $[M+H]^+$ calculated for $C_{35}H_{46}O_{20}$).

2.2.2. Synthesis of degradation products

2.2.2.1. 3',4',7-Tri-O-(β -hydroxyethyl)quercetin (D1)

TriHer (3',4',7-Tri-O-(β -hydroxyethyl)rutin, 50 mg) was dissolved in 2 M HCl aqueous solution (2.5 mL). The solution was refluxed at 90°C for 90 min and the formation of a precipitate was observed. At the end of the reaction, (monitored by TLC: ethyl acetate-isopropanol-water-acetic acid 7:2:1:0.5, v/v/v/v), the mixture was filtered under vacuum to collect the precipitate. 25 mg of D1 were obtained (88% yield). HPLC purity (254 nm): 97.5%; ESI-MS m/z 435 $[M+H]^+$ calculated for $C_{21}H_{22}O_{10}$.

2.2.2.2. 3',4',5,7-Tetra-O-(β -hydroxyethyl)quercetin (D2)

TetraHer (3',4',5,7-Tetra-O-(β -hydroxyethyl)rutin, 50 mg) was dissolved in 2 M HCl aqueous solution (2.5 mL). The solution was refluxed at 90°C for 90 min. At the end of the reaction (monitored by TLC: ethyl acetate-isopropanol-water-acetic acid 7:2:1:0.5, v/v/v/v), the solvent was evaporated under reduced pressure. The crude product was purified by silica gel column chromatography using dichloromethane-methanol (98:2, v/v) mixture as eluent to give pure D2 (29.9 mg, 90% yield). HPLC purity (254 nm): 88.7%; ESI-MS m/z 479 [M+H]⁺ calculated for C₂₃H₂₆O₁₁.

2.2.2.3. 3',4'-Di-O-(β -hydroxyethyl)quercetin (D3)

DiHer (3',4'-Di-O-(β -hydroxyethyl)rutin, 75 mg) was dissolved in 2 M HCl aqueous solution (2 mL). The solution was refluxed at 90°C for 90 min. At the end of the reaction (monitored by TLC: ethyl acetate-isopropanol-water-acetic acid 7:2:1:0.5, v/v/v/v), the solvent was evaporated under reduced pressure. The crude product was purified by silica gel column chromatography using dichloromethane-methanol (95:5, v/v) mixture as eluent to give pure D3 (38 mg, MW: 390.3, 90% yield). HPLC purity (254 nm): 95%; ESI-MS m/z 391 [M+H]⁺ calculated for C₁₉H₁₈O₉.

2.2.2.4. ¹H and ¹³C NMR analyses

¹H and ¹³C experiments were performed on a JEOL Eclipse ECP 300 FT MHz spectrometer (Jeol Ltd. Tokyo, Japan) operating at 7.05 T. Chemical shifts are reported in part per million (ppm). The spectra were collected in d₆-DMSO (triHer, diHer and tetraHer) and in d₅-pyridine (D1, D2 and D3).

2.3. Forced degradation study

2.3.1. Stress studies

Stress studies were carried out on TRX solution at a concentration of 1 mg mL^{-1} . For acidic degradation study TRX was dissolved in 1 N HCl and the solution was left in the dark at room temperature and 50°C for 4 h and 24 h. The degradation in alkaline conditions was done in 1 N NaOH and the solution was left in the dark at room temperature and 50°C for 4 h and 24 h. To test the stability in neutral solution, TRX was dissolved in water and left at room temperature or at 50°C for 4 h, 24 h and 48 h. For oxidative conditions, the degradation was performed in a 5% hydrogen peroxide solution and it was left in the dark at room temperature for 4 h, 24 h and 48 h. The degradation with radical initiator was done dissolving TRX in 5 mM 4,4'-azobis(4-cyanopentanoic acid) aqueous solution and it was left in the dark at room temperature for 24 h and 48 h. Photodegradation studies were carried out, at room temperature, by exposing a thin layer (5 mg) of TRX to daylight and UV-light (365 nm) for 14 days and 4 h, respectively. Before LC-MS analyses, acidic and alkaline samples were firstly neutralized by addition of a suitable amount of NaOH and HCl, respectively, and then diluted by adding an appropriate volume of mobile phase. The samples arising from other stress conditions were analysed at 0.25 mg mL^{-1} after dilution with mobile phase. For comparison purposes, a freshly prepared aqueous solution of TRX was diluted at 0.25 mg mL^{-1} and analysed as above. The forced degradation study, restricted to the acidic conditions, was performed also on the purified diHer, triHer and tetraHer derivatives.

2.3.2. MS and LC-MSⁿ analysis

A Thermo Finnigan LCQ Deca XP Plus system equipped with a quaternary pump, a Surveyor AS autosampler, and a vacuum degasser was used for LC-MS analysis (Thermo Electron Corporation, Waltham, MA, USA). The flow injection analysis of the TRX solution ($1 \text{ } \mu\text{g mL}^{-1}$, $\text{CH}_3\text{CN:H}_2\text{O}$ 50:50, v/v) before degradation was done

in positive ionization at a flow rate of 5 $\mu\text{L min}^{-1}$. The LC-MSⁿ analyses were performed on a Phenomenex Gemini NX C18 (100 x 2 mm I.D., 3 $\mu\text{m dp}$) column as a stationary phase maintained at 25°C. The mobile phase (flow rate: 0.2 mL min^{-1}) was composed of eluent A: ammonium bicarbonate buffer (10 mM, pH 9.2) and eluent B: CH₃CN using the following gradient elution: after 10 min of 17% solvent B, it was increased up to 25% in 5 min and then maintained for other 5 min. Then, solvent B was decreased in 0.5 min to 17% and maintained for 7.5 min for the equilibration. The total run time was 28 min. The sample injection volume was 5 μL . The eluate was injected into the electrospray ion source (ESI) and the MS and MSⁿ spectra were acquired and processed using the Xcalibur[®] software (Thermo Electron Corporation). The operating conditions of the ion trap mass spectrometer in positive ion mode were the following: spray voltage, 5.00 kV; source current, 80 μA ; capillary temperature, 350°C; capillary voltage, 30.0 V; tube lens offset, -60 V; multipole 1 offset, -2.00 V; multipole 2 offset, -7.50 V; sheath gas flow (N₂), 60 Auxiliary Units; sweep gas flow (N₂), 6 Auxiliary Units. Data were acquired both in full scan and product ion scan (MS2 and MS3) modes using mass scan range m/z 100-1000. The collision energy was optimized at 32-37%.

2.4 LC-UV stability indicating method

2.4.1. LC-UV analyses

A Shimadzu HPLC system, consisting in two LC-10AD Vp module pumps and a DGU-14-A on-line vacuum degasser, was used. The analyses were carried out on a Phenomenex (Torrance, CA, USA) Kinetex EVO C18 100 Å column (150 x 3 mm, 5 $\mu\text{m dp}$) with a Phenomenex EVO C18 security guard column. The mobile phase (flow rate 0.6 mL min^{-1}) was composed of eluent A, ammonium bicarbonate buffer (10 mM, pH 9.2), and eluent B, acetonitrile, while the initial ratio A:B was set at 84:16 (v/v). The elution was done using the following gradient: from 0 to 8 min, the composition was increased from 16.0 to 22.0% B and then maintained 7 min. From

15 min, the percentage of eluent B was decreased in 1 min to 16.0% and then maintained 6 min for column equilibration. The eluents A and B were filtered through a 0.45 μm PVDF membrane filter prior the use. A SIL-10AD Vp autosampler was used for the injection of samples (5 μL). The SPD-M10A Vp photodiode array detector was used to detect TRX and the degradation products at 254 nm. A LC solution 1.24 software was used to process the chromatograms. All the analyses were carried out at room temperature.

2.4.2. Preparation of standard stock solutions for validation process

The standard stock solution of purified triHer (200 $\mu\text{g mL}^{-1}$) was prepared by dissolving an appropriate amount (about 40 mg) in 200 mL of water, whereas D1 combined stock solution was prepared by dissolving about 7 mg of D1 in 50 mL of DMSO (final concentration 140 $\mu\text{g mL}^{-1}$). To obtain the working solutions used in the validation protocol both triHer and DP stock solutions were properly diluted using water or a mixture of eluent A-eluent B-DMSO (50:10:40, v/v/v) respectively.

2.4.3. Preparation of test solutions

2.4.3.1. Test solution for triHer assay of TRX batches

About 30 mg of TRX were accurately weighed and dissolved with water in a 50 mL volumetric flask. An aliquot of 2 mL of the solution was then diluted to 25 with water. The sample was analysed by LC-UV after filtration over 0.45 μm PVDF membrane filter.

2.4.3.2. Test solution for degradation product assay of TRX batches

About 60 mg of TRX were weighed and dissolved in 10 mL of a mixture of eluent A-eluent B-DMSO (50:10:40, v/v/v). The sample was analysed by LC-UV after filtration through 0.45 μm PVDF membrane filter.

2.4.3.3. Test solutions for triHer assay in TRX formulations

Venolen[®] capsules: the content of 10 capsules was mixed and about 340 mg of the mixture were weighted and transferred into a 200 mL volumetric flask and filled up to volume with water. An aliquot of 3 mL of the resulting solution was then diluted to 100 mL in water. Fleboside[®] coated tablets: 10 coated tablets were finely grounded in a mortar and about 700 mg of the mixture were weighted and transferred into a 500 mL volumetric flask. An aliquot of 50 mL of water were added and the mixture was sonicated for 5 min. Afterwards, the volumetric flask was filled up to volume with water. An aliquot of 3 mL of the solution was then diluted to 50 mL with water. Fleboside[®] ampoules: the content of 5 ampoules was accurately mixed and 3 mL of the resulting mixture were diluted to 100 mL with water. An aliquot of 3 mL of the solution was further diluted to 100 mL with water. Finally, the samples were analysed by LC-UV after filtration over 0.45 µm PVDF membrane filter.

2.4.3.4. Test solutions for degradation product assay in TRX formulations

Venolen[®] capsules: the contents of 10 capsules of the drug product Venolen[®] were mixed and about 340 mg of the mixture were weighted and transferred into a 50 mL volumetric flask. After addition of 20 mL of eluent A-eluent B-DMSO (50:10:40, v/v/v), the solution was stirred for 20 min and then filled up to volume. Fleboside[®] coated tablets: 10 coated tablets were finely grounded in a mortar and about 700 mg of the mixture were weighted and transferred into a 50 mL volumetric flask. The mixture was sonicated for 5 min with 20 mL of eluent A-eluent B-DMSO (50:10:40, v/v/v) and the volumetric flask was filled up to volume with the same solvent. Fleboside[®] ampoules: the contents of 5 ampoules were accurately mixed and 3 mL of the resulting mixture were diluted to 25 mL with an eluent A-eluent B-DMSO (50:10:40, v/v/v) mixture. The samples were analysed by LC-UV after filtration over 0.45 µm PVDF membrane filter.

2.4.3.5. Stability of stock solutions

A 1 mg mL⁻¹ stock solution of TRX, triHer and D1 were prepared in a solvent mixture constituted by eluent A-eluent B-DMSO (50:10:40, v/v/v). The stability of the stock solutions was assessed analysing the solutions immediately after their preparation, at the end of the study (3 weeks) and after two months of storage. The stock solutions were stored at 4°C and remained stable throughout the study.

2.4.4. Validation procedure

2.4.4.1. System suitability

The system suitability parameters, resolution (Rs), area repeatability and asymmetry factor (As) were calculated as previously reported²⁷.

2.4.4.2. Selectivity

To assess the method selectivity, a mixture of purified tetraHer, diHer and triHer was dissolved in 1 N HCl (t = 4 h, T = 50°C) and analysed by LC-UV. The chromatographic separation of tetraHer, diHer, triHer, D1, D2, D3 and other impurities, arising from the degradation in acidic condition, was evaluated after LC-UV analysis by calculation of the resolution factors (Rs). Moreover, the selectivity was evaluated by preparing a combined placebo constituted by the excipients of the drug products: Venolen[®] capsules (ascorbic acid and titanium dioxide); Fleboside[®] coated tablets (titanium dioxide, gum arabic, corn starch, talc, PVP, colloidal silica, magnesium stearate, calcium carbonate, kaolin, orange yellow (E110), indigotine (E132), sucrose and the active ingredient carbazochrome) and Fleboside[®] ampoules (sodiumchloride and carbazochrome). For LC-UV analysis, the solutions were prepared following the same protocol of test solutions.

2.4.4.3. Robustness

The robustness was determined by varying two parameters: the mobile phase pH and the percentage composition of eluents. The influence of the mobile phase pH was determined at three different values of pH: 9.0, 9.2 and 9.4 being 9.2 the reference value by analysing the same mixture of the standards used for the selectivity. The influence of mobile phase composition was assessed by modifying the initial and final percentages of eluent B ($\pm 5\%$ compared to the reference values). In all cases the effects of the changes applied to the method have been evaluated by calculating the resolution factors (R_s).

2.4.4.4. LOD-LOQ

The determination of LOD and LOQ was based on signal-to-noise ratio: this was evaluated by comparing measured signals from samples of triHer and D1 at low concentrations with those of blank samples and by establishing the minimum concentration at which analytes can be reliably detected (LOD; $S/N = 3$) or quantified (LOQ; $S/N = 10$).

2.4.4.5. Linearity

Linearity of the method was evaluated at five equispaced concentration levels by diluting the standard stock solutions to give solutions over the range 50–150% of label claim for triHer and 0.075–0.5% for D1. These were injected in triplicate and the peak areas were inputted into a Microsoft Excel[®] spread-sheet to plot calibration curves. To fulfil basic requirements such as homoscedasticity and linearity, the Bartlett test and the lack-of-fittest were respectively performed at 95% significance level.

2.4.4.6. Precision

Precision was evaluated in terms of repeatability and intermediate precision. The repeatability was investigated using six separate solutions prepared by appropriate dilution of the stock solutions of triHer and D1 at 100% and 0.2% of label claim respectively. Each solution was injected in duplicate and the peak areas obtained were used to calculate means and RSD values. The intermediate precision was checked on three different days, by preparing and analysing in triplicate three solutions prepared as reported for the repeatability; the means and RSD values were calculated from peak areas.

2.4.4.7. Accuracy

To assess accuracy, freshly prepared placebo of the drug products was spiked with various amounts of triHer at 50 - 150% concentration levels and D1 at 0.075 - 0.5% concentration levels. Each solution was injected in triplicate and the peak areas were used to calculate means and RSD values and compared with those obtained with standard solutions.

3. Results and discussion:

3.1. MS and LC-MSⁿ studies on TRX

Mass spectrometry source conditions were optimized by flow injection analysis on TRX. Analyses were performed in positive ionization mode showing the presence of at least three principal ions at m/z 787, 743, 699 corresponding to the $[M+H]^+$ of triHer (four isomers possible), diHer (six isomers possible) and tetraHer (one only isomer), respectively. No ions corresponding to the monoHer (four isomers possible) were detected. The MS2 experiments on each parent ion gave a fragment ion corresponding to the loss of the sugar moiety (308 u), while MS3 experiments gave the sub-subsequent loss of the hydroxyethyl group (44 u) (Table 1).

Compound	MW	MS (<i>m/z</i>)	MS2 (<i>m/z</i>)	MS3 (<i>m/z</i>)
diHer	698	699 [M+H] ⁺	391 [M+H-308] ⁺	347 [M+H-308-44] ⁺
triHer	742	743 [M+H] ⁺	435 [M+H-308] ⁺	391 [M+H-308-44] ⁺
tetraHer	786	787 [M+H] ⁺	479 [M+H-308] ⁺	435 [M+H-308-44] ⁺
D1	434	435 [M+H] ⁺	391 [M+H-44] ⁺	347 [M+H-88] ⁺
			373 [M+H-62] ⁺	
D2	478	479 [M+H] ⁺	435 [M+H-44] ⁺	391 [M+H-88] ⁺
			391 [M+H-88] ⁺	373 [M+H-62] ⁺
D3	390	391 [M+H] ⁺	347 [M+H-44] ⁺	303 [M+H-88] ⁺

Table 1. Mass data of principal Hers in TRX and DPs (D1, D2 and D3)

This first result confirmed that TRX is a mixture of different compounds. Chromatographic conditions for LC-MSⁿ analyses were setup to obtain the best separation of the Hers and, after degradation, the potential, more lipophilic, DPs. The presence of a polar sugar moiety in Hers but not in the corresponding DPs, combined with the variable number of hydroxyethyl groups, made the chromatographic separation of the analytes a challenging task. In first instance we investigated the role of the aqueous mobile phase pH, by testing various acidic and alkaline buffers on different stationary phases featured by lipophilic (Phenomenex Luna C18(2)) or aromatic/polar (Phenomenex Sinergy Polar) interactions respectively. In all cases when the mobile phase was acidified, the elution order of Hers was tetraHer, triHer and diHer, even if the peaks of triHer and diHer co-eluted (data not shown); conversely, the use of an alkaline mobile phase gave good results in terms of separation of Hers. Accordingly, the stationary phase which gave the best results was the Phenomenex Gemini NX C18, stable in a wide pH range (from 2 to 13), maintained at 25°C. The mobile phase (flow rate 0.2 mL min⁻¹) was composed of eluent A: ammonium bicarbonate buffer (10 mM, pH 9.2) and eluent B: CH₃CN

using a gradient elution. In the chromatogram depicted in Figure 1, the peaks at retention time of 3.03, 4.76 and 5.74 min correspond to tetraHer, diHer and triHer, respectively. The different elution order in acidic conditions respect to alkaline conditions could be attributed to the presence of different steric interactions of the three Hers with the stationary phase used due to the ionization grade at different pH, the number of free hydroxyl groups of the single Hers and the presence of the sugar moiety. The LC-MS analysis confirmed the molecular weight of the three principal Hers: indeed the ions at m/z 787, 699 and 743 correspond to the protonated molecules $[M+H]^+$ of tetraHer, diHer and triHer, respectively. With the mentioned chromatographic separation, the analysis in mass range of the three ions gave rise only to one predominant peak, stating that only one principal isomer could be considered for each one.

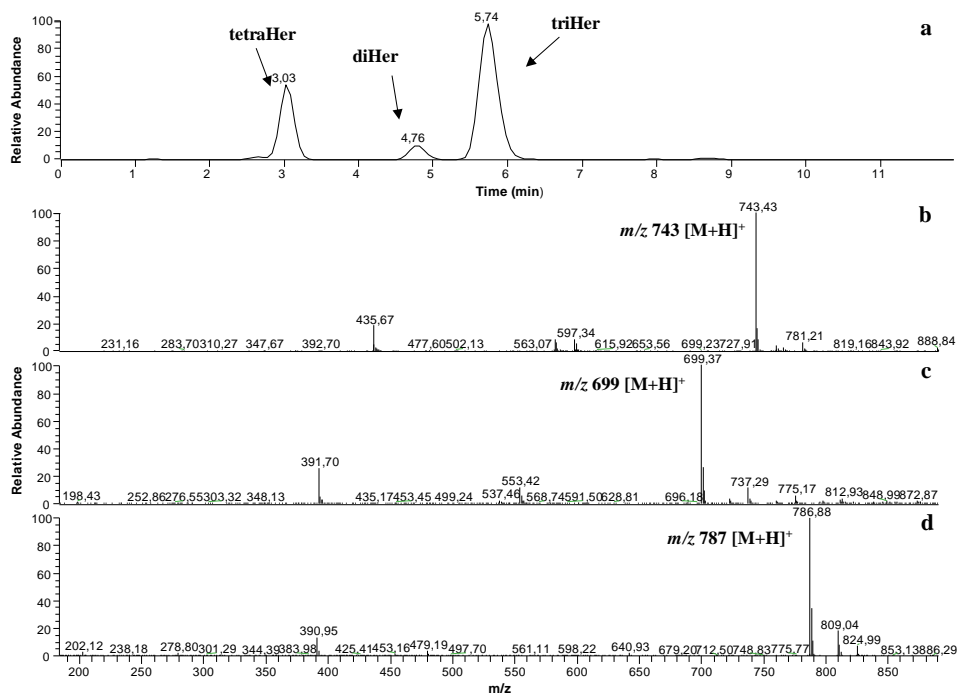


Figure 1. a) LC-MS chromatogram of TRX; b) ESI+ full MS of triHer; c) ESI+ full MS of diHer; d) ESI+ full MS of tetraHer

3.2. LC–MS data on TRX forced degradation

In order to characterize the intrinsic chemical stability of TRX, a forced degradation study was performed following the requirements of ICH guidelines [28]. Furthermore, to avoid unrealistic degradation pathways, the stress conditions were optimized to obtain a 10 - 15% degradation of the parent compound. In acidic conditions (1 N HCl, 50°C), the formation of three peaks eluting at 11.71, 16.13 and 17.86 min respectively was evident after 4 h (Figure 2). Their positive ESI-MS spectra gave rise to the base peaks at m/z 479, 435 and 391, corresponding to the loss of rutinose moiety (308 u with respect to tetraHer, triHer and diHer, respectively), attributable to the Hers aglycones (D2, D1 and D3, respectively). The structure was confirmed also from the MS2 and MS3 analyses (Supplemental 1). As expected, for prolonged exposure to the acidic conditions, the intensity of D2, D1 and D3 increased while the intensity of triHer, diHer, tetraHer decreased (data not shown). Moreover, the exposure of TRX to 1 N HCl at room temperature did not cause the cleavage of the O- β -glycosidic bond of Hers, implying that the temperature is a key parameter for its stability. In alkaline, oxidative conditions and in the presence of both UV light and sunlight TRX did not undergo degradation (Table 2). The degradation in acidic conditions was also repeated on the pure Hers obtained by column chromatography and not commercially available as standard. As a result, it was demonstrated that D1 is the direct degradation product of triHer, D2 of tetraHer and D3 of diHer. Overall, these data allowed to propose the degradation scheme of TRX reported in Figure 3, in which D1 can be also defined the stability indicator of the mixture.

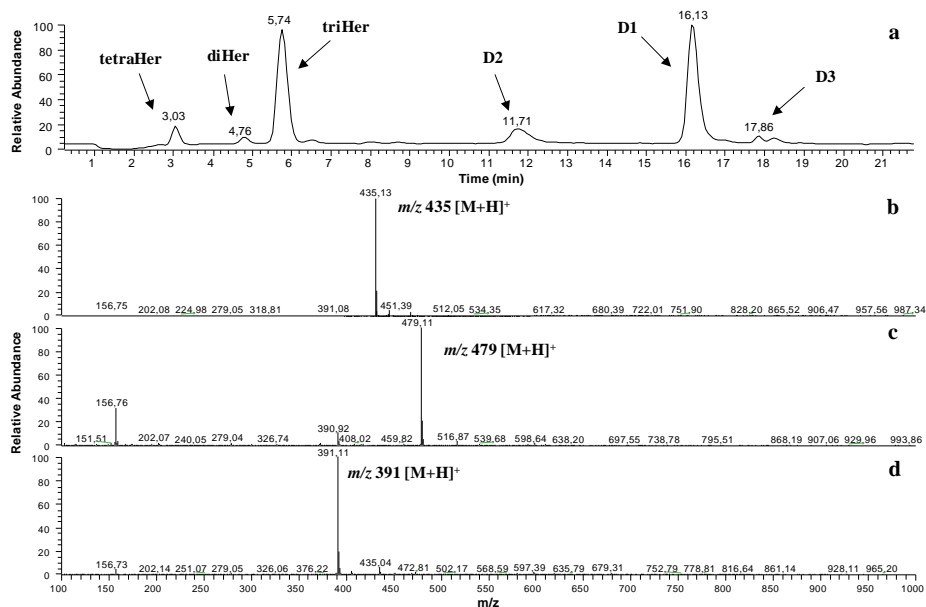


Figure 2. a) LC-MS chromatogram of TRX degradation in 1 N HCl, 50°C and 4 h; b) ESI+ full MS of D1; c) ESI+ full MS of D2; d) ESI+ full MS of D3

Analyte	Stressor	Temperature (°C)	Time	Degradation Products
TRX	1N HCl	RT	24h	-
	1N HCl	50	4h	D1, D2 and D3
	1N NaOH Neutral	50	24h	-
	5% H ₂ O ₂	RT	48h	-
	4 4'-azobis(4-cyanopentanoic acid)			
	UV light (λ=365 nm)			
Sunlight	RT	14 days	-	
diHer triHer tetraHer	1N HCl	50	4h	D3 D1 D2

Table 2. Results of the forced degradation studies of TRX and purified Hers

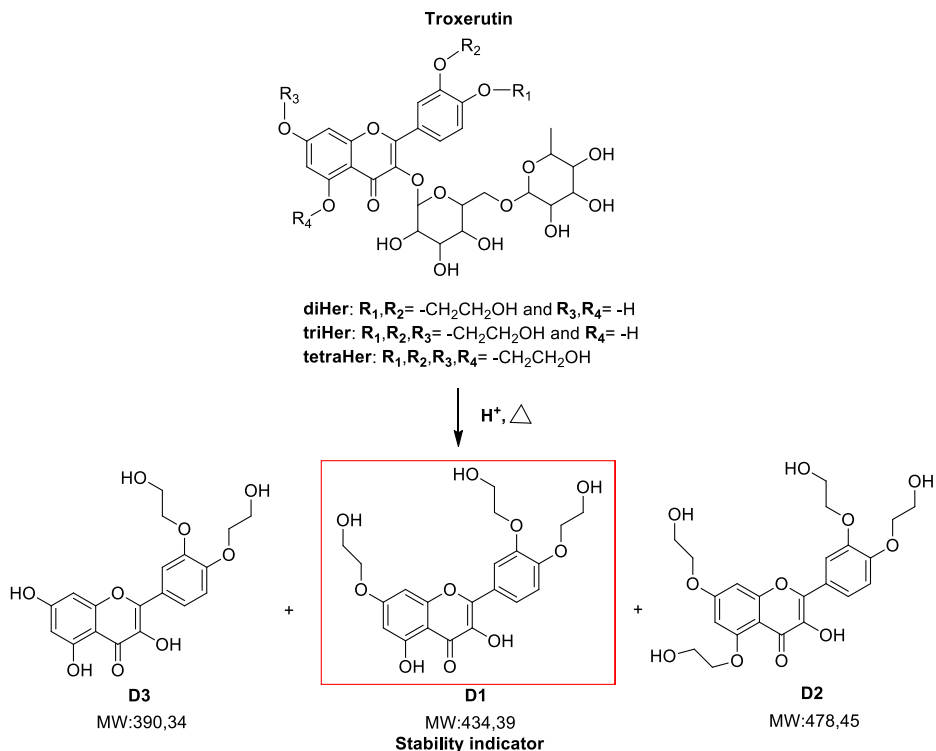


Figure 3. Degradation pathway of TRX

3.3. Purification of Hers, synthesis of DPs and their structural characterization

Since pure Hers are not commercially available, the only possibility was to obtain them from TRX chromatographic separation. Even though this is a challenging task, the availability of pure Hers may lead to significant novelty, improving both the analytical characterization of TRX and the pharmacological knowledge of its components. The purification of TRX resulted very complex and time-consuming but the use of flash silica gel and a gradient elution with a mixture of ethyl acetate-isopropanol-water-acetic acid gave rise to obtain the three products present in the mixture at a good purity. The NMR spectra of triHer were in perfect agreement with the previous reported in literature²⁵ and the ¹³C NMR chemical shift of tetraHer were all consistent with that of triHer except for the C5 upfield from 156.64 to 153.40 ppm, caused by the presence of the hydroxyethyl group in this position. The low concentration and the coelution with triHer (as predictable in acid elution) were the

major problems encountered in the separation of diHer from the mixture. As a consequence, HPLC-UV purity of diHer resulted, for these reasons, of 63% but the only impurity present was triHer, confirmed also from the NMR spectra. The analysis of diHer ^{13}C NMR spectrum evidenced C4' and C3' chemical shifts of 150.53 and 147.69 ppm respectively (consistent with the presence of the hydroxyethyl substitution) and the downfield of the C7 (165.19 ppm) attributable to the free phenolic group. All these data prompted to confirm the isolation and the characterization of three single isomers: diHer (3',4',-Di-O-(β -hydroxyethyl)rutin), triHer (3',4',7-Tri-O-(β -hydroxyethyl)rutin) and tetraHer (3',4',5,7-Tetra-O-(β -hydroxyethyl)rutin) (Supplemental 2 and 3). The synthesis of DPs was performed both to confirm their structures and to allow the development and validation of the stability indicating LC-UV method. The preparation of D1, D2 and D3, starting from purified Hers, was performed based on the forced degradation data; indeed, the synthetic protocol was optimized by adjusting the hydrochloric acid concentration and the time of reaction to obtain the desired products in good yield and high purity. For D2 and D3 the purification through a silica column chromatography was also required. Furthermore, the poor solubility of DPs in the common solvents was overcome solubilizing them in basic medium (*e.g.* ammonium bicarbonate buffer) with an aliquot of DMSO. Similarly, DPs were dissolved in pyridine- d_5 to carry out ^1H NMR and ^{13}C NMR analyses. The NMR analyses of the DPs confirmed the position of hydroxyethyl substituents. The upfield of the C5 of D2 (160.43 ppm) in respect to the same position of D1 and D3 (161.74 and 162.01 ppm respectively) and the downfield of the C7 of D3 (165.73 ppm) in respect to the same position of D1 and D2 (165.18 and 163.81 ppm respectively), prompted to confirm the synthesis and the characterization of three single isomers: D3 (3',4'-Di-O-(β -hydroxyethyl)quercetin), D1 (3',4',7-Tri-O-(β -hydroxyethyl)quercetin) and D2 (3',4',5,7-Tetra-O-(β -hydroxyethyl)quercetin) as reported in Figure 4,5 and 6.

	<table border="1"> <thead> <tr> <th></th> <th>R¹</th> <th>R²</th> <th>R³</th> <th>R⁴</th> </tr> </thead> <tbody> <tr> <td>diHer</td> <td>^A-CH₂^BCH₂OH</td> <td>^A-CH₂^BCH₂OH</td> <td>-H</td> <td>-H</td> </tr> <tr> <td>triHer</td> <td>^A-CH₂^BCH₂OH</td> <td>^A-CH₂^BCH₂OH</td> <td>^A-CH₂^BCH₂OH</td> <td>-H</td> </tr> <tr> <td>tetraHer</td> <td>^A-CH₂^BCH₂OH</td> <td>^A-CH₂^BCH₂OH</td> <td>^A-CH₂^BCH₂OH</td> <td>^A-CH₂^BCH₂OH</td> </tr> </tbody> </table>		R ¹	R ²	R ³	R ⁴	diHer	^A -CH ₂ ^B CH ₂ OH	^A -CH ₂ ^B CH ₂ OH	-H	-H	triHer	^A -CH ₂ ^B CH ₂ OH	^A -CH ₂ ^B CH ₂ OH	^A -CH ₂ ^B CH ₂ OH	-H	tetraHer	^A -CH ₂ ^B CH ₂ OH	^A -CH ₂ ^B CH ₂ OH	^A -CH ₂ ^B CH ₂ OH	^A -CH ₂ ^B CH ₂ OH	<table border="1"> <thead> <tr> <th></th> <th>R¹</th> <th>R²</th> <th>R³</th> <th>R⁴</th> </tr> </thead> <tbody> <tr> <td>D3</td> <td>^A-CH₂^BCH₂OH</td> <td>^A-CH₂^BCH₂OH</td> <td>-H</td> <td>-H</td> </tr> <tr> <td>D1</td> <td>^A-CH₂^BCH₂OH</td> <td>^A-CH₂^BCH₂OH</td> <td>^A-CH₂^BCH₂OH</td> <td>-H</td> </tr> <tr> <td>D2</td> <td>^A-CH₂^BCH₂OH</td> <td>^A-CH₂^BCH₂OH</td> <td>^A-CH₂^BCH₂OH</td> <td>^A-CH₂^BCH₂OH</td> </tr> </tbody> </table>		R ¹	R ²	R ³	R ⁴	D3	^A -CH ₂ ^B CH ₂ OH	^A -CH ₂ ^B CH ₂ OH	-H	-H	D1	^A -CH ₂ ^B CH ₂ OH	^A -CH ₂ ^B CH ₂ OH	^A -CH ₂ ^B CH ₂ OH	-H	D2	^A -CH ₂ ^B CH ₂ OH	^A -CH ₂ ^B CH ₂ OH	^A -CH ₂ ^B CH ₂ OH	^A -CH ₂ ^B CH ₂ OH
	R ¹	R ²	R ³	R ⁴																																						
diHer	^A -CH ₂ ^B CH ₂ OH	^A -CH ₂ ^B CH ₂ OH	-H	-H																																						
triHer	^A -CH ₂ ^B CH ₂ OH	^A -CH ₂ ^B CH ₂ OH	^A -CH ₂ ^B CH ₂ OH	-H																																						
tetraHer	^A -CH ₂ ^B CH ₂ OH	^A -CH ₂ ^B CH ₂ OH	^A -CH ₂ ^B CH ₂ OH	^A -CH ₂ ^B CH ₂ OH																																						
	R ¹	R ²	R ³	R ⁴																																						
D3	^A -CH ₂ ^B CH ₂ OH	^A -CH ₂ ^B CH ₂ OH	-H	-H																																						
D1	^A -CH ₂ ^B CH ₂ OH	^A -CH ₂ ^B CH ₂ OH	^A -CH ₂ ^B CH ₂ OH	-H																																						
D2	^A -CH ₂ ^B CH ₂ OH	^A -CH ₂ ^B CH ₂ OH	^A -CH ₂ ^B CH ₂ OH	^A -CH ₂ ^B CH ₂ OH																																						
H	diHer	triHer	tetraHer	D3	D1	D2																																				
6	6.36 (s; 1H)	6.36 (s; 1H)	6.54 (s; 1H)	6.62 (s; 1H)	6.63 (s; 1H)	6.67 (s; 1H)																																				
8	6.71 (s; 1H)	6.72 (s; 1H)	6.80 (s; 1H)	6.70 (s; 1H)	6.78 (s; 1H)	6.90 (s; 1H)																																				
2*	7.84 (s; 1H)	7.84 (s; 1H)	7.83 (s; 1H)	8.41 (s; 1H)	8.40 (s; 1H)	8.37 (s; 1H)																																				
5'	7.10 (d; 1H; J=8.7Hz)	7.13 (d; 1H; J=7.05Hz)	7.10 (d; 1H; J=8.58Hz)	7.31(d;J=9Hz)	7.29 (d; 1H; J=8.55Hz)	7.28 (d; 1H; J=8.88Hz)																																				
6'	7.70 (d; 1H; J=8.1Hz)	7.70 (d; 1H; J=8.50Hz)	7.71(d; 1H; J=8.58Hz)	8.12 (d; 1H; J=8.25Hz)	8.22 (d; 1H; J=8.58Hz)	8.17 (d; 1H; J=8.25Hz)																																				
1''	5.39 (d; 1H; J=5.7Hz)	5.42 (d; 1H; J=5.82Hz)	5.26 (d; 1H; J=7.05Hz)	-	-	-																																				
6''	1.02 (d; 3H; J=3.3Hz)	0.96 (d; 3H; J=4.59Hz)	0.98 (d; 3H; J=6.12Hz)	-	-	-																																				
H sugar	3.05-3.75 (m; 10H)	3.06-3.75 (m; 10H)	3.05-3.76 (m; 10H)	-	-	-																																				
H-A	3.95-4.1 (m; 4H)	4.06-4.11 (m; 6H)	4.06-4.14 (m; 8H)	4.33-4.41 (m; 4H)	4.01-4.08 (m; 6H)	4.18-4.36 (m; 8H)																																				
H-B	3.17-3.37 (m; 4H)	3.23-3.75 (m; 6H)	3.22-3.78 (m; 8H)	4.13-4.19 (m; 4H)	3.76-4.01 (m; 6H)	4.44-4.60 (m; 8H)																																				
	(300MHz, d ₆ -DMSO) δ (ppm)			(300MHz, d ₆ -Py) δ (ppm)																																						

Figure 4. ¹HNMR of purified Hers and synthesized DPs (D1, D2 and D3)

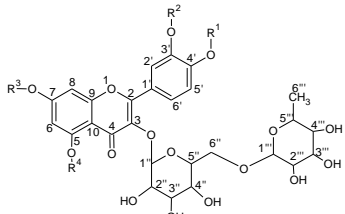
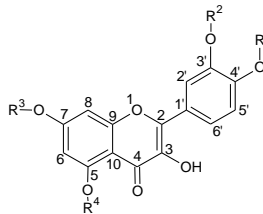
																																										
	<table border="1"> <thead> <tr> <th></th> <th>R¹</th> <th>R²</th> <th>R³</th> <th>R⁴</th> </tr> </thead> <tbody> <tr> <td>diHer</td> <td>A⁻ B⁻ -CH₂CH₂OH</td> <td>A⁻ B⁻ -CH₂CH₂OH</td> <td>-H</td> <td>-H</td> </tr> <tr> <td>triHer</td> <td>A⁻ B⁻ -CH₂CH₂OH</td> <td>A⁻ B⁻ -CH₂CH₂OH</td> <td>A⁻ B⁻ -CH₂CH₂OH</td> <td>-H</td> </tr> <tr> <td>tetraHer</td> <td>A⁻ B⁻ -CH₂CH₂OH</td> <td>A⁻ B⁻ -CH₂CH₂OH</td> <td>A⁻ B⁻ -CH₂CH₂OH</td> <td>A⁻ B⁻ -CH₂CH₂OH</td> </tr> </tbody> </table>		R ¹	R ²	R ³	R ⁴	diHer	A ⁻ B ⁻ -CH ₂ CH ₂ OH	A ⁻ B ⁻ -CH ₂ CH ₂ OH	-H	-H	triHer	A ⁻ B ⁻ -CH ₂ CH ₂ OH	A ⁻ B ⁻ -CH ₂ CH ₂ OH	A ⁻ B ⁻ -CH ₂ CH ₂ OH	-H	tetraHer	A ⁻ B ⁻ -CH ₂ CH ₂ OH	A ⁻ B ⁻ -CH ₂ CH ₂ OH	A ⁻ B ⁻ -CH ₂ CH ₂ OH	A ⁻ B ⁻ -CH ₂ CH ₂ OH	<table border="1"> <thead> <tr> <th></th> <th>R¹</th> <th>R²</th> <th>R³</th> <th>R⁴</th> </tr> </thead> <tbody> <tr> <td>D3</td> <td>A⁻ B⁻ -CH₂CH₂OH</td> <td>A⁻ B⁻ -CH₂CH₂OH</td> <td>-H</td> <td>-H</td> </tr> <tr> <td>D1</td> <td>A⁻ B⁻ -CH₂CH₂OH</td> <td>A⁻ B⁻ -CH₂CH₂OH</td> <td>A⁻ B⁻ -CH₂CH₂OH</td> <td>-H</td> </tr> <tr> <td>D2</td> <td>A⁻ B⁻ -CH₂CH₂OH</td> <td>A⁻ B⁻ -CH₂CH₂OH</td> <td>A⁻ B⁻ -CH₂CH₂OH</td> <td>A⁻ B⁻ -CH₂CH₂OH</td> </tr> </tbody> </table>		R ¹	R ²	R ³	R ⁴	D3	A ⁻ B ⁻ -CH ₂ CH ₂ OH	A ⁻ B ⁻ -CH ₂ CH ₂ OH	-H	-H	D1	A ⁻ B ⁻ -CH ₂ CH ₂ OH	A ⁻ B ⁻ -CH ₂ CH ₂ OH	A ⁻ B ⁻ -CH ₂ CH ₂ OH	-H	D2	A ⁻ B ⁻ -CH ₂ CH ₂ OH	A ⁻ B ⁻ -CH ₂ CH ₂ OH	A ⁻ B ⁻ -CH ₂ CH ₂ OH	A ⁻ B ⁻ -CH ₂ CH ₂ OH
	R ¹	R ²	R ³	R ⁴																																						
diHer	A ⁻ B ⁻ -CH ₂ CH ₂ OH	A ⁻ B ⁻ -CH ₂ CH ₂ OH	-H	-H																																						
triHer	A ⁻ B ⁻ -CH ₂ CH ₂ OH	A ⁻ B ⁻ -CH ₂ CH ₂ OH	A ⁻ B ⁻ -CH ₂ CH ₂ OH	-H																																						
tetraHer	A ⁻ B ⁻ -CH ₂ CH ₂ OH	A ⁻ B ⁻ -CH ₂ CH ₂ OH	A ⁻ B ⁻ -CH ₂ CH ₂ OH	A ⁻ B ⁻ -CH ₂ CH ₂ OH																																						
	R ¹	R ²	R ³	R ⁴																																						
D3	A ⁻ B ⁻ -CH ₂ CH ₂ OH	A ⁻ B ⁻ -CH ₂ CH ₂ OH	-H	-H																																						
D1	A ⁻ B ⁻ -CH ₂ CH ₂ OH	A ⁻ B ⁻ -CH ₂ CH ₂ OH	A ⁻ B ⁻ -CH ₂ CH ₂ OH	-H																																						
D2	A ⁻ B ⁻ -CH ₂ CH ₂ OH	A ⁻ B ⁻ -CH ₂ CH ₂ OH	A ⁻ B ⁻ -CH ₂ CH ₂ OH	A ⁻ B ⁻ -CH ₂ CH ₂ OH																																						
Carbon	DiHer	TriHER	TetraHER	D3	D1	D2																																				
2	157.23 ^{b1}	156.56 ^{a1}	158.23	148.0	151.3	150.83																																				
3	133.71	133.73	135.97	136.5	138.55	136.75																																				
4	173.43	173.07	172.50	176.1	177.32	171.1																																				
5	157.03 ^{b1}	156.64 ^{a1}	153.40	162.01	161.74	160.43																																				
6	99.02	98.48	98.06	98.1	98.43	98.88																																				
7	165.19	164.72	163.27	165.73	165.18	163.81																																				
8	93.01	92.91	93.92	92.90	92.60	94.15																																				
9	160.69	160.94	159.78	158.50	156.93	158.73																																				
10	106.0	105.16	108.47	106.50	105.22	108.09																																				
1 [*]	123.18	122.42	122.61	122.14	124.96	124.15																																				
2 [*]	112.90	112.73	112.72	112.86	113.67	113.79																																				
3 [*]	147.69	147.53	147.49	143.25	143.59	143.16																																				
4 [*]	150.53	150.87	150.46	146.90	147.1	146.73																																				
5 [*]	114.87	114.28	114.29	114.60	114.54	114.13																																				
6 [*]	123.23	122.57	122.16	120.8	123.09	121.75																																				
A	70.89	70.57	70.57	70.8	71.34	71.26																																				
A [*]	71.17	71.80 ^{b2}	71.89 ^{b4}	70.9	71.64	71.62																																				
A ^{**}	-	71.80 ^{b2}	71.89 ^{b4}	-	72.15	69.13																																				
A ^{***}	-	-	71.89 ^{b4}	-	-	63.14																																				
B	59.86 ^{a2}	59.36	59.34	60.98	60.66	62.91																																				
B [*]	60.06 ^{a2}	59.54 ^{b3}	59.52 ^{b5}	60.78	60.77	60.75																																				
B ^{**}	-	59.54 ^{b3}	59.52 ^{b5}	-	60.78	60.65																																				
B ^{***}	-	-	59.52 ^{b5}	-	-	60.54																																				
1 ^{**}	101.75	101.34	101.78	-	-	-																																				
2 ^{**}	74.71	74.21	74.65	-	-	-																																				
3 ^{**}	76.97	76.43	76.62	-	-	-																																				
4 ^{**}	70.24	70.23	70.21	-	-	-																																				
5 ^{**}	76.34	76.06	75.90	-	-	-																																				
6 ^{**}	67.71	67.22	67.00	-	-	-																																				
1 ^{***}	102.03	101.03	100.93	-	-	-																																				
2 ^{***}	70.44	70.66	70.44	-	-	-																																				
3 ^{***}	68.84	68.36	68.31	-	-	-																																				
4 ^{***}	72.39	70.56	70.57	-	-	-																																				
5 ^{***}	71.88	70.34	70.32	-	-	-																																				
6 ^{***}	18.28	17.80	17.81	-	-	-																																				
	(300MHz, d ₆ -DMSO) δ (ppm)			(300MHz, d ₆ -Py) δ (ppm)																																						
	^{a1-2} : interchangeable signals																																									
	^{b1-5} : overlapped signals																																									

Figure 5. ¹³CNMR of purified Hers and synthesized DPs (D1, D2 and D3)

4.3.4. LC-UV method development

In the relevant literature a stability indicating HPLC method for TRX analysis is not reported. In fact, all the methods previously mentioned^{20-23,26} were used for the determination of TRX as triHer. Based on the LC-MS method conditions used in the investigation of the chemical stability of TRX, a LC-UV method was developed and validated. In order to achieve the separation of all the degradation products, a Kinetex EVO C18 stationary phase was used enhancing the peak shape of Hers and DPs (Figure 6a). Finally, the mobile phase composition was fine-tuned in order to obtain the required separation of all the analytes. Moreover, the analysis of a sample of TRX degraded in acidic conditions revealed the presence of D1 as the only DP. This confirmed that D1 can be considered the indicator of stability of TRX in stability studies (Figure 6b). The results obtained and the availability of the purified standards of triHer and D1 (Figure 7) suggested that the present LC-UV method can be used for the quantification of triHer and D1 in TRX drug substance and drug products.

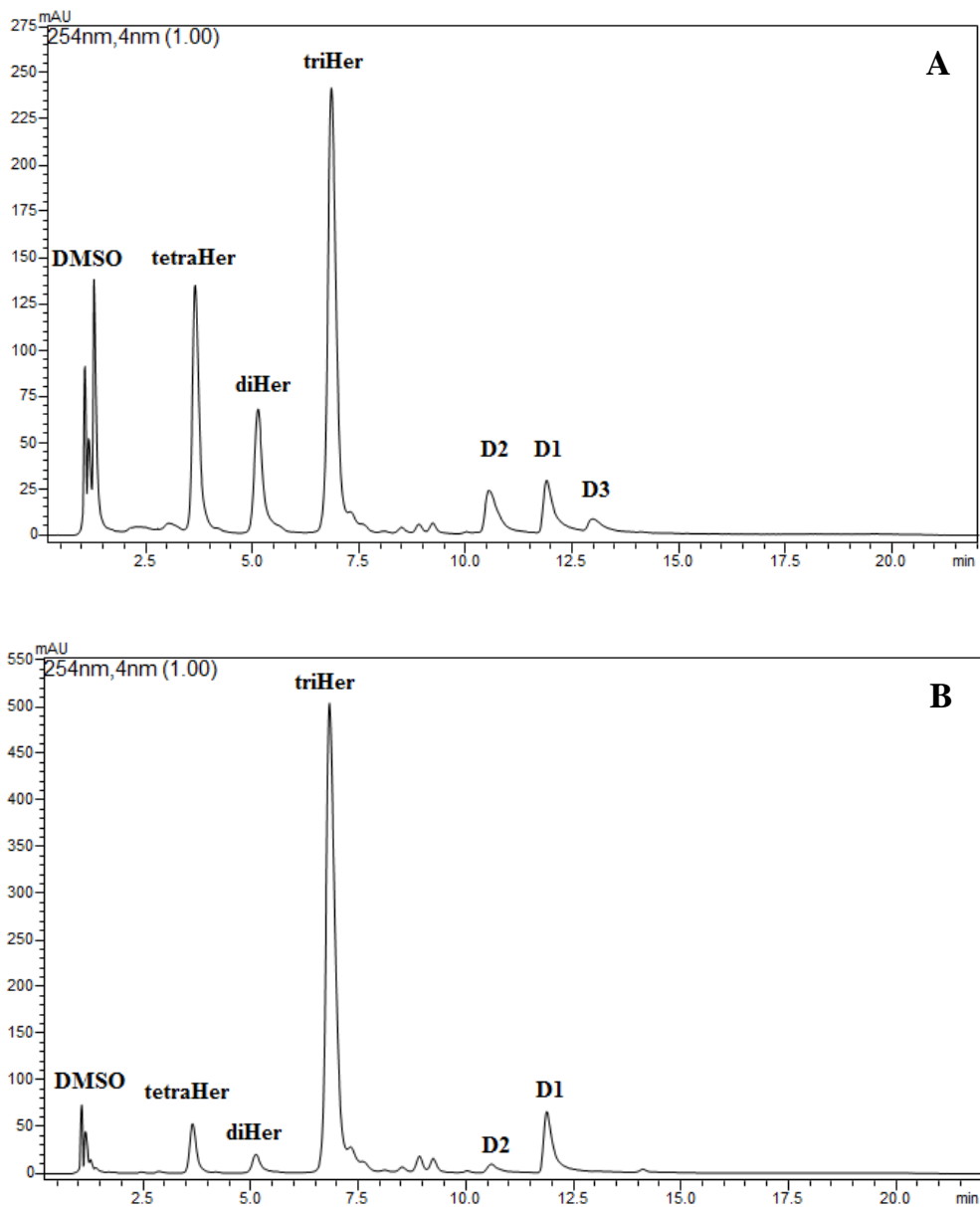


Figure 6. a) LC-UV chromatogram of tetraHer, diHer and triHer standards in acidic solution (1 N HCl, $t = 4$ h, 50°C). b) LC-UV chromatogram of TRX in the presence of 1 N HCl (4 h, 50°C)

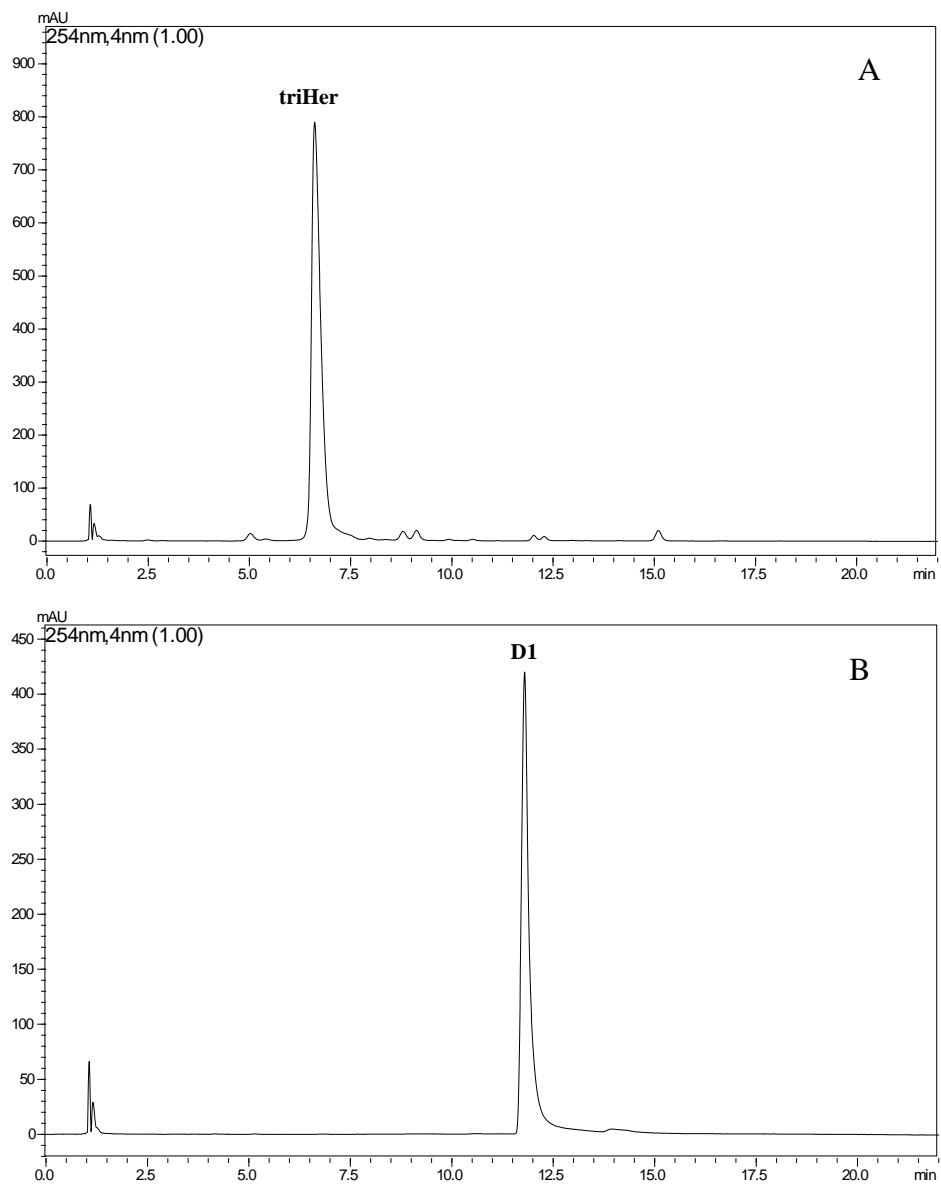


Figure 7. a) LC-UV chromatogram of purified standard triHer (conc. 0.25 mg/mL). b) LC-UV chromatogram of synthetic standard D1 (conc. 0.25 mg/mL)

3.5. Method validation

The method was validated following the ICH guidelines²⁹.

3.5.1. Selectivity

The chromatogram reported in Fig. 4.a showed no peak interfering with analytes; the adjacent chromatographic peaks tetraHer/diHer, diHer/triHer, triHer/D2, D2/D1 and D1/D3 were separated with resolution factors greater than 2 suggesting that the impurities arising from degradation did not affect the selectivity of the method. For the whole validation procedure, triHer and D1 were considered; however, the selectivity of the method was evaluated by using all the analytes. To overcome the limited availability of D2 and D3 synthetic standards, the formation of DPs was obtained in situ from purified Hers at equal concentration, in the presence of HCl. Nevertheless, the attribution of the chromatographic peaks was confirmed by the injection of the corresponding synthetic standard. The chromatograms of the placebo solutions obtained by using the mixture of excipient used for Venolen[®] capsule, Fleboside[®] tablets and Fleboside[®] ampoules are reported in Figure 8. In the case of Fleboside[®] medicinal product the API carbazochrome, present in combination with TRX, was included in the excipient blend excluding its interference with analytes. Overall, these data highlighted the selectivity of the method.

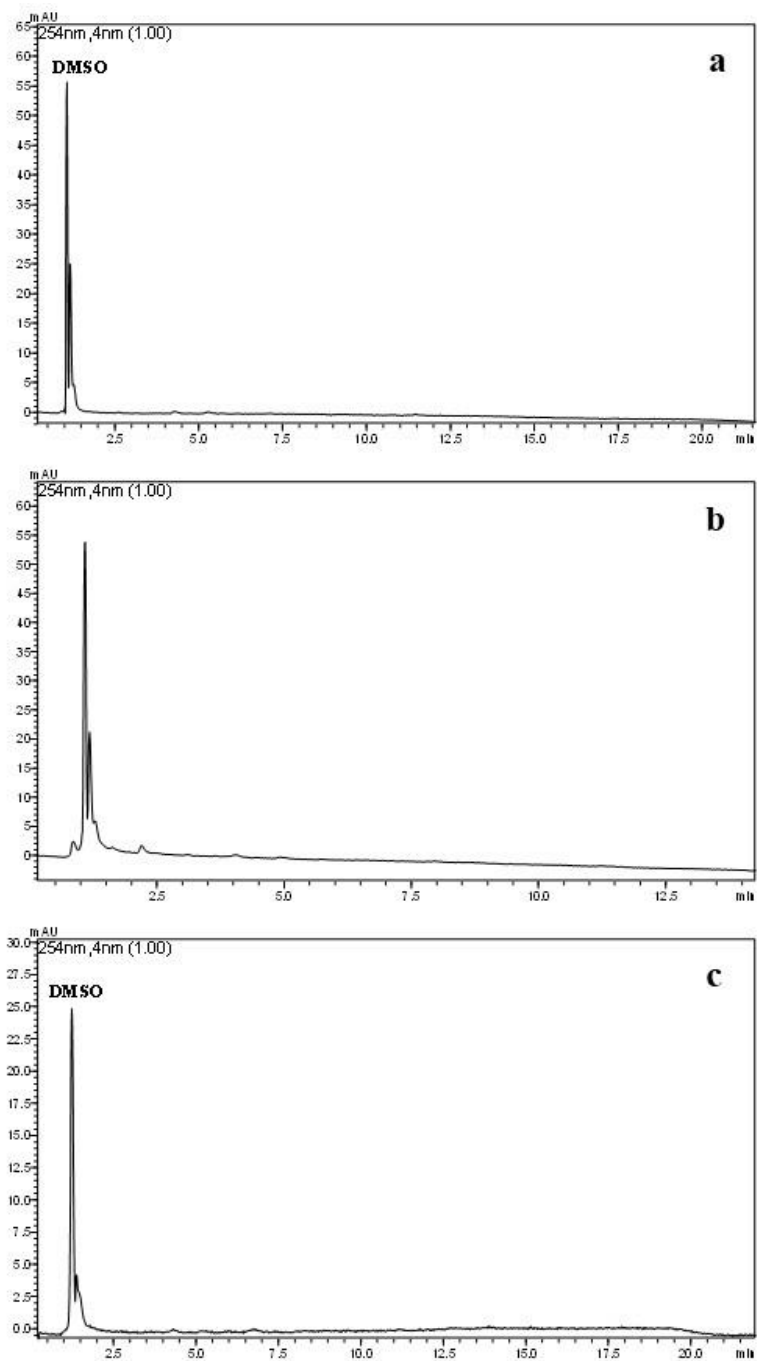


Figure 8. LC-UV chromatograms of the placebo solutions obtained by using the mixture of excipient used for a) Venolen[®] capsule, b) Fleboside[®] tablets and c) Fleboside[®] ampoules

3.5.2. System suitability

The suitability of the chromatographic system was demonstrated by comparing the obtained values, reported in Table 3, with the acceptance criteria of the CDER guidance document³⁰.

Analyte	Retention time (Rt, min)	Relative Retention time (RRt, min)	Repeatability of peak area ^a	Asymmetry factor	Resolution factors
tetraHer	3.652	0.53	0.87	1	4.4 (tetraHer/diHer)
diHer	5.123	0.75	0.72	1.2	3.7 (diHer/triHer)
triHer	6.845	1	0.76	1.5	8.2 (triHer/D2)
D2	10.542	1.54	1.84	2	3.7 (D2/D1)
D1	11.891	1.74	1.24	2	2.2 (D1/D3)
D3	12.975	1.90	2.02	1.7	
^a RSD values for six replicates					

Table 3. System Suitability parameters

3.5.3. Robustness

As for selectivity, the robustness of the method was evaluated by using all the analytes. The role of the most critical parameters (pH and mobile phase composition) has been studied by introducing small but deliberate variations. As reported (Table 4), the resolution values were always greater than 2.0 also in the case of some potential critical pair of adjacent peaks (*e.g.* D1/D3).

Factor	Δ	$Rs_{\text{tetraHer/diHer}}$	$Rs_{\text{diHer/triHer}}$	$Rs_{\text{triHer/D2}}$	$Rs_{\text{D2/D1}}$	$Rs_{\text{D1/D3}}$
Method ^a		4.38	3.74	8.16	3.68	2.16
pH	9.0	3.49	2.76	8.73	4.15	2.02
	9.4	6.42	4.22	2.47	2.00	2.00
% eluant B	-5%	4.20	6.90	7.49	2.00	2.20
	+5%	4.22	3.13	7.96	2.91	2.22

^a the nominal values of the method were reported in the experimental part

Table 4. Resolution values

3.5.4. LOD-LOQ

LOD and LOQ were determined at 254 nm, by analysing progressively low concentration solution of triHer and D1. LOD values for triHer and D1 were 0.4 $\mu\text{g mL}^{-1}$ and 2.5 $\mu\text{g mL}^{-1}$ respectively while LOQ values for triHer and D1 were 2.5 $\mu\text{g mL}^{-1}$ and 4.0 $\mu\text{g mL}^{-1}$ respectively.

3.5.5. Linearity

Five concentration levels within the range 50 - 150% of label claim of triHer were considered to study the linearity. For D1 at 0.2% level of concentration, a range value of 0.075-0.5% was used. Since the Bartlett test evidenced no significant difference ($p > 0.05$) among the variance values of replicates at different concentration levels the best fit was obtained using an unweighted linear regression model. The linearity was observed in the expected concentration ranges, demonstrating their suitability for analysis. The results of the regression statistics for the analytes were reported in Table 5. The square of the correlation coefficient ($r^2 > 0.999$) demonstrated a significant correlation between the concentration of analytes and the detector response; however, it was neither a proof of linearity, nor a useful measure of the calibration variability. Hence the lack-of-fit-test were performed on these data; the significance values ($p > 0.05$) obtained for all analytes indicated that a linear

regression model provides a good interpolation of the experimental data. Moreover, the evaluation of residual plot confirmed that underlying assumption like homoscedasticity was met as well as the goodness of fit of the regression model. Finally, the confidence interval of the y-intercepts includes zero; moreover, the relative residual standard deviations, expressed as percentage, were calculated and used to assess the precision of the regression: all values were < 1% except for those corresponding to D1 and triHer for degradation product (1.9 and 1.9%, respectively).

	triHer	D1
Range ($\mu\text{g mL}^{-1}$)	20 - 60	5.1-35
Slope (a)	10783.9	14360.3
Standard error (SE) (a)	4387.6	4607.1
Intercept (b)	-5665.5	-1437.3
(b) C.I.^a	-13007.7 – 1676.7	-6097.9 – 3223.3
F	18122.7 $p < 0.01$	17165.6 $p < 0.01$
R²	0.9993	0.9992
RRSD^b	1.0	1.9
^a 95% confidence interval		
^b Relative residual standard deviation		

Table 5. Five levels calibration graphs for triHer and D1: unweighted regressions $y = ax + b$; three replicates for each level ($n = 15$)

3.5.6. Precision

The results obtained for the intra-day and inter-day are shown in Table 6. In all instances, RSD values were less than 2%, confirming the precision of the method.

Analyte	Level %	Intraday variation (n=12 RSD%)	Interday variation (n= 9 RSD%)
triHer	100	1.5	1.4
D1	0.2	1.2	1.1

Table 6. Intraday and interday precision values for triHer and D1

3.5.7. Accuracy

Accuracy has been determined by application of the analytical procedure to recovery studies, where known amount of standards was spiked into the placebo. The results of accuracy studies were shown in Table 7. The average recovery values were 98.8 and 97.9 for triHer and D1 respectively demonstrating that the method was accurate within the desired range of concentrations.

Level %	triHer	Level %	D1
50	98.1	0.075	97.6
75	99.0	0.1	97.4
100 ^a	99.2	0.2 ^b	99.4
125	98.2	0.3	97.2
150	99.7	0.5	98.1
Mean	98.8	Mean	97.9
SD	0.68	SD	0.88
RSD	0.7	RSD	0.9

^a 100% of label claim is equivalent to 40 µg mL⁻¹ of triHer

^b 0.2% of label claim is equivalent to 14 µg mL⁻¹ of D1

Table 7. Accuracy: Recovery data for triHer and D1.

3.6. Analysis of TRX in drug substances and drug products

The LC-UV method was applied for the quantification of triHer and D1 in the API batches and in commercial drug products of TRX. LC-UV chromatograms of test solutions for triHer assay were reported in Figure 9 and 10. The LC-UV method allowed the quantification of the triHer due to the availability of a pure standard of triHer obtained by the procedure of purification described (concentration ranged between $40.82 \mu\text{g mL}^{-1}$ and $51.33 \mu\text{g mL}^{-1}$). In the test solutions of degradation product assay in TRX formulations (Figure 11 and 12) the formation of D1 was observed only in Fleboside[®] ampoules where it was quantified in $4 \mu\text{g mL}^{-1}$ corresponding to 0.06% level. The attribution of D1 as stability-indicator is confirmed by the superimposition of LC-UV chromatograms of Fleboside[®] ampoules and TRX API batch (Figure 13).

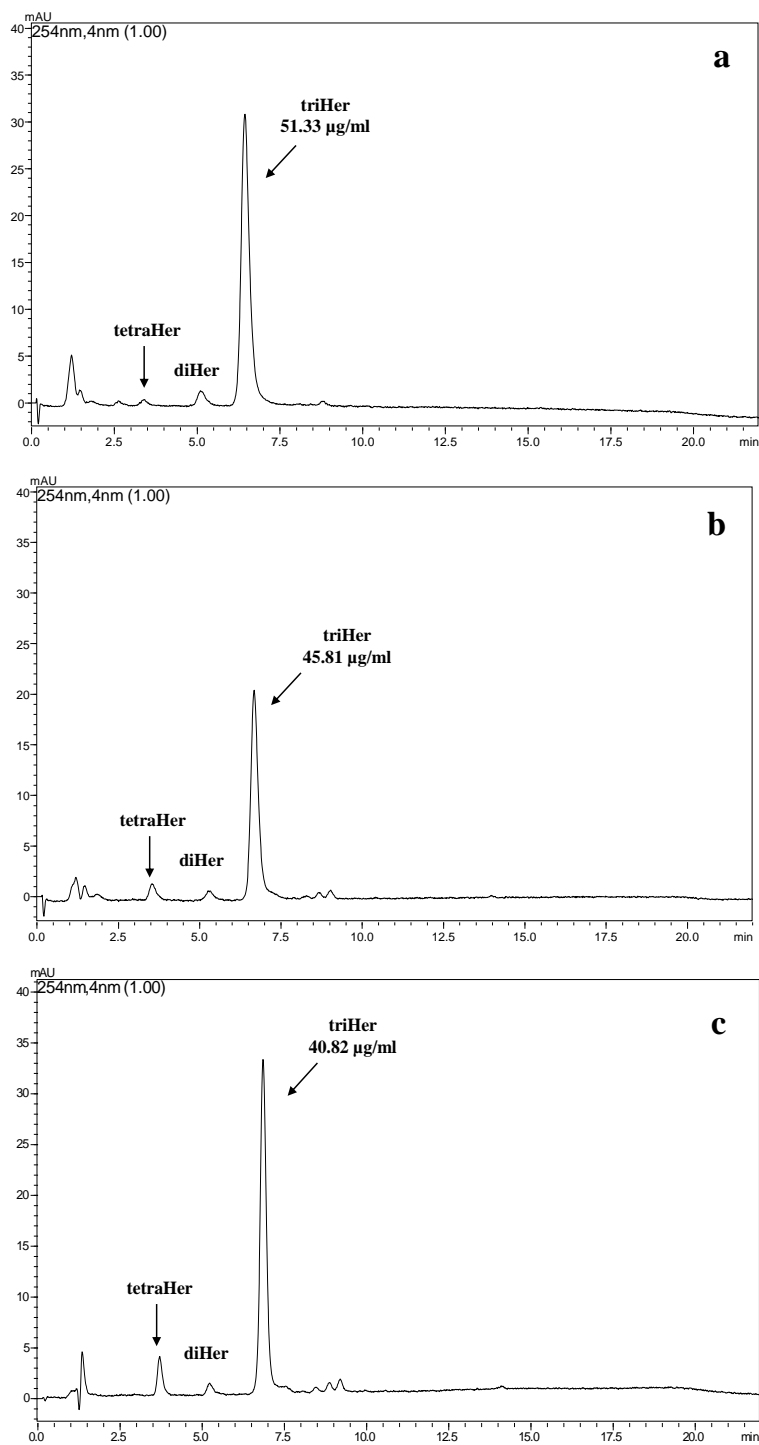


Figure 9. LC-UV chromatograms of test solution for triHer assay in a) TRX batch n° 335539190, b) TRX batch n° 33553C024 and c) TRX batch n° 33553T164

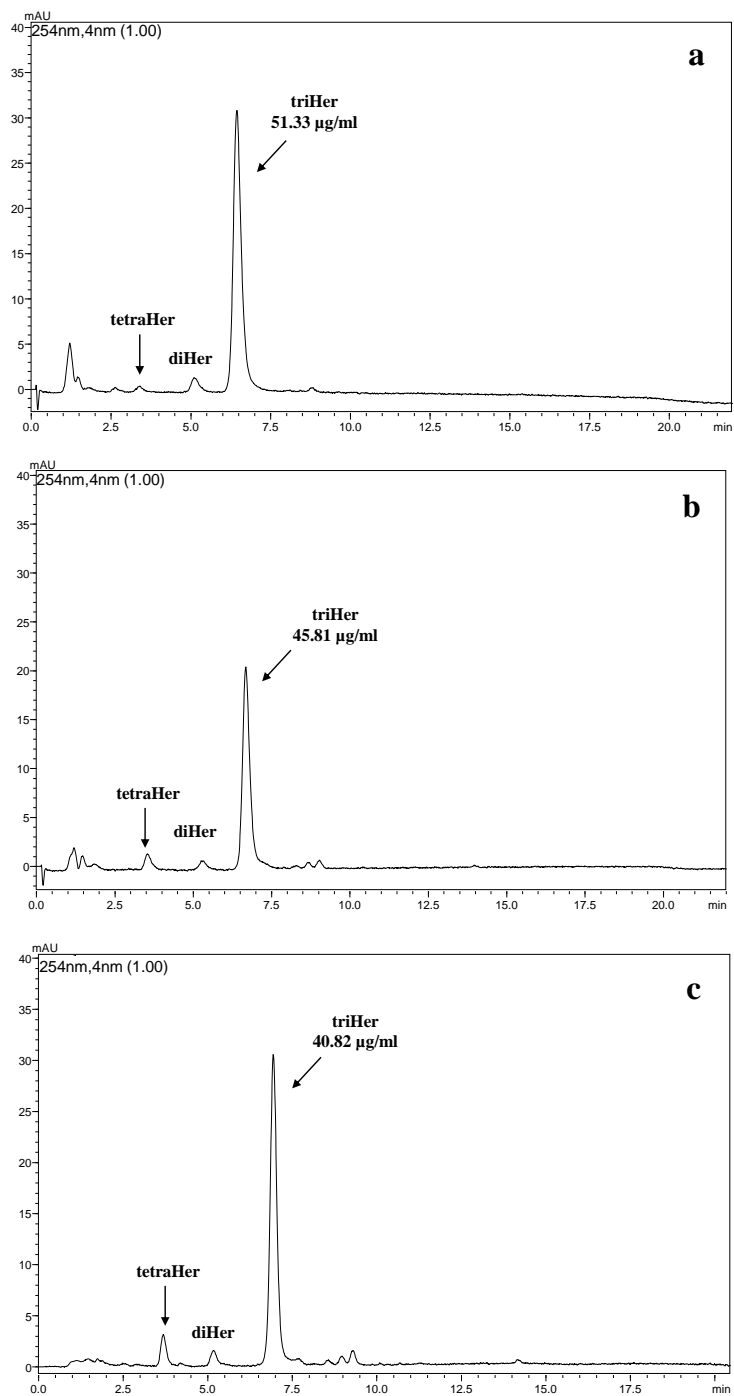


Figure 10. LC-UV chromatograms of test solution for triHer assay in a) Fleboside[®] coated tablets, b) Venolen[®] capsules and c) Fleboside[®] ampoules

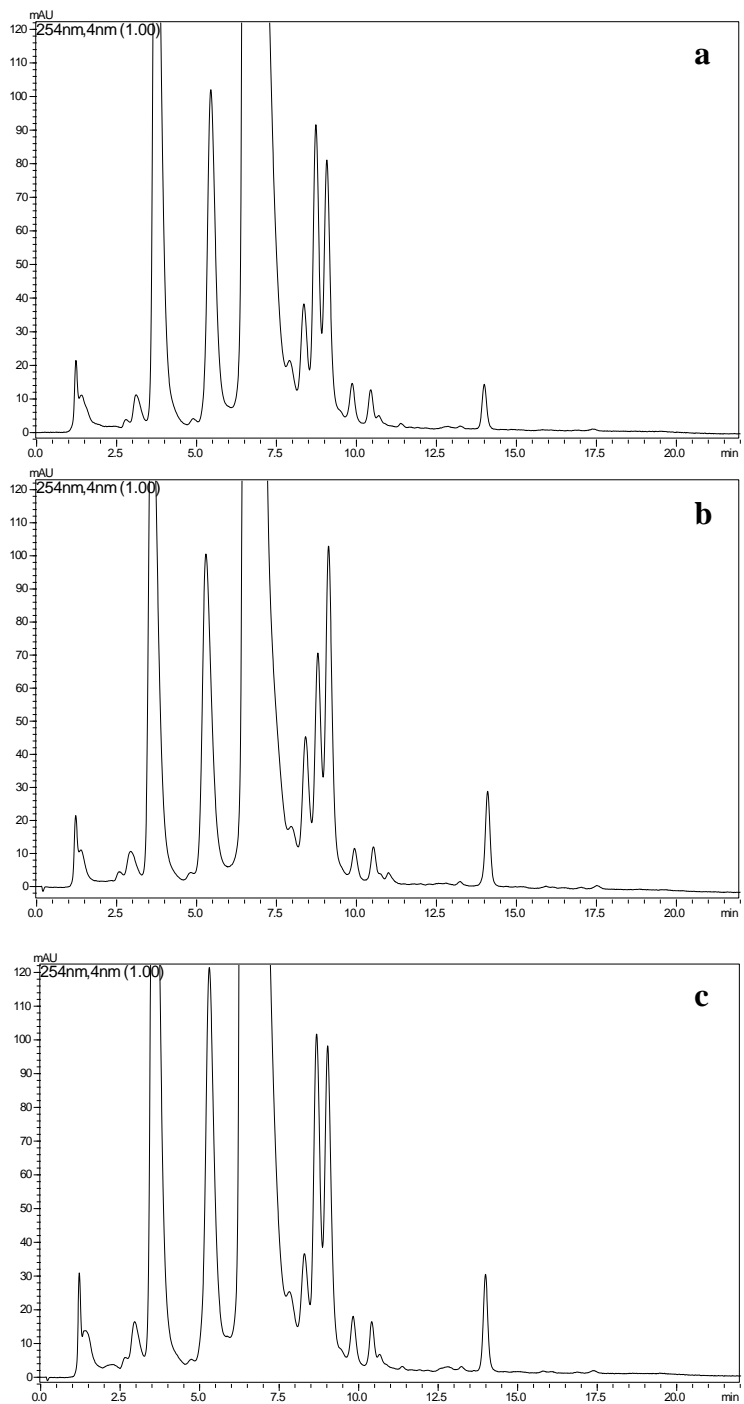


Figure 11. LC-UV chromatograms of test solution degradation product assay in a) TRX batch n° 335539190, b) TRX batch n° 33553C024 and c) TRX batch n°33553T164

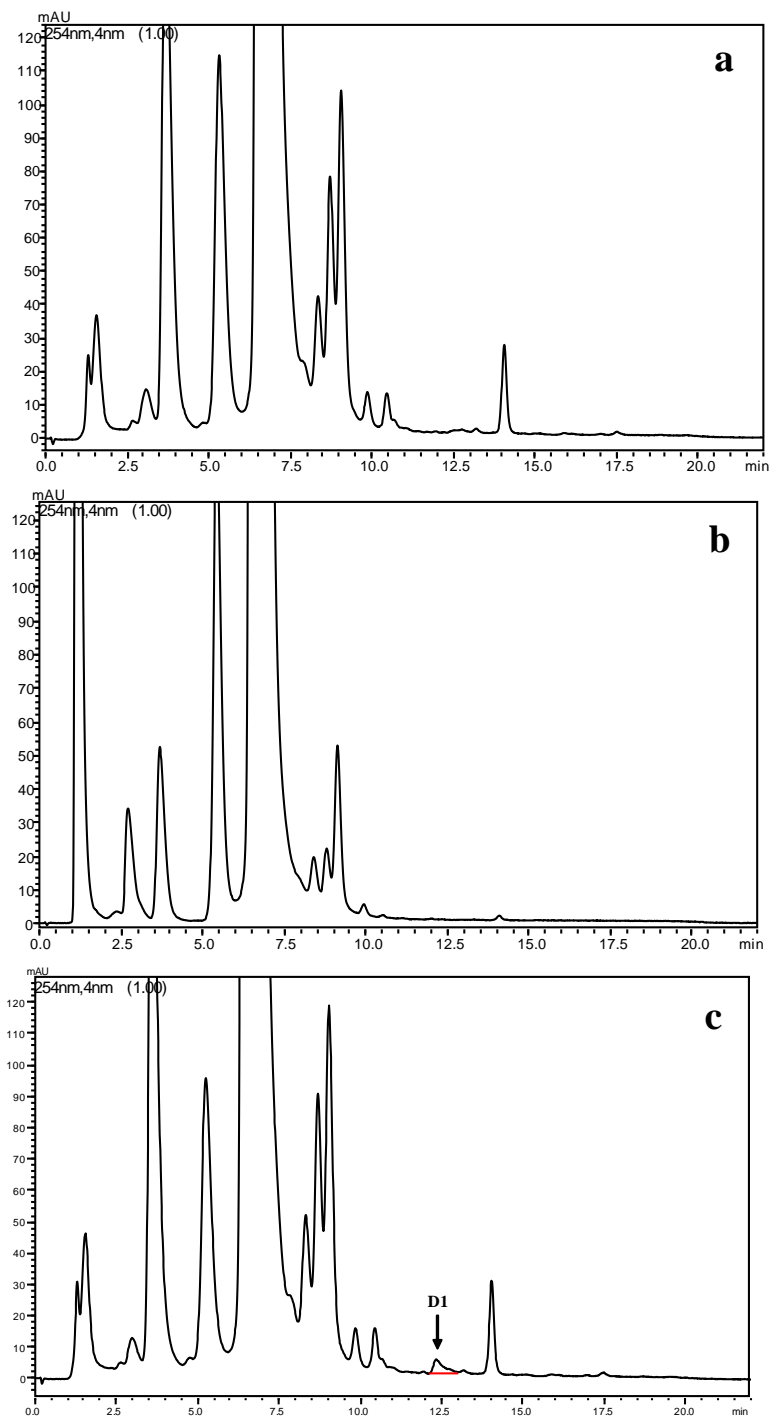


Figure 12. LC-UV chromatograms of test solution degradation product assay in a) Fleboside[®] coated tablets, b) Venolen[®] capsules and c) Fleboside[®] ampoules

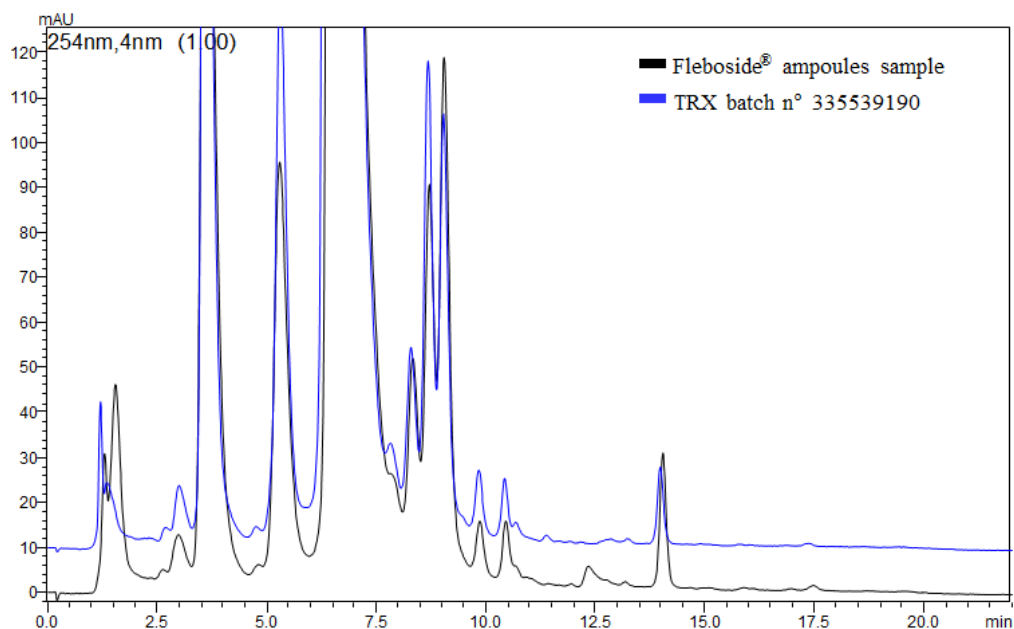


Figure 13. LC-UV chromatograms of test solution degradation product assay in Fleboside[®] ampoules overimposed to TRX batch n° 335539190

4. Conclusion:

In this work, it was proposed for the first time the degradation pathway of TRX mixture based on a complete forced degradation study performed by LC-MS, following the ICH guidelines. The isolation and the characterization of three predominant components of TRX and the synthesis and characterization of all the DPs allowed the development and the validation of a sensitive and robust LC-UV stability indicating method. The method was also successfully applied for the quantification of triHer and D1, in both drug substances and drug products.

References:

1. J.D. Xu, L.-W. Zhang, Y.-F. Liu, Synthesis and antioxidant activities of flavonoid derivatives, troxerutin and 3',4',7-triacetoxyethoxyquercetin. *Chin. Chem. Lett.* **24**, 223–226 (2013).
2. H. G. Montano, G. S. Silva, Renato C. Rocha, N. Z. A. Jimenez, R. C. Pereira, P.S.T. Brioso, Phytoplasma in fava d'anta tree (*Dimorphandra gardneriana*) in Brazil, *Bull. of Insectol.* **60** (2), 147–148 (2007).
3. L. Paniwnyk, E. Beaufoy, J. P. Lorimer, T. J. Mason, The extraction of rutin from flower buds of *Sophora japonica*. *Ultrason. Sonochem.* **8**, 299–301 (2001).
4. European Pharmacopoeia, 9th edition, 2017, pp. 3856.
5. R. van den Berg, G. R. M. M. Haenen, H. van den Berg, W. van der Vijgh, A. Bast, The predictive value of the antioxidant capacity of structurally related flavonoids using the Trolox equivalent antioxidant capacity (TEAC) assay, *Food Chem.* **70**, 391–395 (2000).
6. M. Kessler, G. J. L. Ubeaud, Anti- and pro-oxidant activity of rutin and quercetin derivatives. *J. Pharm. Pharmacol.* **55**, 131–142 (2003).
7. S. H. Fan, Z. F. Zhang, Y. L. Zheng, J. Lu, D. M. Wu, Q. Shan, B. Hu, Y.-y. Wang, Troxerutin protects the mouse kidney from D-galactose-caused injury through anti-inflammation and anti-oxidation. *Int. Immunopharmacol.* **9**, 91–96 (2009).
8. N. A. Panat, D. K. Maurya, S. S. Ghaskadbi, S. K. Sandur, Troxerutin, a plant flavonoid, protects cells against oxidative stress-induced cell death through radical scavenging mechanism. *Food Chem.* **194**, 32–45 (2016).
9. S. Zhang, H. Li, L. Zhang, R. Wang, M. Wang, Effects of troxerutin on cognitive deficits and glutamate cysteine ligase subunits in the hippocampus of streptozotocin-induced type 1 diabetes mellitus rats. *Brain Res.* **1657**, 355–360, (2017).

10. S. Babri, G. Mohaddes, I. Feizi, A. Mohammadnia, A. Niapour, A. Alihemmati, M. Amani, Effect of troxerutin on synaptic plasticity of hippocampal dentate gyrus neurons in a (-amyloid model of Alzheimer's disease: an electrophysiological study. *Eur. J. Pharmacol.* **732**, 19–25 (2014).
11. T. Baluchnejadmojarad, N. Jamali-Raeufy, S. Zabihnejad, N. Rabiee, M. Roghani, Troxerutin exerts neuroprotection in 6-hydroxydopamine lesion rat model of Parkinson's disease: possible involment of PI3 K/ER β signalling. *Eur. J.Pharmacol.* **801**, 72–78 (2017).
12. R. Vinothkumara, R.V. Kumara, V. Karthikkumara, P. Viswanathanb, J. Kabalimoorthyc, N. Nalinia, Oral supplementation with troxerutin (trihydroxyethylrutin), modulates lipid peroxidation and antioxidant statusin 1, 2-dimethylhydrazine-induced rat colon carcinogenesis. *Environ. Toxicol. Pharmacol.* **37**, 174–184 (2014).
13. K. N. S. Thomas, S. George, V. Arivalagan, A. Mani, I. Siddique, N. Namasivayam, The in vivo antineoplastic and therapeutic efficacy of troxerutin on rat preneoplastic liver: biochemical, histological and cellular aspects. *Eur. J. Nutr.* **56**, 2353–2366 (2017).
14. G. Xu, X. Tang, Troxerutin (TXN) potentiated 5-Fluorouracil (5-Fu) treatment of human gastric cancer through suppressing STAT3/NF-kB and Bcl-2 signaling pathways. *Biomed. Pharmacother.* **92**, 95–107 (2017).
15. Y. Gui, A. Li, F. Chen, H. Zhou, Y. Tang, L. Chen, S. Chen, S. Duan, Involvement of AMPK/SIRT1 pathway in anti-allodynic effect of troxerutin in CCI-induced neuropathic pain. *Eur. J. Pharmacol.* **769**, 234-241 (2015).
16. R. Geetha, M. K. Radika, E. Priyadarshini, K. Bhavani, C. V. Anuradha, Troxerutin reverses fibrotic changes in the myocardium of high fat high-fructose diet-fed mice. *Mol. Cell Biochem.* **407**, 263–279 (2015).

17. Y. Yu, G. Zheng, Troxerutin protects against diabetic cardiomyopathy through NF-KB/AKT/IRS1 in a rat model of type 2 diabetes. *Mol. Med. Rep.* **15**, 3473–3478 (2017).
18. D. K. Maurya, S. Balakrishnan, V. P. Salvi, C. K. Nair, Protection of cellular DNA from γ -radiation-induced damages and enhancement in DNA repair by troxerutin. *Mol. Cell. Biochem.* **280**, 57–68 (2005).
19. R. Badalzadeh, B. Baradaran, A. Alihemmati, B. Yousefi, A. Abbaszadeh, Troxerutin preconditioning and ischemic postconditioning modulate inflammatory response after myocardial Ischemia/Reperfusion injury in rat model. *Inflammation* **40**, 136–143 (2017).
20. F. Liu, Y. Xu, L. Rui, S. Gao, H. Dong, Q. Guo, Liquid chromatography/tandem mass spectrometry assay for the quantification of troxerutin in human plasma. *Rapid Commun. Mass Spectrom.* **20**, 3522–3526 (2006).
21. G. J. Yang, P. Liu, X. L. Qua, M. J. Xub, Q. S. Qua, C. Y. Wang, X. Y. Hu, Z.Y. Wang, The simultaneous separation and determination of six flavonoids and troxerutin in rat urine and chicken plasma by reversed-phase high-performance liquid chromatography with ultraviolet–visible detection. *J. Chromatogr. B* **856**, 222–228 (2007).
22. X. Cui, M. Zhang, X. Guan, L. Yin, Y. Sun, J. P. Fawcett, J. Gu, LC-MS–MS determination of troxerutin plasma and its application to a pharmacokinetic study. *Chromatography* **73**, 165–169 (2011).
23. N. J. R. Hephsebah, D. Nihitha, A. A. Kumar, Reverse phase HPLC method development and validation for the simultaneous quantitative estimation of troxerutin and calcium dobesilate in tablets. *Int. J. Pharm. Pharm. Sci.* **6**, 333–339 (2014).
24. N. Dimova, Hplc-separation and UV-spectral identification of O-(β -hydroxyethyl)-rutins. *Compt. Rend. Acad. Bulg. Sci.* **65**, 1681–1690 (2012).

25. Y. M. Xiao, P. Mao, Z. Zhao, L. R. Yang, X. F. Lin, Regioselective enzymatic acylation of troxerutin in nonaqueous medium. *Chin. Chem. Lett.* **21**, 59–62 (2010).
26. A. Ammar, M. El-attug, A. Belaid, S. Sadaawi, R. Kamour, A. Ashames, T. Almog, S. Alsharif, Separation of complexed semi-synthetic flavonoids by using fused core column in short time. *J. Chem. Pharm. Res.* **8**, 438–443 (2016).
27. S. Aprile, R. Canavesi, M. Bianchi, G. Grosa, E. Del Grosso, Development and validation of a stability-indicating HPLC-UV method for the determination of thiocolchicoside and its degradation products. *J. Pharm. Biomed. Anal.* **132**, 66–71 (2017).
28. ICH, Q1A (R2), Stability Testing of New Drug Substances and Products: Text and Methodology, International Conference on Harmonisation, Geneva, November 2005.
29. ICH, Q2A (R1), Validation of Analytical Procedures: Text and Methodology, International Conference on Harmonisation, Geneva, November 2005.
30. Center for Drug Evaluation and Research, U.S. Food and Drug Administration. Reviewer Guidance, Validation of Chromatographic Methods; FDA, Rockville, MD, November 1994.

Chapter 4

4. Synthesis and Degradation of Adenosine 5'- Tetraphosphate by Nicotinamide and Nicotinate Phosphoribosyltransferases

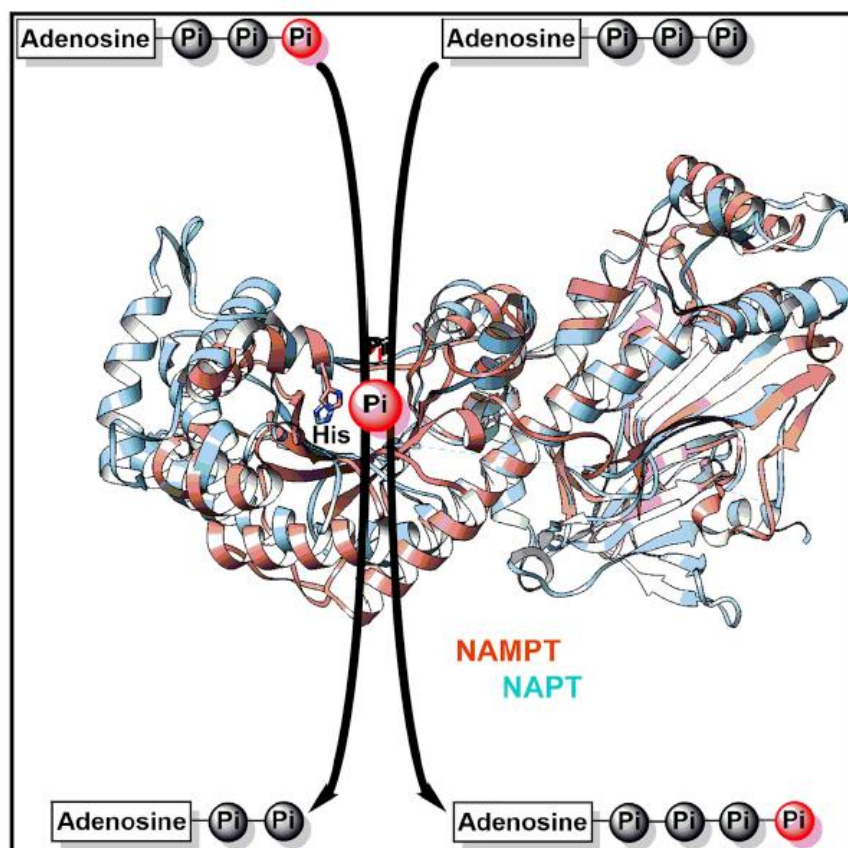
Adolfo Amici,^{1,4} Ambra A. Grolla,^{2,4} Erika Del Grosso,² Roberta Bellini,² Michele Bianchi,² Cristina Travelli,² Silvia Garavaglia,² Leonardo Sorci,¹ Nadia Raffaelli,³ Silverio Ruggieri,³ Armando A. Genazzani,^{2,*} and Giuseppe Orsomando^{1,5,*}

¹Department of Clinical Sciences, Section of Biochemistry, Polytechnic University of Marche, Via Ranieri 67, 60131 Ancona, Italy

²Department of Pharmaceutical Sciences, Università del Piemonte Orientale, Via Bovio 6, 28100 Novara, Italy

³Department of Agricultural, Food and Environmental Sciences, Polytechnic University of Marche, Via Brecce Bianche 10, 60131 Ancona, Italy

⁴Co-first author, ⁵Lead Contact, *Corresponding Authors

Graphical Abstract:**Abstract:**

Adenosine 5'-tetrphosphate (Ap₄) is a ubiquitous metabolite involved in cell signaling in mammals. Its full physiological significance remains unknown. Here we show that two enzymes committed to NAD biosynthesis, nicotinamide phosphoribosyltransferase (NAMPT) and nicotinate phosphoribosyltransferase (NAPT), can both catalyze the synthesis and degradation of Ap₄ through their facultative ATPase activity. We propose a mechanism for this unforeseen additional reaction, and demonstrate its evolutionary conservation in bacterial orthologs of mammalian NAMPT and NAPT. Furthermore, evolutionary distant forms of NAMPT were inhibited *in vitro* by the FK866 drug but, remarkably, it does not block

synthesis of Ap4. In fact, FK866-treated murine cells showed decreased NAD but increased Ap4 levels. Finally, murine cells and plasma with engineered or naturally fluctuating NAMPT levels showed matching Ap4 fluctuations. These results suggest a role of Ap4 in the actions of NAMPT, and prompt to evaluate the role of Ap4 production in the actions of NAMPT inhibitors.

1. Introduction:

Nicotinamide phosphoribosyltransferase (NAMPT) and nicotinate phosphoribosyltransferase (NAPT) are structurally similar NAD biosynthetic enzymes belonging to the class of dimeric type II phosphoribosyltransferases (PRTases)¹. They bind nicotinamide (Nam) or nicotinic acid (Na) as the respective substrate, catalyzing their reversible transfer to the ribose 5-phosphate moiety of the phosphoribosyl pyrophosphate (PRPP), with production of nicotinamide mononucleotide (NMN) or nicotinate mononucleotide (NaMN) and pyrophosphate (PPi). Both classical niacin vitamins, Nam and Na, are physiologically physiologically relevant precursors for NAD; Nam is used in the amidated salvage route, whereas Na is used in the deamidated route, also known as the Preiss-Handler pathway². The two metabolic routes contribute to the overall NAD pool in mammals with different efficiency and in different combinations depending on the tissue³, cell type⁴, and metabolic status⁵. In such metabolic context, NAMPT and NAPT are also recognized as rate-limiting^{6,7} and thus considered as key druggable targets^{8,9}. Besides the PRTase reaction above, these two enzymes are known to catalyze a facultative ATP hydrolysis (ATPase). Most studies on this subject have been carried out on human NAMPT^{10,11}, *Salmonella typhimurium* NAPT¹²⁻¹⁶, and human NAPT¹⁷. Such ATPase activity is intriguing since it couples weakly, i.e., not stoichiometrically, to the PRTase and involves the formation of a phosphor-His intermediate at the active site (phosphorylated H247 in human/ murine NAMPT, H219 in *S. typhimurium* NAPT, and H213 in human NAPT). Therefore, NAMPT and NAPT are uniquely

ATP-sensitive enzymes that have mechanistically evolved to regulate their own NMN/NaMN synthesis by linkage to an ATP-dependent autophosphorylation process. This link, however, is not mandatory and both enzymes readily synthesize pyridine mononucleotides even in the absence of ATP, albeit with decreased catalytic efficiency^{11,16}. At physiological Mg^{2+} -ATP concentrations, NAMPT and NAPT are probably phosphorylated, providing efficient capturing of the pyridine substrate and conversion to the corresponding product. Thus, their ATPase activity is seen as an *in vivo* thermodynamic drive toward NMN/NaMN synthesis and, in this view, intracellular ATP is the fuel that, via these enzymes, allows recycling to NAD of the two niacin moieties even at very low intracellular concentration^{11,13}

The complexity is further increased by the functional pleiotropism of NAMPT within mammalian organisms. Besides regulating intracellular NAD homeostasis⁷, NAMPT is subject to a circadian transcriptional control by the CLOCK machinery¹⁸, it belongs to systemic regulatory networks^{19,20}, and it is a serum-circulating secreted protein known as PBEF²¹ or visfatin²², which has an additional property as an immunomodulating cytokine²³⁻²⁵. Recently, the TLR4 receptor in human lung, which mediates the innate immunity response, has been identified as the receptor of circulating NAMPT²⁶, but controversies remain regarding the secretion mechanism of the enzyme, the involvement of NAMPT catalytic activity in the cytokine function²⁷, and the bioavailability of enzyme reactants in extracellular fluids⁶. As to NAPT, no extracellular function has been yet ascribed to this protein, but its presence in human sera as a circulating active enzyme has been recently reported⁴.

This work started from the serendipitous finding of an unpredicted reaction product formed *in vitro* by NAMPT and NAPT from the ATP substrate. We identified this product as adenosine 5'-tetrphosphate (Ap4) and proved it to be enzymatically formed by a phosphor-transfer reaction to ATP, i.e., an unforeseen additional reaction catalyzed by such type II PRTases. Ap4 is known as the most potent vasoactive purinergic mediator in mammals, circulating in plasma at nanomolar

concentrations, and exerting vasoconstriction through activation of the P2X1 receptor²⁸. Thus, the ability to synthesize Ap4 could be important for the extracellular signaling roles of these enzymes. Moreover, as Ap4 has long been known in mammals as an intracellular molecule of unclear metabolic origin²⁹, our data identify two of the enzymes likely to contribute to its homeostasis.

2. Results:

2.1 Ap4 Is an Authentic ATP-Derived Product of the NAMPT-Catalyzed Reaction

Initial C18-HPLC assays aiming to evaluate ATP usage by murine NAMPT showed the time-dependent formation of an unpredicted product in the reaction mixture, distinct from ADP (Figure 1A). Its UV spectrum was typical of an adenylate compound, i.e., superimposable to that of both ATP and ADP (Figure 1B). The unknown product was absent in control mixtures including heat-inactivated enzyme, or missing individual mixture components ATP and Mg²⁺ ions (not shown). Furthermore, the H247E mutant³⁰, which is ATP insensitive despite its retained NMN synthesis capability (Table 1), did not form any of this product (Figure 1C). This ruled out any non-enzymatic origin and suggested that it was a novel ATP-derived product of NAMPT. The novel product was purified by TSK-DEAE chromatography for further characterization (Figure 1D). The purified species was lyophilized to remove the volatiles and resuspended in suitable solutions at concentrations that were calculated spectrophotometrically based on the adenosine content (see Methods section). The solubilized species was found to be stable through several freezing/thawing cycles, and was next subjected to chemical, enzymatic, and liquid chromatography-electrospray ionization mass spectrometry (LC-ESI-MS) analyses. We identified a phosphate/adenosine stoichiometry of 4:1 (Figure 2A), a progressive digestion by alkaline phosphatase to ATP, ADP, AMP, and adenosine in this order (Figure 2B), digestion by phosphodiesterase to AMP and then to adenosine (Figure 2C), and a mass spectrum under the X peak of m/z 586

[M-H]⁻ (Figure 2D). Orthogonal analysis of these results identified the purified NAMPT product as Ap4. Parallel enzyme digestion tests of a pure Ap4 standard yielded results identical to those obtained with the purified NAMPT product. Moreover, the NAMPT product and the Ap4 standard co-eluted after chromatography in two distinct separations, i.e., ion-pair reverse phase (Figure 2E) and anion exchange (Figure 2F). Taken together, this evidence indicates the novel NAMPT product is indeed an authentic Ap4.

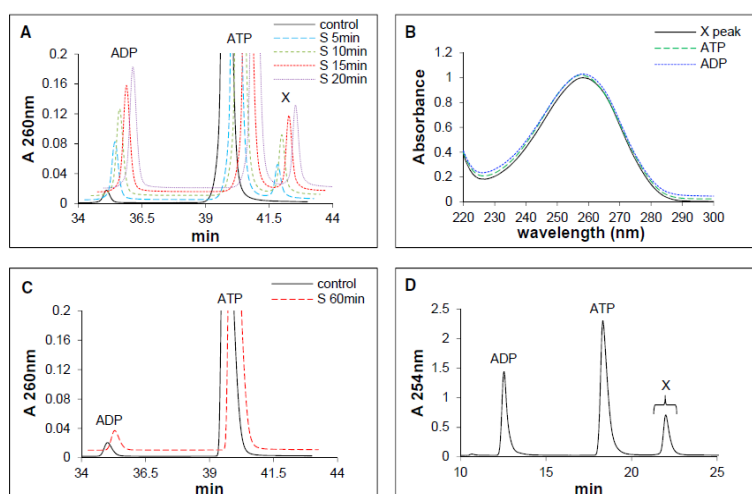


Figure 1. Identification of Ap4 as a New Enzymatic Product A. Analytical C18-HPLC UV profiles from a typical ATPase activity assay (“S”) of murine NAMPT wild-type (~15 mM) incubated in the presence of 2.4 mM ATP. The horizontal axis shows only the region that visualizes the result. “X” indicates the newly identified reaction product. The “control” refers to a parallel blank mixture without the enzyme showing no hydrolysis of ATP and its negligible contamination by ADP. B. UV spectra of the peaks in (A), at comparable maxima corresponding to 1 absorbance unit. C. Analytical C18-HPLC UV profiles from a reaction assay carried out as in (A) but using the murine NAMPT mutant H247E (~40 mM). D. Preparative HPLC purification by TSK-DEAE chromatography of the enzymatically formed species X (the fractions collected are within the curly bracket)

Enzyme species	treatment	PRTase rates (mU/mg) ^a		ATPase rates (mU/mg) ^b			
		NMN synthesis	NaMN synthesis	ATP consumption	ADP synthesis	Pi synthesis	Ap4 synthesis
murine NAMPT wild type	None	31.1 (4.77)	5.86 (0.59)	8.54 (1.02)	5.82 (1.08)	3.19 (1.40)	2.66 (0.47)
	+FK866	Nd	Nd	10.4 (0.12)	9.58 (0.83)	9.02 (1.64)	1.51 (0.27)
murine NAMPT H247E	None	3.21 (0.20)	Nd	Nd	≤0.02	≤0.02	Nd
	+FK866	Nd	Nd	Nd	≤0.02	≤0.03	Nd
human NAPT wild type	None	Nd	16.0 (1.15)	1.48 (0.08)	1.17 (0.10)	1.14 (0.21)	0.16 (0.04)
	+FK866	Nd	15.5 (0.88)	1.57 (0.07)	1.25 (0.04)	1.31 (0.03)	0.19 (0.03)
human NAPT H213A	None	Nd	76.4 (11.2)	≤0.10	≤0.10	≤0.10	Nd
	+FK866	Nd	81.1 (3.82)	≤0.10	≤0.10	≤0.10	Nd
<i>Acinetobacter</i> NadV wild type	None	30.6 (1.84)	Nd	1.14 (0.09)	1.01 (0.08)	0.89 (0.08)	0.12 (0.02)
	+FK866	8.04 (2.06)	Nd	23.4 (2.96)	14.9 (1.22)	6.17 (1.65)	8.54 (2.06)
<i>Staphylococcus</i> PncB wild type	None	Nd	441 (56.7)	13.0 (0.39)	8.54 (0.25)	4.06 (0.11)	4.48 (0.14)
	+FK866	Nd	424 (47.0)	14.3 (0.59)	9.38 (0.37)	4.44 (0.16)	4.94 (0.21)

Table 1. PRTase and ATPase Activities by Orthologous NAMPT and NAPT Enzymes

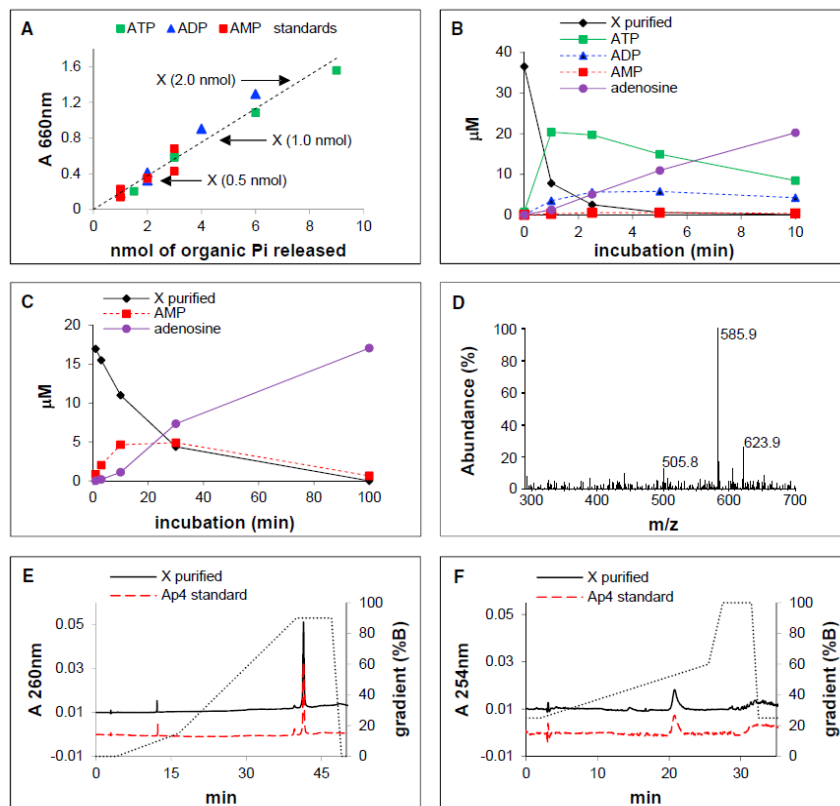


Figure 2. Structural Assessment of the Enzyme-Formed Ap4 Product. A. Molar ratio in the purified species X between the organic phosphate released after chemical digestion and quantified by malachite green, and the adenosine content quantified by UV absorption (arrows). A reference curve was created from the indicated standards, all with known Pi/adenosine stoichiometry. B. Time course digestion of the purified species X by calf intestine alkaline phosphatase (see also Figure S1A). C. Time course digestion of the purified species X by snake venom phosphodiesterase I (including a contaminating 50-nucleotidase that causes AMP-toadenosine conversion, see also Figure S1B). D. LC-ESI-MS analysis of the purified species X. E. Analytical C18-HPLC UV profiles of the purified species X and an Ap4 standard (both ~0.8 nmol). Dotted line, the methanol gradient applied for elution. F. Analytical TSK-DEAE-HPLC UV profiles of the purified species X and an Ap4 standard (both 0.8 nmol average). Dotted line, the salt gradient applied for elution

2.2 Investigation of Ap4 formation and its modulation [31]

Co-authors deeply studied the following aspects related to Ap4 synthesis and its modulation:

- Mechanism of enzymatic formation of Ap4.
- ATP hydrolysis and Phosphor Transfer by Evolutionary Distant Type II PRTases.
- In vitro Modulation of Murine NAMPT ATPase versus PRTase Activities.

2.3 LC-MSⁿ bioanalytical method for the quantification of Ap4 and other five analytes related to NAMPT activity in murine cells and Plasma

With the aim to quantify Ap4 and ATP, ADP, Nam, NMN and NAD, a new LC-MSⁿ bioanalytical quantitative method has been developed. MS source conditions were set up by flow injection analysis on analytes standards. Analyses were performed in both positive and negative ionization mode, according to the chemical features of each compound. Mass/Mass spectra are reported in Figure 3A. To perform a quantitative method, all the analytes of interest were monitored in Single Reaction Monitoring Mode (SRM) or Multiple Reaction Monitoring Mode (MRM) or in Mass/Mass Mode (MS²) (Figure 3B). Under a chromatographic point of view, The stationary phase was constituted by a Phenomenex Luna HILIC (150 x 2 mm, 3 μ m) protected with a security guard (Luna HILIC, 4 x 2 mm) maintained at 25°C. While, the mobile phase was composed of eluent A: ammonium acetate buffer (100 mM, pH 5.8) and eluent B: CH₃CN using an isocratic elution (30:70; A:B; v:v). The flow rate was set at 200 μ l min⁻¹ for 20 min, with an injection volume of 5 μ l (Figure 3C). The LC-MSⁿ bioanalytical method was assessed for the following parameters: % Recovery, % matrix effect, LOD (Lower Limit of Detection) and LOQ (Lower Limit of Quantification) and linearity (Figure 4).

The sample preparation was performed with a protein precipitation approach with organic solvents as described in the experimental section.

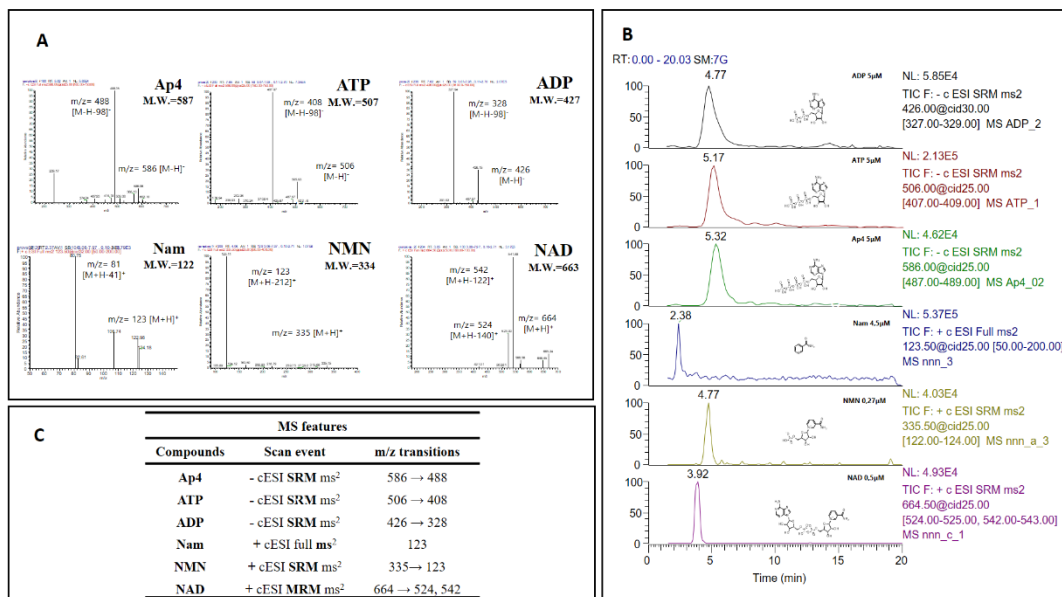


Figure 3. A. MS/MS spectra of Ap4, ATP, ADP, Nam, NMN and NAD collected with flow injection analysis with a flow rate of $5 \mu\text{l min}^{-1}$. B. LC-MS analysis of standard compounds. C. MS parameters developed for the compounds detection

A % Recovery			
	Sample Conc (μM)	% recovery in cells	% recovery in mice plasma
Ap4	1.0	35.7	97
ATP	10	90.1	93
ADP	10	106.4	-
Nam	2.5	52.8	-
NMN	0.2	118.0	-
NAD	2.0	88.2	-

B % Matrix Effect			
	Sample Conc (μM)	% ME in cells	% ME in mice plasma
Ap4	1.0	99.4	90
ATP	10	160.2	96
ADP	10	88.8	-
Nam	1.0	94.5	-
NMN	0.1	87.2	-
NAD	1.0	74.5	-

C		
	LOD (μM)	LOQ (μM)
Ap4	0,03	0,1
ATP	0,3	1,0
ADP	0,3	0,8
Nam	0,2	0,5
NMN	0,003	0,01
NAD	0,02	0,05

D Linearity						
	Ap4	ATP	ADP	Nam	NMN	NAD
Range (μM)	0.1-3.1	1-150	0.5-160	0.5-13.5	0.01-0.27	0.70-6.25
Slope (m)	717949	2765798	850556	2042510	4533738	2565136
Intercept (q)	23497	-1129875	-289108	22202	9454	339534
R ²	0.9991	0.9982	0.9956	0.9993	0.9966	0.9966

Figure 4. A. Recovery was evaluated by comparing the response ratio of the analyte physiologically present in the biological sample with the response ratio after adding the analyte before the PP and the evaporation treatment. B. The matrix effect was evaluated for each compound by comparing the response ratio in presence of matrix with the response ratio in the absence of it. C. LOD and LOQ. D. Linearity was performed using the external calibration method and it was calculated as unweighted linear regression $y = ax + b$

2.4 *In Vivo* Regulation of Ap4 Levels by NAMPT in Murine Cells and Plasma

We proceeded to evaluate Ap4 levels in mammalian cells and their dependence on NAMPT *in vivo*. For this we used an in-house B16 melanoma cell line previously shown to be enriched in NAMPT³². We had previously engineered³³ an overexpressing cell line (B16 FLAG-NAMPT) expressing ca. 160% of wild-type NAMPT levels, and a silenced cell line (B16 shNAMPT Low) expressing less than 20% of wild-type NAMPT (see Figure 5 for expression levels). The levels of the nucleotides of interest determined by LC-ESI-MS in these cells are reported in Table 2. The overall data show a low ATP/ADP ratio that has also been observed by

others³⁴ in the same cell type (B16), as well as higher than expected Nam levels, which can be explained by the presence of high micromolar concentrations of Nam in the commercially available medium in which cells were grown (32.7 mM, as depicted in the product datasheet). It is unlikely that the low ATP/ADP ratio, as well as the high Nam/NAD ratio, are instead given by degradation during sample preparation, as standards were processed in parallel with no sign of degradation. As expected, NMN and NAD levels correlated with NAMPT expression. More surprisingly, the Nam levels were lower in shNAMPT compared with wild-type NAMPT. Notably, we could measure intracellular Ap4 levels at 0.527 ± 0.068 nmol/mg. Such levels were increased in cells overexpressing NAMPT and reduced in cells silenced for the enzyme. We also observed an almost doubling of the Ap4 content in wild-type cells treated with FK866 (Table 2). Such doubling was accompanied by the depletion of NMN and NAD, as expected, and by a marked reduction of Nam. These data, taken together, suggest that NAMPT is a source of intracellular Ap4, although we cannot rule out the possibility that other enzymes also contribute. The effect observed in the presence of FK866 could in part be explained by the uncoupling of the two reactions, as shown by the experiments performed on the purified enzymes, and in part could suggest that a cellular homeostatic control is present. Ap4 levels under conditions of metabolic perturbation were also evaluated. We assayed Ap4 levels in cells grown for 20 hr in serum-free conditions, in low-glucose conditions (normal concentration of 4.5 g/L to a low concentration of 1 g/L), and in both low-glucose and serum-free conditions. Levels of Ap4 were reduced in all three conditions but were statistically reduced only when cells were grown in low concentration of glucose (Figure 6A). On the contrary, NMN levels were statistically reduced only when cells were grown in the absence of serum (Figure 6B). Treating cells with H₂O₂ (500 mM) reduced both Ap4 and NMN levels, but this change was not statistically significant. Furthermore, given the extracellular role of secreted NAMPT, we decided to explore whether we could detect Ap4 in murine plasma and

whether circulating NAMPT levels correlated with plasma Ap4 levels. To this end, we sampled blood from mice for both NAMPT (via an ELISA assay) and Ap4 levels (by LC-ESI- MS). In most samples Ap4 was detectable with a global mean of 562 ± 114 nM ($n = 23$). This is similar to a previous report of Ap4 in human plasma at 255.6 ± 82.4 nM²⁸. In addition, these Ap4 levels, despite their inter- and intra-subject variability, showed a good correlation with extracellular NAMPT levels (Figure 6C, $R^2 = 0.41$). Not surprisingly, Ap4 also correlated, to a greater extent, with ATP levels measured in parallel (Figure 6D, $R^2 = 0.81$). These data are consistent with the notion that extracellular NAMPT may be one of the enzymes that participates in the synthesis of Ap4, and that Ap4 is derived enzymatically from ATP.

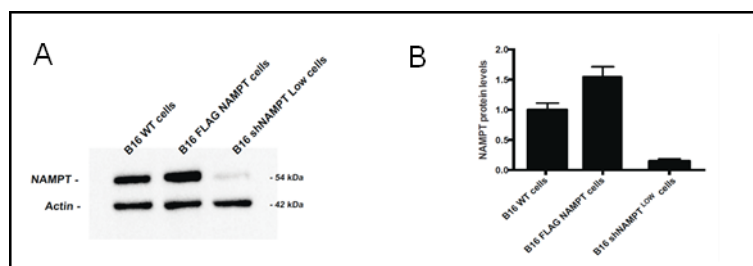


Figure 5. Mouse B16 cells with modulated expression of NAMPT. Crude protein extracts were obtained from wild type B16 cells or from the same cells after lentiviral transfection with either FLAG-NAMPT or shNAMPT Low constructs, respectively inducing a stable NAMPT over-expression or its silencing. After electrophoresis, membrane transfer, and immunostaining with specific antibodies (A), the NAMPT protein levels were quantified relatively to the housekeeping beta-Actin signal by densitometry analysis (B)

nmol/mg of protein						
B16 cells	Ap4	ATP	ADP	Nam	NMN	NAD
WT (n=9)	0.527 (0.068)	9.107 (1.595)	8.992 (2.056)	4.344 (0.721)	0.039 (0.007)	4.489 (1.524)
WT +FK866 (n=7)	0.923 (0.101)**	5.882 (0.605)	7.654 (1.385)	3.056 (0.535)	0.010 (0.002)*	Nd
FLAG-NAMPT (n=3)	1.073 (0.175)**	17.22 (0.546)	13.32 (0.454)	2.417 (0.097)	0.212 (0.068)***	6.940 (0.122)
shNAMPT Low (n=5)	0.329 (0.075) ^{ns}	5.347 (1.027)	5.972 (1.125)	3.281 (0.311)	0.026 (0.005) ^{ns}	2.135 (0.289)

Table 2. Adenylate and pyridine compounds in melanoma B16 cells with modulated intracellular expression of NAMPT (see Figure 5), or treated with 100 nM FK866 for 24 hours, were collected and evaluated for their nucleotides levels by LC-ESI-MS analysis. B16 WT, wild-type cells. B16 shNAMPT Low, cells engineered for NAMPT silencing. B16 FLAG-NAMPT, cells engineered for NAMPT over-expression. Data are represented as the mean and SEM (in parentheses) from n experiments, as indicated. Statistical analysis for Ap4 values: p=0.09 (ns) for B16 shNAMPT Low cells vs B16 WT cells; p=0.0048 (**) for B16 FLAG NAMPT cells vs B16 WT cells; p=0.0047 (**) for B16 WT+FK866 cells vs B16 WT cells. Statistical analysis for NMN values: p=0.19 (ns) for B16 shNAMPT Low cells vs B16 WT cells; p=0.0009 (***) for B16 FLAG NAMPT cells vs B16 WT cells; p=0.045 (*) for B16 WT+FK866 cells vs B16 WT cells. Nd, below the detection limit

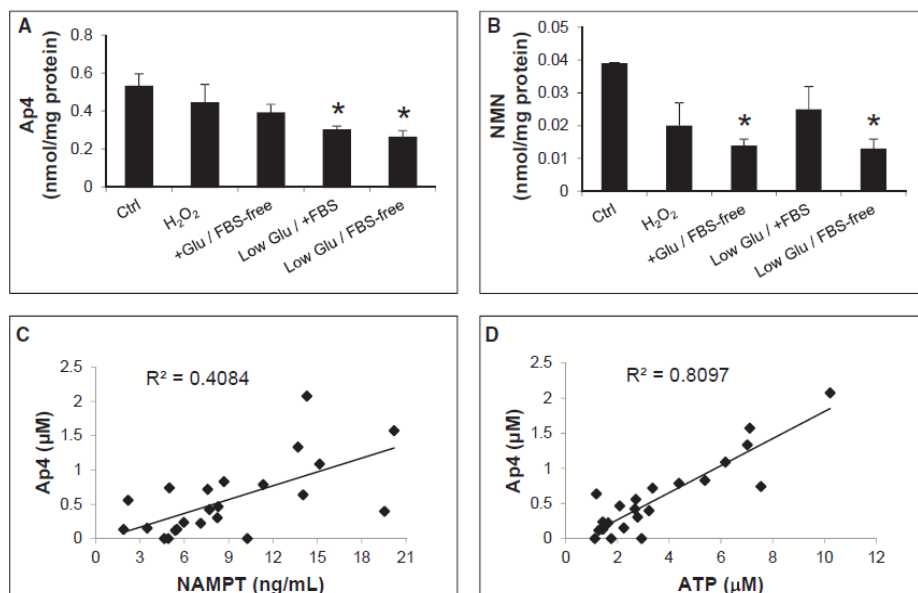


Figure 6. A and B. Ap4 (A) and NMN (B) levels evaluated by LC-ESI-MS in B16 wild-type cells under metabolism perturbations obtained by growth for 20 hr in serum (fetal bovine serum [FBS])-free conditions, in low-glucose (Low Glu) conditions (from 4.5 to 1.0 g/L), in both low-glucose and serum-free conditions, or treatment with 500 mM H₂O₂. *p = 0.05 for Ap4 levels of B16 in Low Glu/+FBS condition versus ctrl cells; *p = 0.029 for Ap4 levels of B16 in Low Glu/FBS-free condition versus ctrl cells; *p = 0.03 for NMN levels of B16 in +Glu/FBS-free condition versus ctrl cells; *p = 0.05 for NMN levels of B16 in Low Glu/FBS-free condition versus ctrl cells. Values represent the mean + SEM from a triplicate assay. C and D. The Ap4 levels measured by LC-ESI-MS in the plasma of healthy male C57BL/6 mice (n = 23 total analyzed samples) and their correlation with extracellular NAMPT (C) and ATP (D). The linear regression value (R^2) is highlighted

3. Discussion:

Ap4 was first described in the early 1950s as a contaminant of commercial ATP preparations³⁵, and re-emerged in the literature about 50 years later as an extracellular vasoactive compound^{28,36}. It has a broad distribution in prokaryotes and eukaryotes, including mammalian tissues and plasma, and has been identified as an *in vitro* by-product of a number of ATP-dependent enzymatic reactions²⁹. Given the lack of any dedicated enzyme to its synthesis, Ap4 *in vivo* is thought to arise from the promiscuous activity of multiple enzymes, and no information about its physiological regulation is currently available. Yet, given that Ap4, at sub-nanomolar concentrations, is one of the most potent vasoconstrictors known to date²⁸, and nanomolar concentrations of Ap4 can modulate the intraocular pressure

in the rabbit eye³⁶, it seems unlikely that its production would not be regulated. These actions of extracellular Ap4 are also mediated by P2X receptors^{28,36} that belong to a structural family of membrane ion channels, with a widespread tissue distribution in mammals, where they underlie a variety of functions, including excitatory effects on smooth muscle cells (depolarization/contraction), Ca²⁺ uptake into neurons (neuromodulator responses), and release of pro-inflammatory cytokines such as interleukin 1b from immune cells³⁷. On the other hand, intracellular functions of Ap4 are only putative at present but potentially relevant in fundamental biological processes like, for example, the cellular protein turnover, as suggested by the observed *in vitro* targeting of Ap4 to AMP-forming ligases, aminoacyl-tRNA synthetases³⁸, and the ubiquitin-activating enzyme E1 of the proteasome system³⁹.

3.1 Mechanism of the enzymatic formation of Ap4

To our knowledge, the data presented here establish for the first time that two enzymes belonging to the class of type II PRTases, long thought to be committed to NAD synthesis in living cells with a non-obligatory accompanying use of ATP, are also capable of synthesizing Ap4. We propose a mechanism shared by NAMPT and NAPT, where the known ATP hydrolysis is coupled to a new phosphor-transfer reaction that, via the same E-P complex intermediate, leads to Ap4 synthesis. Notably, the facultative ATPase of both enzymes has been extensively studied in the past as a paradigm for energy use^{11,14}, but the reaction as such went partially unnoticed due to its cryptic nature and, most likely, to the lack of a stoichiometric evaluation of all reactants involved. Nevertheless, in support of our model, mechanisms similar to the proposed one apply to other enzymes forming covalent intermediates during their catalytic cycle. For example, glucose-6-phosphatase⁴⁰, transglutaminases⁴¹, and nucleotidases⁴² are all known to catalyze branched-pathway reactions characterized by double-displacement mechanisms and formation of

covalently modified enzyme intermediates (phosphorylated or acylated) that preserve the transfer potential of the group undergoing transfer.

One peculiarity of NAMPT and NAPT is that such use of ATP may occur independently from NMN/NaMN synthesis, the intrinsically catalyzed reaction for which they were originally classified and that remains the focus of most current studies. Notably, only NAMPTs and NAPT from both bacterial and mammalian sources are known to use ATP hydrolysis and to catalyze a dual PRTase reaction, whether ATP coupled or ATP uncoupled^{11,13,17,43}. The other classified PRTase members, including adenine (EC 2.4.2.7), hypoxanthine/guanine (EC 2.4.2.8), uracil (EC 2.4.2.9), orotate (EC 2.4.2.10), quinolinate (EC 2.4.2.19), and dioxotetrahydropyrimidine (EC 2.4.2.20) PRTases are widely considered to be ATP insensitive, albeit supporting experimental evidence exists in only a few cases^{44,45}. To confirm this, we have tested the ATP dependence of a bacterial quinolinate PRTase and a member of the hypoxanthine/guanine PRTase family. The results showed the ATP insensitivity of both these PRTases (Figure 6A and 6B)³¹. It should also be noted that quinolinate PRTase, the closest functional and structural relative of NAMPT and NAPT¹, lacks the conserved His residue that is essential for Ap4 formation according to our scheme and catalyzes a reaction of irreversible nature due to a decarboxylation step occurring along with the phosphoribosyl transfer⁴⁶, so that there is no need of ATP hydrolysis to drive the reaction. On the contrary, in both NAMPT and NAPT, ATP is used to establish the formation of a phosphohistidine intermediate^{10,12} that has been shown to potentiate their PRTase activity^{11,16}, thereby enhancing cellular NAD synthesis. Nonetheless, in both NAMPT and NAPT, the reaction coupling ATP hydrolysis to NMN/NaMN synthesis is not stoichiometric and only a small part of the energy released from the hydrolysis is efficiently captured^{11,12}. This appreciable thermodynamic leak suggests additional roles exerted by the facultative ATPase reaction, perhaps independent from coupling. In this regard, our finding that it may drive Ap4 synthesis is an intriguing explanation. This

is also supported by the observed catalytic similarity between mammalian and bacterial orthologs (Table 1), which suggests an intrinsic role for the Ap4 synthesis mediated by these enzymes, fully conserved throughout evolution.

3.2 LC-MSⁿ bioanalytical method development

To quantify the intracellular levels of Ap4, ATP, ADP, Nam, NMN and NAD in both murine cells and murine plasma, a new LC-MSⁿ bioanalytical method has been developed. The source parameters were set up according to the chemical features of the compounds. Ap4, ATP and ADP gave a better response in negative ionization mode, due to the phosphate moieties on their structures. While Nam, NMN and NAD gave better results in positive ionization mode due to the contemporary presence of pyridine and adenine moiety with the absence of free phosphate moieties which characterize their structures. MS/MS ion fragmentations were studied to develop a SRM or MRM scans for each analyte. Only for Nam, the scan performed was a MS/MS mode, cause the low mass of the analyte which made impossible to have a stabilization of the mother and daughter ions during the fragmentation (Figure 3).

The Chromatographic conditions were optimized to satisfy these features: (1) good peaks shape; (2) retention times far enough from the death time of the column and not too high, to get a method as faster as possible; (3) to avoid matrix effects; (4) to have all the analytical parameters in the common ranges of agreement.

Various stationary phases were tested (such as C18, C8, Biphenyl, F5, Synergy Polar and Kinetex HILIC) with various methods, without any success. In the end, we opted for a Luna HILIC column which, thanks to a silica surface covered with cross-linking diol groups, allows a polar selectivity under hydrophilic liquid chromatography conditions. In order to have satisfactory % matrix effects values, an isocratic run analysis was performed as described in the experimental section. Gradient elutions were tested but no one gave positive results under this aspect. In fact, matrix is constituted essentially by polar small molecules and salts which is important to keep

them separated from our analytes of interest, in terms of retention time. % matrix effects values were reported in Figure 4B.

For what concern the sample preparation, the strategy chose to clean up the biological samples was the protein precipitation with organic solvents (ppt). It is a quick technique, not expensive and suitable for large batch of samples. The limiting point of this technique is that is not always the best option, cause it could be tricky to find out the right solvents and solvents ratio for having a good extraction. Nowadays, the ppt is the most common way to extract adenylate and pyridine compounds⁴⁷, even if the recovery is not always greater than 80% for all the molecules studied. We developed two different ppt sample preparations for each matrix analyzed. The best conditions of ppt for having the highest % recovery values were used and the % recovery values were described in figure 4A. % recovery resulted slightly low for Ap4 and Nam. It could be due to the high polarity of both of these compounds, associated to the small structure of Nam. These facts could tend Ap4 and Nam to precipitate with the huge amount of protein in the matrices analyzed. The linearity was set using the external calibration method because all the analytes investigated are physiologically present in the cells or plasma samples. Nevertheless, the calibration curves of each compound were linear in the calibration range as demonstrated by the correlation coefficients reported in the last line of the table (Figure 4D).

Each biological sample was analyzed in analytical triplicate.

3.3 *In vitro* and *in vivo* Ap4 production and modulation

Focusing on murine NAMPT, whether as an intracellular enzyme acting in the amidated NAD-salvaging route³ that chiefly regulates NAD homeostasis⁷ or as an extracellular cytokine^{25,27}, we provide evidence for an Ap4 synthesis of potential relevance at both the cellular and systemic level. First, the NAMPT ATPase is modulated *in vitro* by several compounds targeting the enzyme active site, suggesting a capability to synthesize Ap4 from ATP both intracellularly, in the presence of PRTase reactants, and extracellularly, in the absence of most of them⁴⁸. Second, *in vivo* Ap4 levels correlate with intracellular and, to some extent, extracellular NAMPT expression levels (Table 2; Figure 6C), pointing that NAMPT may regulate Ap4 homeostasis in different mammalian tissues. Third, metabolic perturbation in cells is able to modulate both Ap4 and NMN synthesis, albeit to different extents (Figures 6A and 6B). Fourth, the treatment with FK866, a selective inhibitor of NAMPT PRTase, but not of NAMPT ATPase (Table 1), downregulates intracellular NAD levels^{9,49}, but in contrast it upregulates intracellular Ap4 levels (Table 2). This latter observation further indicates that the intrinsic and facultative reactions catalyzed by NAMPT should be equally considered when investigating the effects of NAMPT inhibitors.

Indeed, an additional finding from our work is that NAD and FK866 exert opposite effects on NAMPT regarding its Ap4 synthesis, respectively inhibiting or potentiating it. Both compounds target NAMPT at the active site but, while NAD competes with PRPP¹¹, FK866 binds at the dimer interface and competes with Nam for binding^{1,49}. In keeping with such distinct binding sites, we observed that FK866 behaves like Nam in potentiating the ATPase activity, while NAD behaves like PRPP in preventing it. This leads to suggest that FK866 binding to the catalytic pocket of NAMPT, contrary to NAD binding, does not block ATP binding and its catalytic processing. Furthermore, as reflected by the picomolar versus nanomolar Ki values reported for FK866 and NAD, respectively¹¹, we found that micromolar

concentrations of FK866 can neutralize the effect of millimolar NAD *in vitro*. Therefore, NAMPT targeting by FK866 results in a novel biological effect, i.e., the rise of physiological Ap4 levels, in addition to the well-documented NAD depletion effect. This should be taken into account when evaluating the actions of this drug.

From the point of view of cell physiology, the coincidental identification of Ap4 synthesis by NAMPT and NAPT might underlie a dual level regulation of NAD biosynthesis: a direct one, through the NMN/NaMN-forming activity, and an indirect one, through Ap4 signaling. In a plausible scenario, for example, Ap4 would reroute protein resources toward *de novo* NAD biosynthesis, which in mammals starts from tryptophan. Indeed, while inhibiting aminoacyl-tRNA synthetases³⁸, Ap4 might support the activity of proteasome³⁹, both processes converging in boosting tryptophan bioavailability. Speculation on the possible involvement of Ap4 in other intracellular pathways is hard to present at the moment, as the physiological targets for Ap4 are only putative.

On the other hand, in an extracellular context, Ap4 has recognized functions on purinergic signaling. In the rabbit eye this established function might be related to local NAMPT³⁵. Furthermore, our observation that ATP and Ap4 are both circulating in murine plasma, where NAMPT is also present (Figures 6C and 6D), confirms earlier reports^{28,48} and suggests the possibility that some extracellular functions of NAMPT might be based on its enzymatic synthesis of Ap4. In this light, it would be worth reassessing the reported cytokine-like functions of extracellular NAMPT^{12,50}. The debate about the existence of a link between the molecular action and the enzymatic function of extracellular NAMPT is not yet settled, and our results provide new important elements that should not be overlooked.

In conclusion, we have shown that NAMPT appears to be directly coupled to intracellular and/or extracellular Ap4 homeostasis in mammals. Given that both the intracellular and extracellular forms of this enzyme are recognized as relevant in a number of disease states⁵¹⁻⁵³, and that Ap4 has been already recognized as a potent

signaling molecule, future work on this enzyme should not disregard this novel function. Further investigation should also encompass the other NAD biosynthetic enzyme, NAPT, endowed with the same catalytic property.

4. Significance:

This study reports additional catalytic properties of NAMPT and NAPT, two ubiquitous enzymes that are crucial for the synthesis of the essential redox co-factor NAD. They share structural similarity and dual location in mammals, i.e., both intracellular and extracellular. Extracellular NAMPT is also regarded as a cytokine endowed with multiple signaling functions, and whether its catalyzed reaction is pertinent to these actions is at present unclear, with contradictory evidence from different experimental settings. From a catalytic point of view, both NAMPT and NAPT appear profligate consumers of ATP. Indeed, they use a facultative ATP hydrolysis to promote their NAD biosynthesis activity by weak energy coupling. This paradigmatic reaction represents the main subject of our investigation. Our most significant finding is that bacterial and mammalian NAMPTs and NAPT can also use ATP to form adenosine 5'-tetraphosphate (Ap₄), a prominent signaling molecule of an as-yet unclear biochemical origin. Based on *in vitro* and *in vivo* evidence, we propose (1) a mechanism for Ap₄ synthesis, (2) a chief contribution of NAMPT to Ap₄ homeostasis in mammals, and (3) a reassessment of the NAMPT drug targeting in this light. Indeed, we demonstrate that *in vivo* targeting of NAMPT by FK866, a drug inhibitor of NAD synthesis, results in a parallel upregulation of Ap₄ levels. This opens up pharmacological scenarios possibly missed before. In a broader perspective, a direct link of NAMPT to Ap₄ formation suggests novel mechanisms by which this enzyme, intracellularly and extracellularly, may exert the plethora of actions that are attributed to it.

Material and methods:*Experimental model and subject details:**Cell Lines*

B16 cells were engineered for NAMPT over-expression or silencing as follows. To generate a stable B16 FLAG-NAMPT cell line overexpressing NAMPT, a FLAG-NAMPT was cloned in the pLV-IRES-GFP bicistronic vector⁵⁶. The lentiviral particles were produced in HEK293T cells transfected with pMDLg/pRRE, pMD2.VSVG, pRSV-Rev⁵⁷, and pLVFLAG- NAMPT-IRES-GFP. Briefly, after 48 h, the cell medium was collected, filtrated, and centrifuged at 100,000 x g for 90 min. The viral particles in the pellet fraction were titrated, resuspended at appropriate concentrations, and used to infect B16 cells. Likewise, a stable B16 shNAMPT Low cell line silencing NAMPT was obtained after B16 infection with lentiviral particles. These particles were produced as described above in HEK293T cells by using a second-generation packaging plasmid system added with GIPZ Mouse Nampt Lentiviral shRNA plasmid. The infected cells were sorted for high levels of GFP (GFP++, called B16 shNAMPT Low cells). All B16 cells were normally cultured in DMEM supplemented with 10 % fetal bovine serum (FBS), 2 mg/mL glutamine, 10 U/mL penicillin and 100 lg/mL streptomycin. Typically, 1.5×10^6 cells were seeded and detached after 24 hours by trypsinization. When required, B16 cells were treated for 24 hours with 100 nM FK866. IC50 for FK866 on these cells is 122 nM at 72 hours. For metabolism perturbation, cells were grown for 20 hours after adhesion in DMEM (4.5 g/L glucose) \pm FBS, or MEM (1.0 g/L glucose) \pm FBS.

Animals

Eight weeks old C57BL/6 healthy male mice were grown and treated under procedures authorized by the animal ethical committee of the University of ‘‘Piemonte Orientale’’ (Novara, Italy).

Method details

Preparative HPLC Chromatography

The Ap4 from Jena Bioscience or from the ATPase assays described below was purified by HPLC onto a Tosoh Bioscience TSKgel DEAE-2SW (250346 mm) column. Elution was carried out at room temperature in volatile buffers, ammonium acetate 0.05M (A) and 1 M (B), at pH 5.5. The gradient applied at 1 mL/min flow rate was: 2.5 min at 25 % B; 23.5 min up to 60 % B; 2 min up to 100 % B; 4 min hold at 100 % B; 1 min down to 25 % B; 6 min hold at 25 % B. After subsequent injections of each sample in aliquots, the fractions corresponding to UV peaks eluting at ~22 min were pooled. The purified Ap4 was quantified from the Abs (260 nm) using an $\epsilon(260 \text{ nm})$ of $15.4 \text{ mM}^{-1}\text{cm}^{-1}$, then frozen and lyophilized.

Chemical and Enzymatic Digestion of the Purified NAMPT Product

Following preparative HPLC chromatography, Ap4 amounts of 0.5, 1 and 2 nmol appropriately lyophilized in cleaned, acid-washed glass tubes, were ashed in a magnesium nitrate/ethanol solution⁵⁸, before the chemically released organic Pi was quantified by Malachite green. A reference curve was created by treating in parallel pure ATP, ADP, and AMP (0.5 to 3 nmol each, from UV calibrated solutions). Alternatively, enzymatic digestions were carried out in either 0.3 mL mixtures containing ~0.4 U/mL calf intestine alkaline phosphatase in the supplied buffer, or 0.2 mL mixtures containing 0.04 mU/mL *Crotalus adamanteus phosphodiesterase I* in 0.1 M Tris/HCl buffer, pH 8.9, 0.1 M NaCl, 15 mM MgCl₂. The mixtures contained 20-40 mM of purified Ap4 and were treated and analysed by C18-HPLC (see Activity assays). The commercial phosphodiesterase used was contaminated by a 5'-nucleotidase activity.

Cloning, Expression, and Purification

The expression constructs used for mouse NAMPT and its H247E mutant are described in Grolla et al.³³, those for human NAPT and its H213A mutant in Galassi et al.¹⁷, that for *Acinetobacter baylyi* NadV in Sorci et al.⁴³, and that for *Streptococcus pyogenes* NadC in Sorci et al.⁵⁵. The expression construct for *Staphylococcus aureus* PncB was obtained in this study by PCR amplification from genomic DNA and cloning into a pET-derived vector. Their transformation into *E. coli* BL21(D3) competent cells, expression by induction with IPTG 0.5 mM for 17h at 26-28 °C, and purification by TALON chromatography were carried out essentially as described in Orsomando et al.⁵⁹. The purified enzymes were finally desalted on PD-10 in 50 mM HEPES/NaOH buffer, pH 7.5, 1mM TCEP, and stored at -80 °C. Their concentration was measured by the Bradford reagent protein assay. All these recombinant proteins were fused to N-terminal and/or C-terminal His-tag tails.

Activity Assays

One unit (U) is defined as the enzyme amount catalyzing 1 mmol/min product formation (or substrate consumption) at 25 °C. Rates were calculated in the linear region of v vs t plots (product accumulation versus time). The PRTase activities of NAMPT and NAPT (either NMN or NaMN synthesis) were measured by adapting a continuous assay based on detection at 340 nm of the NADH formed⁶⁰ in the presence of PncC, NadD, NadE, and ADH as the ancillary enzymes⁴. The mixtures for NAMPT assay contained, in 0.5 mL final volume, 80 mM HEPES/NaOH buffer, pH 7.5, 12 mM MgCl₂, 0.5 mg/mL bovine serum albumin, 75mM ethanol, 30mMsemicarbazide, 4.5mM NH₄Cl, 0.024 U/mL PncC, 0.192 U/mL NadD, 0.081 U/mL NadE, 12.5 U/mL ADH, 1 mM ATP, 0.5 mM PRPP, 0.5 mM Nam, and 20-40 mg/mL of enzyme to be tested. In NAPT assays, PncC was omitted, 50mM K₂HPO₄, pH 7.5, was included in addition¹⁷, and Na 0.5mM was used in place of

Nam. The pyridine substrate was usually added to start the reaction and, when indicated, mixtures were supplied with 2.5 mL of 10 mM FK866 in DMSO (50 mM final). Alternatively, the ATPase activities of NAMPT and NAPT (either ADP or Pi or Ap4 synthesis) were measured by discontinuous assays. The assay mixtures contained, in 0.2 mL final volume, 50 mM HEPES/NaOH buffer, pH 7.5, 5 mM MgCl₂, from 0.25 to 2.5 mM ATP, and from 0.03 to 2.3 mg/mL each enzyme (i.e. 0.5-40 mM based on average MW). The enzyme or ATP were added to start the reaction and, when indicated, mixtures were supplied with 1 mL of 10 mM FK866 in DMSO (50 mM final) or other compounds in water. During incubation, 20 μ L aliquots were collected at different times and stopped on ice by addition of 10 μ L HClO₄ 1.2 M. These aliquots were centrifuged, neutralized by addition of 6.8 μ L K₂CO₃ 1 M, and centrifuged again. For analytical purposes, the supernatants were injected into HPLC for separation and UV detection of both ADP and Ap4 formed, or treated with Malachite Green for VIS detection of the Pi formed⁵⁸. In this latter case, they were quenched with two volumes of Biomol Green reagent, left for 15 min on the bench, and read at 620 nm. A calibrated solution of KH₂PO₄ was used for Pi quantitation. The HPLC analysis was carried out either by ion pair-reverse phase chromatography onto a Supelcosil LC18-S (250346 mm) column as reported³, or by the above anion exchange TSK-DEAE chromatography (see Preparative HPLC). Both HPLC methods allowed separation of Ap4, ATP, ADP, AMP, and adenosine, as verified by coelution with corresponding standards. The integrated peak areas were converted into nanomoles as described³, using the ϵ (260 nm) of 15.4 mM⁻¹ cm⁻¹. Both NMN and NaMN after C18-HPLC were likewise quantified using an ϵ (260 nm) of 3.5 mM⁻¹ cm⁻¹.

Cell Extraction for Western Blot Analysis

To monitor NAMPT expression and stability in the engineered cell lines B16 FLAG-NAMPT and B16 shNAMPT Low, cultured cells were collected and lysed in a 20

mM HEPES/NaOH buffer, pH 7.5, containing 100 mM NaCl, 5 mM EDTA, 1 % Nonidet P-40, 1 mM PMSF, and appropriate aliquots of the Calbiochem Protease Inhibitor Cocktail Set VI. Proteins extracted were quantified by the BCA Protein Assay, separated on SDS-PAGE, blotted onto a nitrocellulose membrane, and stained with monoclonal antibodies specific for NAMPT and beta-Actin. Densitometry analysis was next performed with the Bio-Rad Quantity One program.

Cell Extraction for MS Analysis

The various B16 cells freshly grown and collected were frozen in liquid nitrogen and immediately lysed in 400 μ L water/acetonitrile (1:3 vol/vol). Proteins were precipitated by centrifugation. The supernatant was treated in two different ways before LC-ESI-MS analysis. For quantification of Ap4, ATP and ADP, a 300 μ L aliquot was evaporated in a rotational vacuum concentrator to dryness (for 4 h at 30 $^{\circ}$ C) and reconstituted in 80 μ L water/acetonitrile (1:1 vol/vol). For quantification of Nam, NMN and NAD, 80 μ L of supernatant were directly analyzed. Values in nmol were referred to mg of protein extracted and quantified from the cell lysate.

Mouse Plasma Sampling and Treatment

From 3 mice, blood samples were drawn three times on separate days, while from other 14 mice, a single blood sample was collected. Before LC-ESI-MS analysis, 100 μ L of plasma were added to 300 μ L of methanol, clarified by centrifugation, and then a 320 μ L aliquot was evaporated to dryness and reconstituted in 80 μ L water/acetonitrile (1:1 vol/vol). In parallel, 100 μ L of plasma without dilution were used to quantify the extracellular NAMPT content by means of the NAMPT (Visfatin/PBEF) (mouse/rat) Dual ELISA Kit.

LC-ESI-MS analysis of Pyridine and Adenine Nucleotides

Analyses were carried out onto a Thermo Finnigan LCQ Deca XP Plus system equipped with a quaternary pump, a Surveyor AS autosampler, and a vacuum degasser (Thermo Finnigan). The liquid chromatography was performed on a Phenomenex Luna HILIC column (150 x 2 mm, 3mm) with a Phenomenex Luna HILIC security guard column (4mmx 2 mm), at 25 °C, at 200 µL/min flow rate, under isocratic elution. The mobile phase was composed by a 70:30 (v/v) ratio of acetonitrile and 100 mM ammonium acetate buffer, pH 5.8. The injection volume was 5 mL and the run time was 20 min. The MS detection was performed using two different methods: negative polarity for Ap4 (SRM m/z 586 > 488 C.I.D. 25 eV), ATP (SRM m/z 506 > 408 C.I.D. 25 eV), and ADP (SRM m/z 426 > 328 C.I.D. 30 eV), and positive polarity for Nam (MSMS m/z 123 C.I.D. 25 eV), NMN (SRM m/z 335 > 123 C.I.D. 25 eV), and NAD (MRM m/z 664 > 542, 524 C.I.D. 25 eV). The instrument was set as follows: ion spray voltage, 4 kV; source current, 80 mA; capillary temperature, 350 °C; sheath gas flow (N₂), 60 Auxiliary Units (A.U.); sweep gas flow (N₂): 6.0 A.U., capillary voltage, -15.00 V (negative polarity) and 18.00 V (positive polarity); tube lens offset, -5.0 V (negative polarity) and 10.00 V (positive polarity); multipole 1 offset, 7.50 V (negative polarity) and -5.00 V (positive polarity); multipole 2 offset, 11.00 V (negative polarity) and -8.00 V (positive polarity).

Quantification and statistical analysis

All data represent the mean and SEM or SD of at least 3 independent experiments. T test analysis was carried out by PRISM program. A p value ≤ 0.05 was considered as significant and indicated in figures with asterisks (*). LC-MS data were acquired and processed using the Xcalibur[®] software. For quantification of Ap4, ATP, ADP, Nam, NMN and NAD in cell extracts and plasma samples, calibration curves in the appropriate range were prepared (external calibration method) with a correlation

coefficient (R^2) always > 0.99 ; data were corrected for recovery and matrix effect when present.

References:

1. Marletta, A.S., Massarotti, A., Orsomando, G., Magni, G., Rizzi, M., and Garavaglia, S. Crystal structure of human nicotinic acid phosphoribosyltransferase. *FEBS Open Bio.* **5**, 419–428 (2015).
2. Magni, G., Orsomando, G., Raffelli, N., and Ruggieri, S. Enzymology of mammalian NAD metabolism in health and disease. *Front Biosci.* **13**, 6135–6154 (2008).
3. Mori, V., Amici, A., Mazzola, F., Di Stefano, M., Conforti, L., Magni, G., Ruggieri, S., Raffaelli, N., and Orsomando, G. Metabolic profiling of alternative NAD biosynthetic routes in mouse tissues. *PLoS One* **9**, e113939 (2014).
4. Zamporlini, F., Ruggieri, S., Mazzola, F., Amici, A., Orsomando, G., and Raffaelli, N. Novel assay for simultaneous measurement of pyridine mononucleotides synthesizing activities allows dissection of the NAD(+) biosynthetic machinery in mammalian cells. *FEBS J.* **281**, 5104–5119 (2014).
5. Ruggieri, S., Orsomando, G., Sorci, L., and Raffaelli, N. Regulation of NAD biosynthetic enzymes modulates NAD-sensing processes to shape mammalian cell physiology under varying biological cues. *Biochim. Biophys. Acta* **1854**, 1138–1149 (2015).
6. Hara, N., Yamada, K., Shibata, T., Osago, H., Hashimoto, T., and Tsuchiya, M. Elevation of cellular NAD levels by nicotinic acid and involvement of nicotinic acid phosphoribosyltransferase in human cells. *J. Biol. Chem.* **282**, 24574–24582 (2007).

7. Revollo, J.R., Grimm, A.A., and Imai, S. The NAD biosynthesis pathway mediated by nicotinamide phosphoribosyltransferase regulates Sir2 activity in mammalian cells. *J. Biol. Chem.* **279**, 50754–50763 (2004).
8. Galli, U., Travelli, C., Massarotti, A., Fakhfour, G., Rahimian, R., Tron, G.C., and Genazzani, A.A. Medicinal chemistry of nicotinamide phosphoribosyltransferase (NAMPT) inhibitors. *J. Med. Chem.* **56**, 6279–6296 (2013).
9. Magni, G., Di Stefano, M., Orsomando, G., Raffaelli, N., and Ruggieri, S. NAD(P) biosynthesis enzymes as potential targets for selective drug design. *Curr. Med. Chem.* **16**, 1372–1390 (2009).
10. Burgos, E.S., Ho, M.C., Almo, S.C., and Schramm, V.L. A phosphoenzyme mimic, overlapping catalytic sites and reaction coordinate motion for human NAMPT. *Proc. Natl. Acad. Sci. USA* **106**, 13748–13753 (2009).
11. Burgos, E.S., and Schramm, V.L. Weak coupling of ATP hydrolysis to the chemical equilibrium of human nicotinamide phosphoribosyltransferase. *Biochemistry* **47**, 11086–11096 (2008).
12. Gross, J., Rajavel, M., Segura, E., and Grubmeyer, C. Energy coupling in *Salmonella typhimurium* nicotinic acid phosphoribosyltransferase: identification of His-219 as site of phosphorylation. *Biochemistry* **35**, 3917–3924 (1996).
13. Gross, J.W., Rajavel, M., and Grubmeyer, C. Kinetic mechanism of nicotinic acid phosphoribosyltransferase: implications for energy coupling. *Biochemistry* **37**, 4189–4199 (1998).
14. Grubmeyer, C.T., Gross, J.W., and Rajavel, M. Energy coupling through molecular discrimination: nicotinate phosphoribosyltransferase. *Methods Enzymol.* **308**, 28–48 (1999).

15. Rajavel, M., Lalo, D., Gross, J.W., and Grubmeyer, C. Conversion of a cosubstrate to an inhibitor: phosphorylation mutants of nicotinic acid phosphoribosyltransferase. *Biochemistry* **37**, 4181–4188 (1998).
16. Vinitsky, A., and Grubmeyer, C. A new paradigm for biochemical energy coupling. Salmonella typhimurium nicotinate phosphoribosyltransferase. *J. Biol. Chem.* **268**, 26004–26010 (1993).
17. Galassi, L., Di Stefano, M., Brunetti, L., Orsomando, G., Amici, A., Ruggieri, S., and Magni, G. Characterization of human nicotinate phosphoribosyltransferase: kinetic studies, structure prediction and functional analysis by site-directed mutagenesis. *Biochimie* **94**, 300–309 (2012).
18. Ramsey, K.M., Yoshino, J., Brace, C.S., Abrassart, D., Kobayashi, Y., Marcheva, B., Hong, H.K., Chong, J.L., Buhr, E.D., Lee, C., et al. Circadian clock feedback cycle through NAMPT-mediated NAD⁺ biosynthesis. *Science* **324**, 651–654 (2009).
19. Rehan, L., Laszki-Szczachor, K., Sobieszczanska, M., and Polak-Jonkisz, D. SIRT1 and NAD as regulators of ageing. *Life Sci.* **105**, 1–6 (2014).
20. Yoon, M.J., Yoshida, M., Johnson, S., Takikawa, A., Usui, I., Tobe, K., Nakagawa, T., Yoshino, J., and Imai, S. SIRT1-mediated eNAMPT secretion from adipose tissue regulates hypothalamic NAD⁺ and function in mice. *Cell Metab.* **21**, 706–717 (2015).
21. Samal, B., Sun, Y., Stearns, G., Xie, C., Suggs, S., and McNiece, I. Cloning and characterization of the cDNA encoding a novel human pre-Bcell colony-enhancing factor. *Mol. Cell Biol* **14**, 1431–1437 (1994).
22. Fukuhara, A., Matsuda, M., Nishizawa, M., Segawa, K., Tanaka, M., Kishimoto, K., Matsuki, Y., Murakami, M., Ichisaka, T., Murakami, H., et al. Visfatin: a protein secreted by visceral fat that mimics the effects of insulin. *Science* **307**, 426–430 (2005).

23. Audrito, V., Serra, S., Brusa, D., Mazzola, F., Arruga, F., Vaisitti, T., Coscia, M., Maffei, R., Rossi, D., Wang, T., et al. Extracellular nicotinamide phosphoribosyltransferase (NAMPT) promotes M2 macrophage polarization in chronic lymphocytic leukemia. *Blood* **125**, 111–123 (2015).
24. Skokowa, J., Lan, D., Thakur, B.K., Wang, F., Gupta, K., Cario, G., Brechlin, A.M., Schambach, A., Hinrichsen, L., Meyer, G., et al. NAMPT is essential for the G-CSF-induced myeloid differentiation via a NAD(+)-sirtuin-1-dependent pathway. *Nat. Med.* **15**, 151–158 (2009).
25. Sun, Z., Lei, H., and Zhang, Z. Pre-B cell colony enhancing factor (PBEF), a cytokine with multiple physiological functions. *Cytokine Growth Factor Rev.* **24**, 433–442 (2013).
26. Camp, S.M., Ceco, E., Evenoski, C.L., Danilov, S.M., Zhou, T., Chiang, E.T., Moreno-Vinasco, L., Mapes, B., Zhao, J., Gursoy, G., et al. Unique toll-like receptor 4 activation by NAMPT/PBEF induces NFkappaB signaling and inflammatory lung injury. *Sci. Rep.* **5**, 13135 (2015).
27. Li, Y., Zhang, Y., Dorweiler, B., Cui, D., Wang, T., Woo, C.W., Brunkan, C.S., Wolberger, C., Imai, S., and Tabas, I. Extracellular Nampt promotes macrophage survival via a nonenzymatic interleukin-6/STAT3 signaling mechanism. *J. Biol. Chem.* **283**, 34833–34843 (2008).
28. Tolle, M., Jankowski, V., Schuchardt, M., Wiedon, A., Huang, T., Hub, F., Kowalska, J., Jemielity, J., Guranowski, A., Loddenkemper, C., et al. Adenosine 5'-tetraphosphate is a highly potent purinergic endothelium derived vasoconstrictor. *Circ. Res.* **103**, 1100–1108 (2008).
29. Fraga, H., and Fontes, R. Enzymatic synthesis of mono and dinucleoside polyphosphates. *Biochim. Biophys. Acta* **1810**, 1195–1204 (2011).
30. Wang, T., Zhang, X., Bheda, P., Revollo, J.R., Imai, S., and Wolberger, C. Structure of Nampt/PBEF/visfatin, a mammalian NAD⁺ biosynthetic enzyme. *Nat. Struct. Mol. Biol.* **13**, 661–662 (2006).

31. Amici A., Grolla A. A., Del Grosso E., Bellini R., Bianchi M., Travelli C., Garavaglia S., Sorci L., Raffaelli N., Ruggieri S., Genazzani A. A., Orsomando G. Synthesis and degradation of adenosine 5'-tetrphosphate by nicotinamide and nicotinate phosphoribosyltransferases. *Cell Chemical Biology* **24** (5), 553-564 (2017).
32. Maldi, E., Travelli, C., Caldarelli, A., Agazzone, N., Cintura, S., Galli, U., Scatolini, M., Ostano, P., Miglino, B., Chiorino, G., et al. Nicotinamide phosphoribosyltransferase (NAMPT) is over-expressed in melanoma lesions. *Pigment Cell Melanoma Res.* **26**, 144–146 (2013).
33. Grolla, A.A., Torretta, S., Gnemmi, I., Amoruso, A., Orsomando, G., Gatti, M., Caldarelli, A., Lim, D., Penengo, L., Brunelleschi, S., et al. Nicotinamide phosphoribosyltransferase (NAMPT/PBEF/visfatin) is a tumoural cytokine released from melanoma. *Pigment Cell Melanoma Res.* **28**, 718–729 (2015).
34. Huang, D., Zhang, Y., and Chen, X. Analysis of intracellular nucleoside triphosphate levels in normal and tumor cell lines by high-performance liquid chromatography. *J. Chromatogr. B Analyt Technol. Biomed. Life Sci.* **784**, 101–109 (2003).
35. Marrian, D.H. A new adenine nucleotide. *Biochim. Biophys. Acta* **13**, 278–281 (1954).
36. Pintor, J., Pelaez, T., and Peral, A. Adenosine tetraphosphate, Ap₄, a physiological regulator of intraocular pressure in normotensive rabbit eyes. *J. Pharmacol. Exp. Ther.* **308**, 468–473 (2004).
37. North, R.A. P2X receptors. *Philos. Trans. R. Soc. Lond. B Biol. Sci* **371**, pii: 20150427 (2016).
38. Retailleau, P., Weinreb, V., Hu, M., and Carter, C.W., Jr. Crystal structure of tryptophanyl-tRNA synthetase complexed with adenosine-5' tetraphosphate: evidence for distributed use of catalytic binding energy in amino acid

- activation by class I aminoacyl-tRNA synthetases. *J. Mol. Biol.* **369**, 108–128 (2007).
39. Gunther Sillero, M.A., de Diego, A., Silles, E., and Sillero, A. Synthesis of (di)nucleoside polyphosphates by the ubiquitin activating enzyme E1. *FEBS Lett.* **579**, 6223–6229 (2005).
40. Sukalski, K.A., and Nordlie, R.C. Glucose-6-phosphatase: two concepts of membrane-function relationship. *Adv. Enzymol. Relat. Areas Mol. Biol.* **62**, 93–117 (1989).
41. Chung, S.I., and Folk, J.E. Kinetic studies with transglutaminases. The human blood enzymes (activated coagulation factor 13 and the Guinea pig hair follicle enzyme). *J. Biol. Chem.* **247**, 2798–2807 (1972).
42. Amici, A., Emanuelli, M., Ruggieri, S., Raffaelli, N., and Magni, G. Kinetic evidence for covalent phosphoryl-enzyme intermediate in phosphotransferase activity of human red cell pyrimidine nucleotidases. *Methods Enzymol.* **354**, 149–159 (2002).
43. Sorci, L., Blaby, I., De Ingeniis, J., Gerdes, S., Raffaelli, N., de Crecy Lagard, V., and Osterman, A. Genomics-driven reconstruction of *Acinetobacter* NAD metabolism: insights for antibacterial target selection. *J. Biol. Chem.* **285**, 39490–39499 (2010).
44. Gholson, R.K., Ueda, I., Ogasawara, N., and Henderson, L.M. The enzymatic conversion of quinolinate to nicotinic acid mononucleotide in mammalian liver. *J. Biol. Chem.* **239**, 1208–1214 (1964).
45. Shimosaka, M., Fukuda, Y., Murata, K., and Kimura, A. Purification and properties of orotate phosphoribosyltransferases from *Escherichia coli* K-12, and its derivative purine-sensitive mutant. *J. Biochem.* **98**, 1689–1697 (1985).

46. Bello, Z., Stitt, B., and Grubmeyer, C. Interactions at the 2 and 5 positions of 5-phosphoribosyl pyrophosphate are essential in *Salmonella typhimurium* quinolinate phosphoribosyltransferase. *Biochemistry* **49**, 1377–1387 (2010).
47. Zhang G., Walker A. D., Lin Z., Han X., Blatnik M., Steenwyk R. C., Groeber E. A. Strategies for quantitation of endogenous adenine nucleotides in human plasma using novel ion-pair hydrophilic interaction chromatography coupled with tandem mass spectrometry. *J. Chromatogr. A* **1325**, 129–136 (2014).
48. Hara, N., Yamada, K., Shibata, T., Osago, H., and Tsuchiya, M. Nicotinamide phosphoribosyltransferase/visfatin does not catalyze nicotinamide mononucleotide formation in blood plasma. *PLoS One* **6**, e22781 (2011).
49. Khan, J.A., Tao, X., and Tong, L. Molecular basis for the inhibition of human NMPRTase, a novel target for anticancer agents. *Nat. Struct. Mol. Biol.* **13**, 582–588 (2006).
50. Zhao, Y., Liu, X.Z., Tian, W.W., Guan, Y.F., Wang, P., and Miao, C.Y. Extracellular visfatin has nicotinamide phosphoribosyltransferase enzymatic activity and is neuroprotective against ischemic injury. *CNS Neurosci. Ther.* **20**, 539–547 (2014).
51. Garten, A., Schuster, S., Penke, M., Gorski, T., de Giorgis, T., and Kiess, W. Physiological and pathophysiological roles of NAMPT and NAD metabolism. *Nat. Rev. Endocrinol.* **11**, 535–546 (2015).
52. Grolla, A.A., Travelli, C., Genazzani, A.A., and Sethi, J.K. Extracellular nicotinamide phosphoribosyltransferase, a new cancer metabokine. *Br. J. Pharmacol.* **173**, 2182–2194 (2016).
53. Shackelford, R.E., Mayhall, K., Maxwell, N.M., Kandil, E., and Coppola, D. Nicotinamide phosphoribosyltransferase in malignancy: a review. *Genes Cancer* **4**, 447–456 (2013).

54. Colombano, G., Travelli, C., Galli, U., Caldarelli, A., Chini, M.G., Canonico, P.L., Sorba, G., Bifulco, G., Tron, G.C., and Genazzani, A.A. A novel potent nicotinamide phosphoribosyltransferase inhibitor synthesized via click chemistry. *J. Med. Chem.* **53**, 616–623 (2010).
55. Sorci, L., Blaby, I.K., Rodionova, I.A., De Ingeniis, J., Tkachenko, S., de Crecy-Lagard, V., and Osterman, A.L. Quinolate salvage and insights for targeting NAD biosynthesis in group A streptococci. *J. Bacteriol.* **195**, 726–732 (2013).
56. Enomoto, M., Bunge, M.B., and Tsoufas, P. A multifunctional neurotrophin with reduced affinity to p75NTR enhances transplanted Schwann cell survival and axon growth after spinal cord injury. *Exp. Neurol.* **248**, 170–182 (2013).
57. Dull, T., Zufferey, R., Kelly, M., Mandel, R.J., Nguyen, M., Trono, D., and Naldini, L. A third-generation lentivirus vector with a conditional packaging system. *J. Virol.* **72**, 8463–8471 (1998).
58. Hess, H.H., and Derr, J.E. Assay of inorganic and organic phosphorus in the 0.1-5 nanomole range. *Anal. Biochem.* **63**, 607–613 (1975).
59. Orsomando, G., Cialabrini, L., Amici, A., Mazzola, F., Ruggieri, S., Conforti, L., Janeckova, L., Coleman, M.P., and Magni, G. Simultaneous single sample determination of NMNAT isozyme activities in mouse tissues. *PLoS One* **7**, e53271 (2012).
60. Balducci, E., Emanuelli, M., Raffaelli, N., Ruggieri, S., Amici, A., Magni, G., Orsomando, G., Polzonetti, V., and Natalini, P. Assay methods for nicotinamide mononucleotide adenylyltransferase of wide applicability. *Anal. Biochem.* **228**, 64–68 (1995).

Chapter 5

5. Proneurogenic effects of trazodone in murine and human neural progenitors

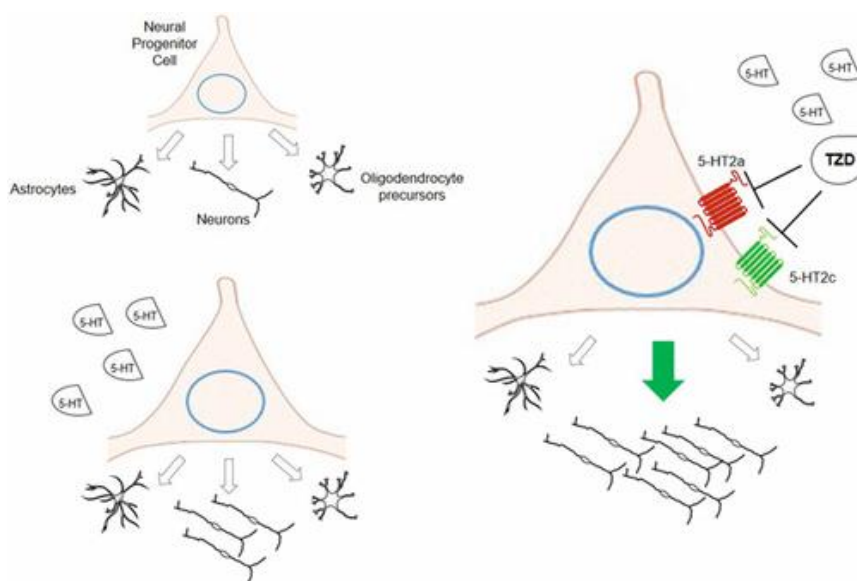
Valeria Bortolotto^{a,c}, Francesca Mancini^d, Giorgina Mangano^d, Rita Salem^{a,c}, Er Xia^{a,c}, Erika Del Grosso^{b,c}, Michele Bianchi^{b,c}, Pier Luigi Canonico^c, Lorenzo Polenzani^d, Mariagrazia Grilli^{a,c,*}

^aLaboratory of Neuroplasticity, ^bLaboratory of Pharmaceutical Analysis, ^cDepartment of Pharmaceutical Sciences, University of Piemonte Orientale “Amedeo Avogadro”, Via Bovio 6, Novara, 28100 Italy

^dAngelini S.p.A - RR&D, Angelini Research Center, Piazzale della Stazione, 00071 S. Palomba-Pomezia (Roma), Italy

* Corresponding author

Graphical Abstract:



Abstract:

Adult hippocampal neurogenesis (ahNG) in mammals is increased by several antidepressant drugs. Trazodone (TZD) is a multimodal antidepressant drug with a unique pharmacological profile. However, TZD effects on ahNG are still unknown and a new bioanalytical tool is essential to deeply understand its mechanism of action in neural progenitor cells (NPC). So, the aim of the work was to develop a new LC-MS bioanalytical method for the quantification of serotonin (5-HT) extracellular levels in primary cultures of murine NPC exposed to different stimuli. For our studies, differentiation media of murine adult hippocampal NPC (ahNPCs) was collected and proceeded for the proteins removal through a protein precipitation step. The liquid chromatography was performed on a Phenomenex Luna HILIC column while the serotonin MS detection was carried out in single reaction monitoring mode. Some LC-MS method parameters were assessed, such as: Selectivity, LLOQ and LOD, Linearity, % Recovery and % Matrix Effect. The method was successfully applied for measuring 5-HT levels in extracellular media of ahNPC. The results collected allowed us to demonstrate that ahNPCs cells do synthesize, release and uptake, by expressed SERT, 5-HT. Indeed, irreversible inhibition of tryptophan hydroxylase, a rate-limiting enzyme in serotonin biosynthesis, resulted in undetectable extracellular levels of 5-HT. Moreover, 5-HT levels are increased in extracellular media when cells were treated with proneurogenic concentrations of TZD (100 nM; 1.25 ± 0.20 ng/mL, $p = 0.07$) and fluoxetine, FLX (1 μ M; 1.76 ± 0.10 ng/mL, $p < 0.01$) *vs* basal vehicle conditions (0.86 ± 0.19 ng/mL). Nevertheless, SERT blockage cannot be considered the main mechanism with which TZD exerts its novel proneurogenic effects.

1. Introduction:

Adult hippocampal neurogenesis (ahNG) is a key and hot topic in the neuroscience research^{1,2}. The search for factors that modulate the birth of new neurons produced preclinical and clinical evidence. In fact, it has been demonstrated that the hippocampal neurogenesis is downregulated in stress and depression conditions^{3,4}. Nevertheless, among multiple signals which are related to this process, the serotonin (5-hydroxytryptamine, 5-HT) homeostasis plays a key role. Indeed, in the case of depression, the chronic modulation by antidepressant agents that inhibit serotonin reuptake in synapsis, leads to an upregulation of neural progenitor cells (NPC) proliferation and neurogenesis^{5,6}. In this context, *in vitro* studies on the murine adult hippocampal NPC (ahNPCs) could help in understanding the proneurogenic potential of antidepressant drugs and the underlying mechanisms. Trazodone (TZD) is a triazolopyridine derivate and can be recognized as the first multimodal antidepressant due to its activities on various targets^{7,8,9}. So far, the potential proneurogenic effect of this compound has never been investigated.

In literature various LC-MS methods are reported to quantify serotonin and other small molecules in biological matrices as cerebrospinal fluid¹⁰, rat brain tissue¹¹, plasma¹², blood¹³, serum¹⁴ and urine¹⁵. However, none of them deals with the analysis of extracellular differentiation media. So, in order to evaluate whether TZD proneurogenic effects require 5-HT synthesis by murine ahNPCs, the aim of the work was to develop a new LC-MS bioanalytical method to quantify 5-HT in extracellular media of murine ahNPCs.

2. Material and Methods:

2.1. Reagents and chemicals

The source of reagent and chemical was as follows: acetonitrile (HPLC grade), formic acid, 5-Hydroxytryptamine hydrochloride (5-HT) trazodone hydrochloride (TZD), DL-P-chlorophenylalanine (PCPA), and fluoxetine hydrochloride were purchased from Sigma-Aldrich (Milan, Italy). Water (HPLC grade) was obtained from Milli-Q RO system.

2.2 LC-MS bioanalytical method

LC-ESI-MS analyses were carried out using a Thermo Finnigan LCQ Deca XP Plus system equipped with a quaternary pump, a Surveyor AS autosampler and a vacuum degasser (Thermo Finnigan, San Jose, CA). The liquid chromatography was performed on a Phenomenex Luna HILIC column (150 x 2 mm, 3 μ m) with a Phenomenex Luna HILIC security guard column (4 mm x 2 mm), at 25 °C, at 200 μ l/min flow rate, under isocratic elution. The mobile phase was composed by a 90:10 ratio of acetonitrile and water (both with 0.2% v/v of formic acid). The injection volume was 5 μ l and the run time was 20 min. The MS detection of serotonin was performed in positive ionization mode. Quantitation was carried out using single reaction monitoring (SRM) mode to monitor the transition m/z 177 > 160 (Collision-Induced dissociation C.I.D. 20 eV). The principle instrument parameters were set as follows: ion spray voltage, 5.2 kV; source current, 80 μ A; capillary temperature, 350°C.

2.3 Preparation of serotonin stock solution

The stock standard solutions of the serotonin were prepared by dissolving its powder accurately weighted amounts (5.0 mg) in 5 ml of water (HPLC grade). The solution was kept in darkness at -24°C. This solution was stable for at least one month and

was diluted in water/acetonitrile with 0.2% formic acid (7:3 vol/vol). before the use to the required concentrations.

2.4 LC-MS method parameters

LC-MS bioanalytical method was assessed for the following parameters: Selectivity, Lower Limit of Quantification (LLOQ), Linearity, % Recovery and % Matrix Effect.

2.4.1 Selectivity

The LC-MS method selectivity has been evaluated by the injection of matrix blank samples arising from six different batches. The presence of matrix components, degradations products and impurities which may interfere with the analyte of interest has been investigated.

2.4.2 Lower Limit of Quantification (LLOQ) and Limit of Detection (LOD)

The determination of LLOQ and LOD was based on signal-to-noise ratio: this was evaluated by comparing measured signals from samples of Serotonin at low concentrations with those of blank samples and by establishing the minimum concentration at which the analyte can be quantified (LLOQ; S/N = 10) and the minimum concentration at which the analyte can be detected (LOD; S/N = 3).

2.4.3 Linearity

The linearity was performed using the internal calibration method. It assessed at six concentration levels in a range of 1 – 100 ng/mL by diluting the standard stock solution in differentiation media treated with acetonitrile with 0.2% formic acid (3:7, vol/vol). These points were injected in analytical triplicate and the peak areas were inputted into a Microsoft Excel[®] spread-sheet to plot calibration curves.

2.4.4 % Recovery (% RE) and % Matrix Effect (% ME)

% Recovery and % Matrix Effect were evaluated at three concentration levels: 1 – 50 – 100 ng/mL preparing three different samples starting from serotonin stock solution: (A) sample prepared in water/acetonitrile with 0.2% formic acid (7:3 vol/vol); (B) sample prepared adding the standard to the blank matrix after the protein precipitation step; (C) sample prepared adding the standard to the blank matrix before the protein precipitation step. Then, % RE and % ME were calculated with the following formula:

$$\% RE = \frac{C}{B} \times 100$$

$$\% ME = \frac{B}{A} \times 100$$

The matrix effect was evaluated also with the post infusion method¹⁶. Briefly, this method consists in the injection of a blank matrix samples on the LC column and at the same time in the continuously flow injection of the sample (A) directly in the ion source. There is an evaluation of the increase and / or suppression of the signal caused by the matrix in proximity of the analyte retention time.

2.5 Animals

Male C57BL/6 (C57BL/6, The Jackson Laboratories, US) mice were acclimated under light- and temperature-controlled conditions in high efficiency particulate air (HEPA)-filtered Thoren units (Thoren Caging System, Hazelton, PA). Mice were housed in number of 3-4/cage with *ad libitum* access to food and water at the animal facility of Piemonte Orientale University. Animal care and handling were carried out according to protocols approved by the European Community Directive and the local Institutional Animal Care and Use Committees (IACUC).

2.6 Isolation and Culture of Adult Hippocampal Neural Progenitor Cells (ahNPCs)

Adult murine hippocampal NPC isolation was performed as previously described¹⁷. Briefly, for each culture preparation three adult male mice (3-4 months-old) were euthanized by cervical dislocation, and their hippocampi dissected. Tissue was digested by a Papain Dissociation System (Worthington DBA, Lakewood, NJ). Cells were plated in NUNC EasyFlask 25 cm² (Thermo Scientific, Waltham, MA) and cultured in serum-free complete proliferation medium [Neurobasal-A with B27 supplement, 2 mM glutamine (Gibco, Life Technologies, Monza, IT), 20 ng/ml recombinant human Epidermal Growth Factor (rhEGF), 10 ng/ml of recombinant human Fibroblast Growth Factor-2 (rhFGF-2, PeproTech, Rocky Hill, NJ) and 4 µg/ml heparin sodium salt (Sigma-Aldrich)]. Passage 1 (P1) neurospheres were dissociated for the first time after ten days *in vitro* (DIV). From P2, dissociation was performed every five days and NPC were replated at a density of 12,000 cells/cm². NPC were used for proliferation and differentiation experiments from P5 to P30. Proliferating NPC were routinely tested for their undifferentiated state by expression of SOX2 (Sry-related HMG box transcription factor) and nestin (Type VI intermediate filament). For irreversible inhibition of tryptophane hydroxylase (TPH), cells were treated with 50 µM of PCPA or vehicle for 72 hours starting from the second day after dissociation. At day 5, cells were dissociated and plated for differentiation.

2.7 Sample preparation for LC-MS analysis

Vehicle- or PCPA-treated ahNPC were differentiated in presence of vehicle, trazodone or fluoxetine. Differentiation media were collected after 24 hours and centrifuged for 10 min at 16,000 g. 140 µl of acetonitrile with 0.2% of formic acid were added to 60 µl of collected media. Proteins were precipitated by centrifugation for 10 min at 11,300 g. An aliquot of 180 µl of supernatant was evaporated to dryness in a rotational vacuum concentrator (for about 4h at 40 °C). The sample was

reconstituted in 80 μ l of water/acetonitrile with 0.2% of formic acid (3:7 vol/vol), before the injection. For quantification of serotonin in differentiation medium, a calibration curve was prepared in blank matrix (differentiation medium treated with acetonitrile with 0.2% of formic acid, 3:7 vol/vol) in the appropriate range.

2.8 Statistical analysis

All experiments were run in triplicates using different cell preparations and repeated at least three times. Data were expressed as mean \pm S.D. and analyzed by one-way analysis of variance (ANOVA), followed by Tuckey's post-hoc test or by Student's *t* test. Statistical significance level was set for *p* values < 0.05.

3. Results and discussion:

3.1 LC-MS bioanalytical method development

To quantify 5-HT extracellular level of murine adult hippocampal neural progenitor cells (ahNPCs), we developed a new LC-MS bioanalytical method. MS source conditions were set up by flow injection analysis of serotonin standard. Analyses were performed in positive ionization mode working in low mass range (< 250 u), considering the low M.W. of 5-HT. Fragmentation mechanism of serotonin has been investigated in order to select the best fragmentation reaction to set up an appropriate Single Reaction Monitoring (SRM) scan suitable for a quantitative study. A collision-induced dissociation energy was optimized at 22 eV on mother ion *m/z* 177 [M+H]⁺ to monitor daughter ion *m/z* 160 [M+H]⁺. The full MS, MS₂ and MS₃ spectra are reported in Figure 1.

During the development of the chromatography part of the method, different stationary phases were considered and tested. Lipophilic stationary phases were excluded, and the attention was focused on the polar one due to the polarity moieties and the small dimension of 5-HT. Phenomenex Synergy Polar, Phenomenex Kinetex

F5, Phenomenex Luna HILIC and Phenomenex Kinetex HILIC were tested. Best results in terms of retention time, peak shapes and matrix effect were obtained with the Phenomenex Luna HILIC (150 x 2 mm, 3 μm). Its polar selectivity under hydrophilic liquid chromatography conditions was essential to increase the serotonin retention time, and so to avoid matrix effect. The main media components, which may cause a matrix effect, have a retention at the death time of the column thanks to their high polarity. The mobile phase was composed by eluent A: water with 0.2% formic acid and eluent B: acetonitrile with 0.2% formic acid using an isocratic method (A/B, 90/10, vol/vol). The flow rate was 200 $\mu\text{l min}^{-1}$ and the elution was kept at 25°C. Some Gradient elution was tested increasing the phase B during the time. We did not obtain positive results, mainly in terms of matrix effect. Nevertheless, the run time was 20 min to allow all the matrix components to elute out of the column and to avoid interference signals from the previous analytical run. We report an LC-MS chromatogram of serotonin with the method developed in Figure 1.

The sample preparation was developed with the aim to have a quick, reproducible and inexpensive procedure, which allows a full recovery in terms of serotonin. There are different techniques for cleaning the biological samples and for extracting 5-HT from biological samples like the protein precipitation from rat brain^{18,19}, plasma²⁰, platelet depleted plasma²¹, CSF^{10,22}, serum^{22,14}, the solid phase microextraction from CSF²³, the solid phase extraction²⁴⁻²⁷ for urine and liquid-liquid extraction for rat brain tissue^{28,29}.

In this context, the approach chosen to clean up the extracellular media was a protein precipitation (ppt) step with acetonitrile 0.2% formic acid. For 60 μL of collected media, 140 μl of ppt solvent was added. This ratio between media and organic solvent is the result of the optimization process. High amount of acetonitrile gave bad results in terms of recovery. At the same time, less amount of acetonitrile did not allow a good protein and matrix components precipitation. 0.2% formic acid

increased the precipitation in all tested conditions. Moreover, an evaporation step was included in the sample preparation protocol, useful to concentrate the biological sample before the injection. This approach allows a satisfactory % RE for the serotonin extraction.

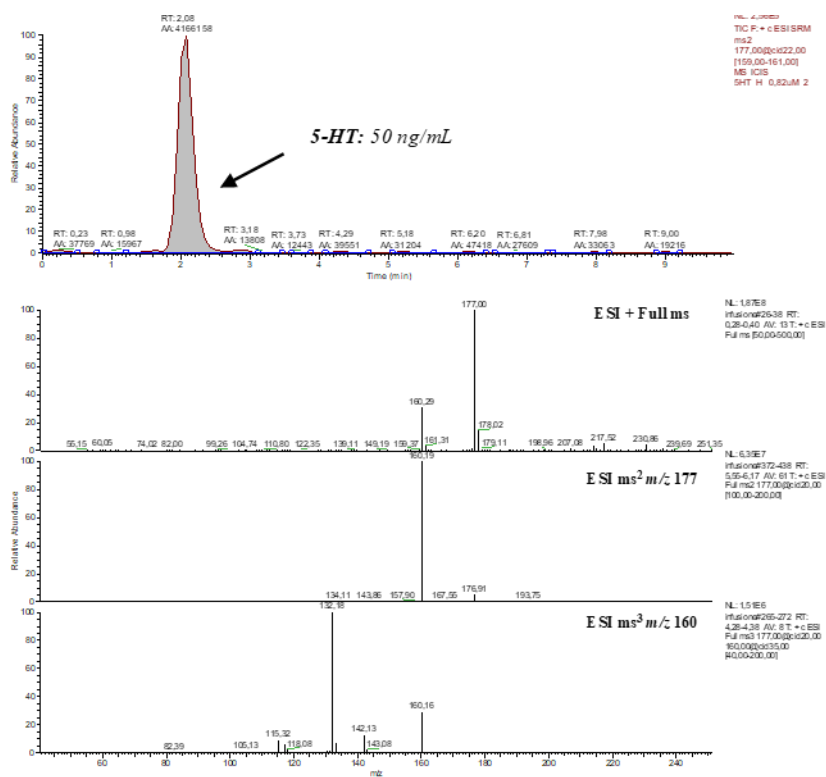


Figure 1. LC-MS chromatogram, ESI + full mass, ESI + MS2 and ESI + MS3 spectra of 5-HT

3.2 LC-MS bioanalytical method parameters

Before analyzing the biological samples, the LC-MS method was assessed for the following method parameters: Selectivity, Linearity, LLOQ and LOD, % RE and % ME.

3.2.1 Selectivity

As shown in Figure 1, The LC-MS method resulted selective for Serotonin. In 5-HT scan there are not any media components, degradation products of impurities which interfere with the serotonin peak.

3.2.2 LLOQ and LOD

LLOQ and LOD were established in 1.00 ng/mL and 0.30 ng/mL, respectively. It is reported in literature other LC-MS bioanalytical methods with even lower values^{20,30,31}. At the same time, the LLOQ and LOD values reached with this method are more than enough to apply it for the study of ahNPCs extracellular concentration of serotonin.

3.2.3 Linearity

The linearity was set using the internal calibration method. The linearity of the method was calculated as unweighted linear regression $y = ax + b$. Nevertheless, the serotonin calibration curve was linear in the calibration range as demonstrated by the correlation coefficient greater than 0.999. All the data regarding the linearity were summarized in Table 1.

Linearity data	
Analyte	Serotonin
Range (ng/ml)	1-100
Slope (m)	35381.7
Intercept (q)	-321.3
R²	0.9992
LLOQ (ng/ml)	1.00
LOD(ng/ml)	0.30

Table 1. Linearity, LLOQ and LOD data

3.2.4 % Recovery and % Matrix Effect

% Recovery and % Matrix Effect are reported in Figure 2A. All the % RE collected at three different levels of concentration were greater than 77 %. So, all of the recovery values were satisfactory, meaning that the serotonin extraction procedure from extracellular media is working properly. Also the % ME show good values, all of them greater than 82 % meaning that there is not an increase or a suppression due to the matrix on serotonin signal in the LC-MS run. The matrix effect has been evaluated also with the post infusion method as described by Matuszewski et al.¹⁶ Also in this case, the matrix effect could be considered more or less of the 10 %, and so negligible.

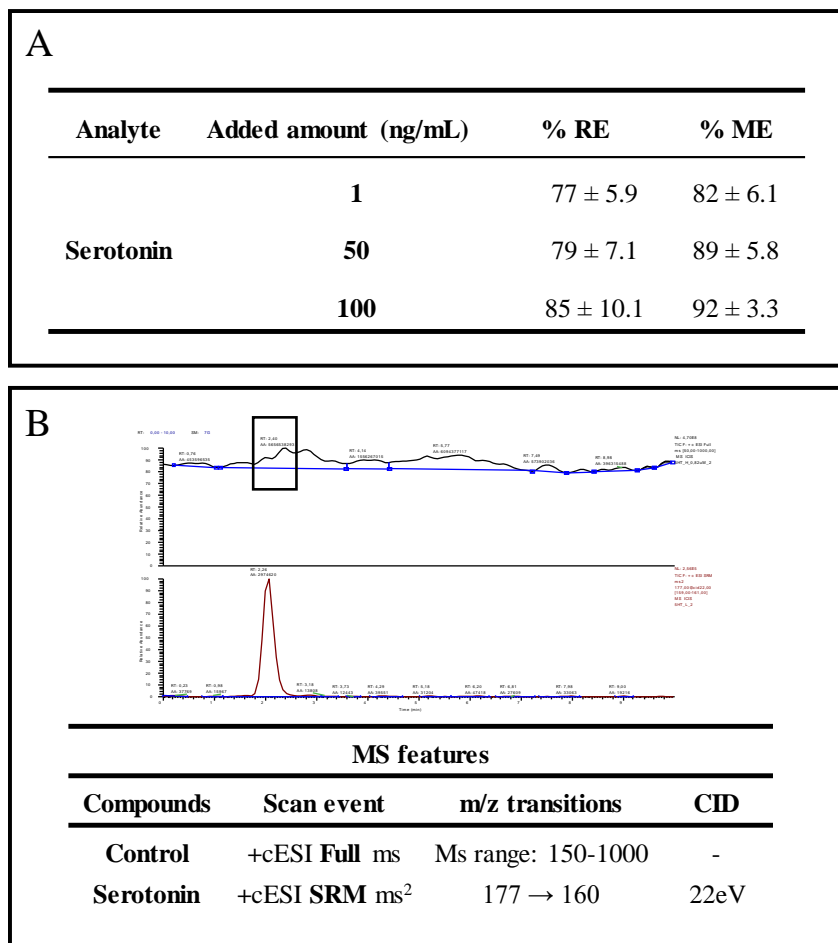


Figure 2. (A) % RE and % ME of serotonin at three different levels. (B) ME evaluated with the post infusion method

3.3 LC-MS bioanalytical method application

The LC-MS method developed was applied to quantify the extracellular levels of 5-HT in primary cultures of ahNPC in presence of different drugs including exposure for 24 h to trazodone and, as a control, fluoxetine (FLX). All the data regarding cell treatment with antidepressant drugs are described by Bortolotto et al.⁷ The same paper establish, for the first time, the *in vitro* proneurogenic effects of TZD at therapeutically relevant concentrations. With the results collected from the LC-MS experiment (Figure 3), we demonstrated: 5-HT levels are increased in extracellular media when cells were treated with TZD (1.25 ± 0.20 ng/mL, $p = 0.07$) and FLX

(1.76 ± 0.10 ng/mL, $p < 0.01$) in proneurogenic concentrations vs vehicle-treated conditions (0.86 ± 0.19 ng/mL). According to this data, fluoxetine (a selective serotonin reuptake inhibitor) treatment showed a statistically significant increase in terms of extracellular serotonin levels, as expected by its established ability to block SERT. Nevertheless, although serotonin extracellular levels are increased in TZD treatment conditions, there is not a statistically significant difference against vehicle condition ($p > 0.05$). According to this data, we could propose the following: (1) SERT blockage cannot be established as a major mechanism by which TZD exerts its proneurogenic effects. (2) Para-chlorophenylalanine (PCPA) treatment reduced 5-HT extracellular levels, making them undetectable (< 0.3 ng/mL, LOD). PCPA is a selective and irreversible inhibitor of tryptophan hydroxylase, a rate-limiting enzyme in serotonin biosynthesis. So, cellular enzyme blockade resulted in depletion of serotonin in the extracellular culture media.

Finally, taking together all of these results, we demonstrated that ahNPCs cells do synthesize and release in the extracellular compartment 5-HT which can also be taken up by SERT expressed on these cells.

Analyte	Samples	Conc \pm sd (ng/mL)	p value
Serotonin	Veh	0.86 \pm 0.19	-
	TZD 100 nM	1.25 \pm 0.20	0.07
	FLX 1 μ M	1.76 \pm 0.10	< 0.01 **
	PCPA 50 μ M	n.d.	-

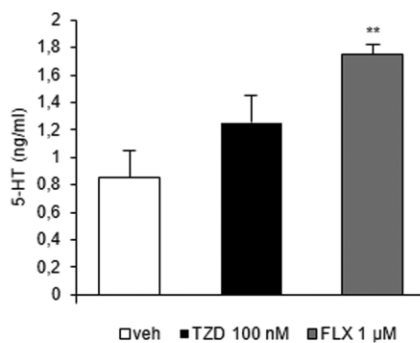


Figure 3. LC-MS analysis of extracellular 5-HT content in our *in vitro* model under basal conditions and after treatment with 1 μ M FLX, 100 nM TZD and 50 μ M PCPA

4. Conclusion:

In this work, it is described a new LC-MS bioanalytical method for the quantification of serotonin extracellular levels. This method has been successfully applied on murine ahNPCs exposed to different antidepressant drugs *vs* basal conditions. Thanks to this protocol some biological aspects regarding TZD proneurogenic mechanism of action were elucidated.

References:

1. Toda T., Parylak S. L., Linker S. B. and Gage F. H. The role of adult hippocampal neurogenesis in brain health and disease. *Mol. Psychiatry*. Ahead of print (2018).
2. Kempermann G., Song H., and Gage F. H. Neurogenesis in the Adult Hippocampus. *Cold Spring Harb. Perspect. Biol.* **7 (9)**, 1-14 (2015).
3. Mirescu C., and Gould E. Stress and adult neurogenesis. *Hippocampus* **16**, 233-238 (2006).
4. Kempermann, G. Krebs J., and Fabel K. The contribution of failing adult hippocampal neurogenesis to psychiatric disorders. *Curr. Opin. Psychiatry* **21**, 290-295 (2008).
5. Malberg J. Implications of adult hippocampal neurogenesis in antidepressant action. *J. Psychiatry Neurosci.* **29 (3)**, 196-205 (2004).
6. Alenina N., Klempin F. The role of serotonin in adult hippocampal neurogenesis. *Behavioural Brain Res.* **277**, 49-57 (2015).
7. Bortolotto V., Mancini F., Mangano G., Salem R., Xia E., Del Grosso E., Bianchi M., Canonico P. L., Polenzani L. and Grilli M. Proneurogenic effects of trazodone in murine and human neural progenitors, *ACS Chem. Neurosci.* **8 (9)**, 2027–2038 (2017).
8. Fagiolini A., Comandini A., Catena Dell’Osso M. and Kasper S. Rediscovering trazodone for the treatment of major depressive disorder. *CNS Drugs* **26**, 1033-1049 (2012).
9. Stahl S.M. Mechanism of action of trazodone: a multifunctional drug. *CNS Spectr.* **14**, 536-546 (2009).
10. Kovac A., Somikova Z., Zilka N., Novak M. Liquid chromatography–tandem mass spectrometry method for determination of panel of neurotransmitters in cerebrospinal fluid from the rat model for tauopathy. *Talanta* **119**, 284-290 (2014).

11. Wojnicz A., Ortiz J. A., Casas A. I., Freitas A. E., López M. G., and Ruiz-Nuño A. Simultaneous determination of 8 neurotransmitters and their metabolite levels in rat brain using liquid chromatography in tandem with mass spectrometry: Application to the murine Nrf2 model of depression. *Clin. Chim Acta.* **453**, 174-181 (2016).
12. Cai H. L., Zhu R. H., and Li H. D. Determination of dansylated monoamine and amino acid neurotransmitters and their metabolites in human plasma by liquid chromatography-electrospray ionization tandem mass spectrometry. *Anal. Biochem.* **396**, 103-111 (2010).
13. Johnsen E., Leknes S., Wilson S. R. and Lundanes E. Liquid chromatography-mass spectrometry platform for both small neurotransmitters and neuropeptides in blood, with automatic and robust solid phase extraction. *Sci. Rep.* **5**, 9308 (2015).
14. Choi J. M., Park W. S., Song K. Y., Lee H. L., and Jung B. H. Development of simultaneous analysis of tryptophan metabolites in serum and gastric juice – an investigation towards establishing a biomarker test for gastric cancer diagnosis. *Biomed. Chromatogr.* **30**, 1963–1974 (2016).
15. El-Beqqali A., Anders Kussak A., Abdel-Rehim M. Determination of dopamine and serotonin in human urine samples utilizing microextraction online with liquid chromatography/electrospray tandem mass spectrometry. *J. Sep. Sci.* **30**, 421 – 424 (2007).
16. Matuszewski B. K., Constanzer M. L. and Chavez-Eng C. M. Strategies for the Assessment of Matrix Effect in Quantitative Bioanalytical Methods Based on HPLC-MS/MS. *Anal. Chem.* **75**, 3019-3030 (2003).
17. Meneghini V., Cuccurazzu B., Bortolotto V., Ramazzotti V., Ubezio F., Tzschentke T. M., Canonico P. L., and Grilli M. The Noradrenergic Component in Tapentadol Action Counteracts μ -Opioid Receptor–Mediated

- Adverse Effects on Adult Neurogenesis. *Mol. Pharmacol.* **85**, 658-670 (2014).
18. He B., Bi K., Jia Y., Wang J., Lv C., Liu R., Zhao L., Xu H., Chen X., and Li Q. Rapid analysis of neurotransmitters in rat brain using ultra-fast liquid chromatography and tandem mass spectrometry: application to a comparative study in normal and insomnic rats. *J. Mass Spectrom.* **48**, 969–978 (2013).
 19. Wei B., Li Q., Fan R., Su D., Chen X., Jia Y., and Bi K. Determination of monoamine and amino acid neurotransmitters and their metabolites in rat brain samples by UFLC–MS/MS for the study of the sedative-hypnotic effects observed during treatment with *S. chinensis*. *J. Pharma. Biomed. Anal.* **88**, 416–422 (2014).
 20. Zhao X. E., Zhu S., Yang H., You J., Song F., Liu Z., and Liu S. Simultaneous determination of amino acid and monoamine neurotransmitters in PC12 cells and rats models of Parkinson’s disease using a sensitizing derivatization reagent by UHPLC–MS/MS. *J. Chrom. B.* **995–996**, 15–23 (2015).
 21. Monaghan P. J., Brown H. A., Houghton L. A., and Keevil B. G. Measurement of serotonin in platelet depleted plasma by liquid chromatography tandem mass spectrometry. *J. Chrom. B.* **877**, 2163–2167 (2009).
 22. Hényková E., Vránová H. P., Amakorová P., Pospíšil T., Zukauskaitė A., Vlcková M., Urbánka L., Novák O., Mares J., Kanovsky P, and Strnad M. Stable isotope dilution ultra-high performance liquid chromatography–tandem mass spectrometry quantitative profiling of tryptophan-related neuroactive substances in human serum and cerebrospinal fluid. *J. Chrom. A.* **1437**, 145–157 (2016).
 23. Cudjoe E., and Pawliszyn J. Optimization of solid phase microextraction coatings for liquid chromatography mass spectrometry determination of neurotransmitters. *J. Chrom. A.* **1341**, 1–7 (2014).

24. Tareke E., Bowyer J. F., and Doerge D. R. Quantification of rat brain neurotransmitters and metabolites using liquid chromatography/electrospray tandem mass spectrometry and comparison with liquid chromatography/electrochemical detection. *Rapid Commun. Mass Spectrom.* **21**, 3898–3904 (2007).
25. Lu H., Yu J., Wang J., Wu L., Xiao H., and Gao R. Simultaneous quantification of neuroactive dopamine serotonin and kynurenine pathway metabolites in gender-specific youth urine by ultra performance liquid chromatography tandem high resolution mass spectrometry. *J. Pharma. Biomed. Anal.* **122**, 42–51 (2016).
26. Moriarty M., Lee A., O’Connell B., Kelleher A., Keeley H., and Furey A. Development of an LC-MS/MS method for the analysis of serotonin and related compounds in urine and the identification of a potential biomarker for attention deficit hyperactivity/hyperkinetic disorder. *Anal. Bioanal. Chem.* **401**, 2481–2493 (2011).
27. Moriarty M., Lehane M., O’Connell B., Keeley H., and Furey A. Development of a nano-electrospray MSⁿ method for the analysis of serotonin and related compounds in urine using a LTQ-orbitrap mass spectrometer. *Talanta.* **90**, 1– 11 (2012).
28. Najmanova, V., Rambousek L., Syslova K., Bubenikova V., Slamberova R., Vales K. And Kacer P. LC-ESI-MS-MS Method for Monitoring Dopamine, Serotonin and Their Metabolites in Brain Tissue. *Chrom.* **73 (S1)**, S143–S149 (2011).
29. Zhang X., Rauch A., Lee H., Xiao H., Rainer G.,and Logothetis N. K. Capillary hydrophilic interaction chromatography/mass spectrometry for simultaneous determination of multiple neurotransmitters in primate cerebral cortex. *Rapid Commun. Mass Spectrom.* **21**, 3621–3628 (2007).

30. Ji C., Li W., Ren X., El-Kattan A. F., Kozak R., Fountain S., and Lepsy C. Diethylation Labeling Combined with UPLC/MS/MS for Simultaneous Determination of a Panel of Monoamine Neurotransmitters in Rat Prefrontal Cortex Microdialysates. *Anal. Chem.* **80**, 9195–9203 (2008).
31. Kim M., Lee J., Yang C. H., and Lee S. Silica stationary phase-based on-line sample enrichment coupled with LC-MS/MS for the quantification of dopamine, serotonin and their metabolites in rat brain microdialysates. *Anal. Chim. Acta.* **923**, 55-65 (2016).

Chapter 6

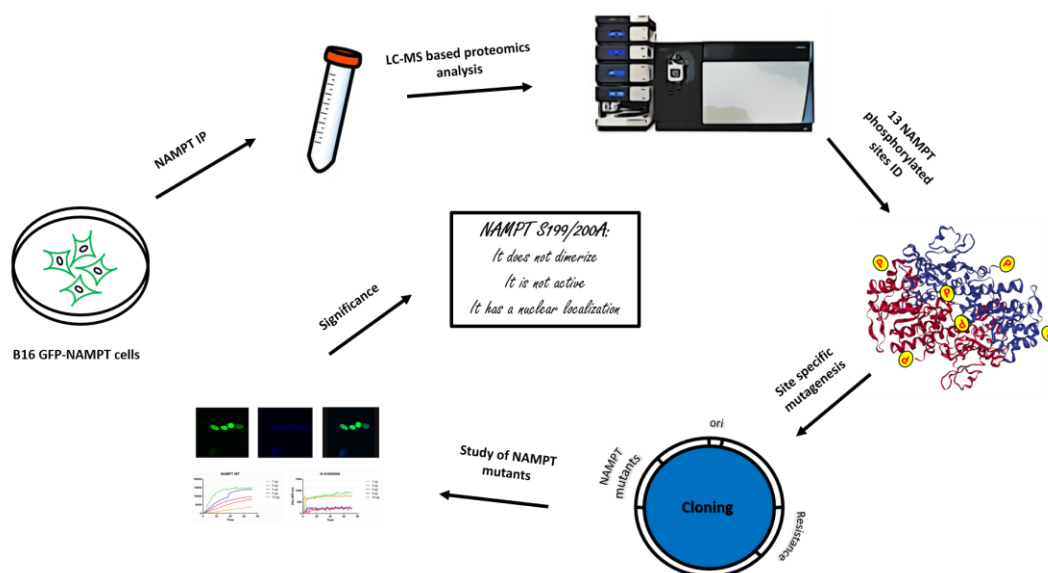
6. Study of Nicotinamide Phosphoribosyltransferase (NAMPT) phosphorylation sites in melanoma cells

Michele Bianchi^a, Cristina Travelli^a, Ambra A. Grolla^a, Giorgia Colombo^a, Erika Del Grosso^a, Adarsh Mayank^b, William D. Barshop^b, James A. Wohlschlegel^b and Armando A. Genazzani^a

^aDepartment of Pharmaceutical Sciences, Università del Piemonte Orientale, Largo Donegani 2, 28100 Novara, Italy

^bDepartment of Biological Chemistry, University of California, Los Angeles, California 90095, United States

Graphical Abstract:



Abstract:

Nicotinamide phosphoribosyltransferase (NAMPT) is a key enzyme involved in nicotinamide adenine dinucleotide (NAD) salvage pathway. NAMPT is a homodimer, that catalyzes the ratio of formation of NMN, precursor of NAD, and by doing so is the bottleneck enzymes in this pathway.

In literature, only two post-translational modifications on NAMPT have been described: the his247 autophosphorylation and the lys53 deacetylation. Surprisingly, no data are available on its phosphorylation sites. Since it is well known that phosphorylation controls the switch-on or switch-off of several enzymes, the aim of our work was to identify, quantify and characterize possible NAMPT phosphorylated sites in murine melanoma cells (B16 cells). Interesting, thirteen phosphorylated sites were identified and label free quantified by LC-MS based proteomics. Based on quantitative data, S199, S200 and S472 NAMPT phosphorylated sites were the more

abundant and by mutagenesis we have characterized at biological level the contribution of each phosphorylation. The mutant S199/200A showed significant differences *vs* NAMPT WT in terms of intracellular localization in melanoma cells, enzymatic activity and dimer formation as recombinant protein, suggesting a possible role of this PTM in controlling both location and the NAMPT enzymatic activity.

This work has identified for the first time that NAMPT is phosphorylated and that this phenomenon may regulate its function and intracellular signaling.

1. Introduction:

Nicotinamide phosphoribosyltransferase (NAMPT) is a dimeric class of type II¹ phosphoribosyltransferase, made up of 491 amino acids and a molecular weight approximal of 55 kDa². NAMPT does exist as an intracellular (iNAMPT) and extracellular (eNAMPT) form³. iNAMPT is localized mainly in cytosol, present in the nucleus and its presence in mitochondria is still uncertain and controversial^{4,5}. eNAMPT has been described for the first time by Samal *et al.* in 1994⁶ and it is known to be a cytokine^{7,8,9}.

NAMPT is the rate-limiting enzyme that contributes to the nicotinamide adenine dinucleotide (NAD) homeostasis in both prokaryotes and eukaryotes¹⁰. NAD may be synthesized from various sources such as tryptophan, nicotinic acid, nicotinamide riboside and nicotinamide, and the pathway^{11,12}.

NAMPT, which is involved NAD salvage pathway, catalysis the PRTase reaction that leads to the synthesis of nicotinamide mononucleotide (NMN), transferring a phosphoribosyl group from 5-phosphoribosyl pyrophosphate (PRPP) to nicotinamide (Nam). Afterwards, NMN adenylyltransferase (NMNAT) synthesizes NAD from NMN. Both the reactions are performed together with a facultative hydrolysis of ATP (ATPase)^{13,14}.

Recently it was attributed to NAMPT a new phosphotransfer reaction which allows the synthesis of adenosine 5'-tetraphosphate, known as Ap₄, in both *in vitro* and *in vivo* studies¹⁵. NAMPT is involved in many inflammatory and metabolic diseases, including cancer¹⁶, such as melanoma^{17,18,19}, breast²⁰, ovarian²¹, lymphomas²², myelofibrosis²³, prostate²⁴, gastric²⁵ and colorectal cancer^{26,27}. Indeed, NAMPT is over-expressed and released as eNAMPT by most of tumor cells and its high levels are correlated to prognosis and overall survival²⁸.

Nevertheless, in literature are reported only two post-translational modifications occurring on NAMPT, the histidine 247 autophosphorylation²⁹ and the of lysine 53 deacetylation³⁰. The first one was well characterized by Burgos et al., and it increases the Nam affinity to the substrate binding site causing 1000-fold increased NMN production. The second one was reported by Yoon et al., 2015 and it is responsible of increasing NAMPT activity and in the secretion of NAMPT in the extracellular space.

However, there are not evidences of NAMPT phosphorylated sites. Phosphorylation is surely one of the most important among the post-translational modifications. It plays key roles in the regulation of many cellular processes (e.g. cell cycle, growth, apoptosis and signalling).

In this scenario, the aim of the work was to identify, to quantify and to characterize NAMPT phosphorylation sites in murine melanoma cells (B16-F10 cells).

2. Results and Discussion:

2.1 Identification and label-free quantitation of NAMPT phosphorylated sites in mouse B16 WT cells

LC-MS based proteomics was the technique chosen for the identification of NAMPT phosphorylated sites in mouse GFP-NAMPT B16 cells. We chose B16 as model because in these cells NAMPT is over-expressed in basal concentration. Our model

has been engineered in order to have a stable expression of GFP fused at N-terminal of NAMPT. The cells conditions were set up as following: untreated cells, starvation (serum-free cells culture media) for 24 h, starvation for 24 h followed by 2 h of complete culture media and protease inhibitors cocktail.

Two different samples preparation protocols were developed. After treatments, cells were harvested, lysed and NAMPT was immunoprecipitated (IP) with GFP traps. Beads were eluted, and samples were split to perform in solution trypsin digestion³¹ and in gel trypsin digestion³².

We identified thirteen phosphorylated sites in mouse B16 WT cells (Figure 1) by LC-MS with a Data Dependent Acquisition mode. The sites identified with two different protocols are slightly different. Only two sites (S472 and Y240) were identified with both samples preparation approaches. The differences of modified sites identified could be due to the different lysis buffers and proteases and phosphatases inhibitor cocktails used during the experiments. Moreover, cells were growth and harvested in two different laboratories.



Figure 1. NAMPT phosphorylated sites identified in melanoma B16 GFP-NAMPT WT cells by LC-MS based proteomics analysis. Thirteen sites were identified performing two different lysis protocols starting from tissue cultures

MS/MS spectra of all the phosphorylated peptides are shown in Figure 2. Data arising from PTMs confirm the identification of the modified sites.

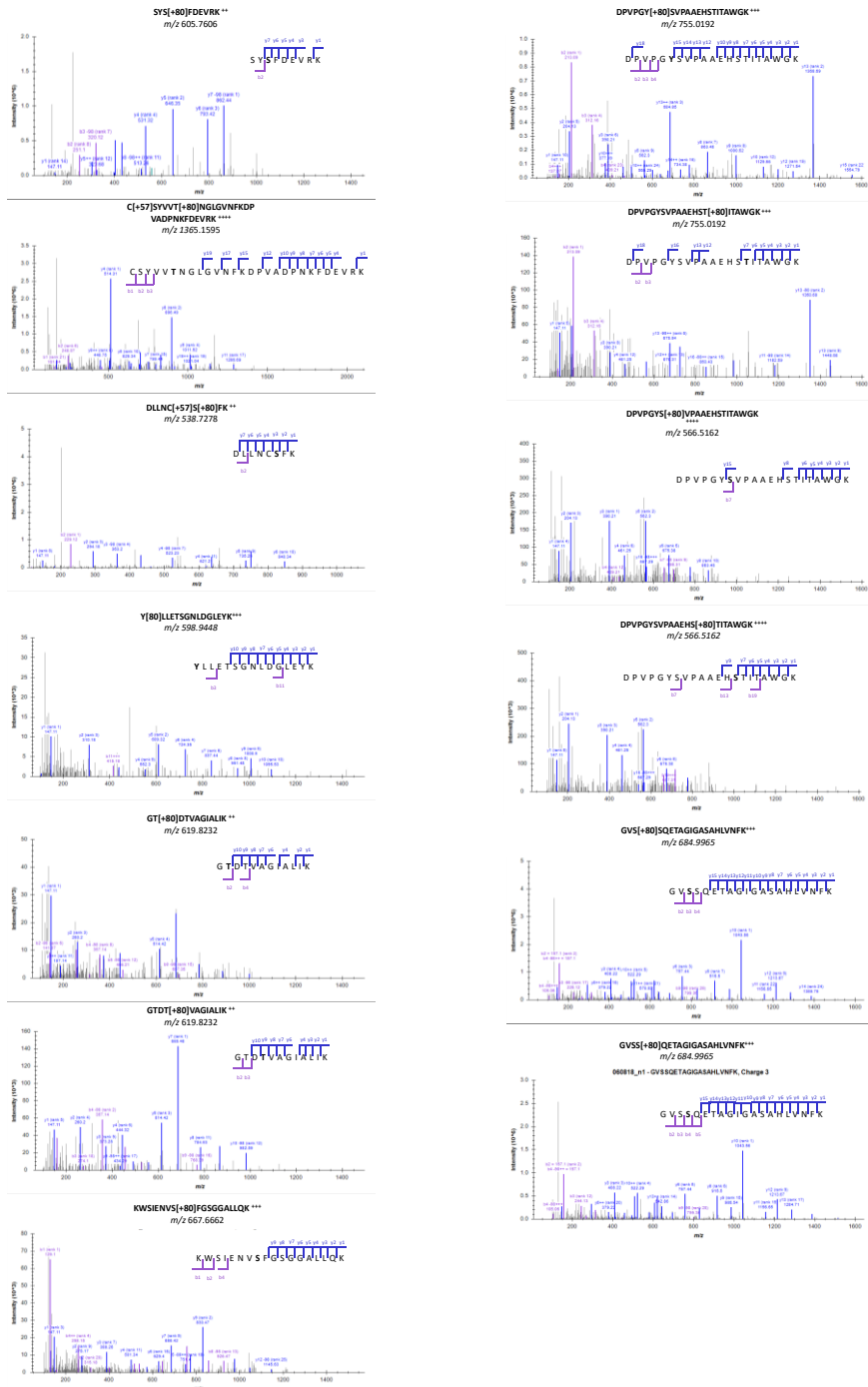


Figure 2. MS/MS Higher-energy Collisional Dissociation (HCD) spectra of phosphorylated NAMPT peptides identified by mass spectrometry

Starting from the same cells and treatments, we analyzed in solution digested samples coming from both sample preparation protocols by LC-MS in Parallel Reaction Monitoring mode (PRM). Target modified peptides were label-free quantified and the area ratio $\times 10^3$ values are reported in table 1.

Peptide modified	aa mod	Sample preparation 1				Sample preparation 2			
		Area ratio $\times 10^3$				Area ratio $\times 10^3$			
		BASAL	Pinhib	STAR	STARfbs	BASAL	Pinhib	STAR	STARfbs
SYS[+80]FDEVRK	S472	1.09	1.24	1.26	1.23	2.81	1.87	3.10	3.84
DLLNC[+57]S[+80]FK	S398	0.10	0.13	0.17	0.05	0.17	0.28	0.45	0.28
C[+57]SYVVT[+80]NGLGVNVFKDPVADPNK	T406							0.05	
Y[+80]LLETSGNLDGLEYK	Y175					0.26	0.07	0.15	0.22
GT[+80]DTVAGIALIK	T218	0.15	0.15	0.21	0.13	0.02	0.15	0.24	0.13
GTDT[+80]VAGIALIK	T220	0.12	0.14	0.17	0.09	0.02	0.17	0.01	0.02
KWSIENV[+80]FGSGGALLQK	S379	0.02	0.02	0.05	0.02		0.01	0.04	0.01
DPVPGY[+80]SVPAAEHSTITAWGK	Y240	1.85	2.36	1.19	1.25		0.41	2.34	0.07
DPVPGYSVPAAEHST[+80]ITAWGK	T249						0.02	0.59	0.01
DPVPGYS[+80]VPAAEHSTITAWGK	S241	1.84	2.22	2.10	1.31		0.19	0.02	0.04
DPVPGYSVPAAEHS[+80]ITAWGK	S248							0.06	
GVSS[+80]QETAGIGASAHLVNFK	S200	2.94	5.10	4.51	6.26		0.16	0.85	0.08
GV[+80]SQETAGIGASAHLVNFK	S199	2.68	4.58	4.13	5.48		0.15	0.95	0.08

Table 1. Label-free quantitation of thirteen NAMPT phosphorylated sites. Data were collected by LC-MS analysis with PRM acquisition mode of the target modified peptides. The average area of three unmodified NAMPT peptides acquired in PRM were used for the normalization of phosphorylated peptides area

Each phosphorylated site has a phosphorylation trend through each treatment. S472 is highly expressed in all the conditions tested even if the trend is different between the two protocols. Also, S199 and S200 are highly phosphorylated, and together with S472 revealed an interesting phosphorylation increase in starvation condition vs untreated samples.

In general, other sites resulted to be quantified in low amounts against the total NAMPT present in each sample. Considering the area values collected from these modified sites, it is difficult to appreciate significant differences between the treatment conditions.

2.2 NAMPT localization in mouse B16 WT cells in starvation conditions

NAMPT intracellular localization is known and it is already reported in literature^{4,5}. With the aim to deeply study NAMPT localization under various stimuli, we started investigating the NAMPT intracellular localization of GFP-NAMPT in mouse B16 WT cells in starvation conditions by laser confocal scanning microscopy analysis (Figure 3). Data confirm that NAMPT in untreated conditions is mainly localized in cytosol. It is interesting that NAMPT starts moving to nuclei after 8 h of starvation. Moreover, NAMPT remains localized in nuclei in the next time points checked at 17 h and 24 h.

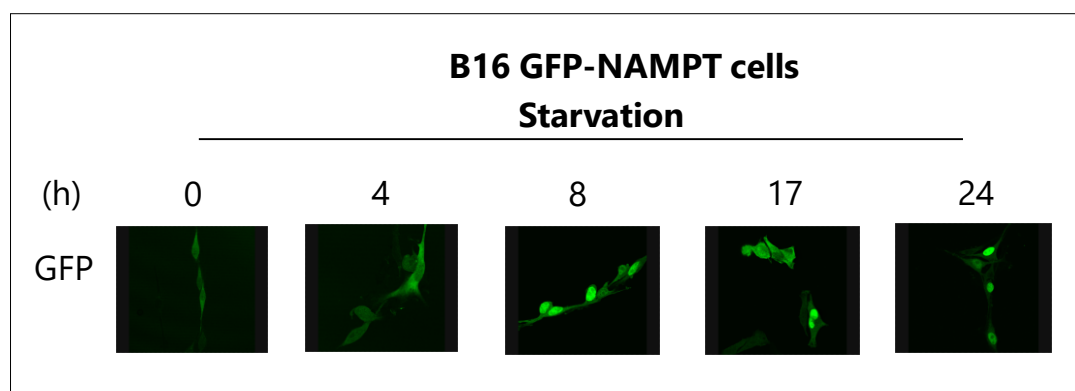


Figure 3. Intracellular NAMPT localization in B16 GFP-nampt WT cells in starvation conditions. We evaluated NAMPT nuclei and cytosol localization in basal conditions (0h starvation), and after 4 h, 8 h, 17 h and 24 h using confocal microscopy

Taking together the data arising from S472, S199 and S200 phosphorylation in B16 WT cells and NAMPT intracellular localization in starvation, we decided to perform LC-MS targeted analysis to study NAMPT phosphorylation trends in nuclei and cytosol fractions of B16 WT cells in starvation conditions.

We set up four experimental conditions: untreated, starvation 8 h, starvation 16 h and 24 h starvation. After harvesting cells, we fractionated nuclei and cytosol and performed the IP with GFP traps (Figure 4A and 4B). After beads elution, samples were in solution trypsin digested and they were analysed by LC-MS in PRM

acquisition mode. Quantitative results of S472, S199 and S200 modified sites are reported in Figure 4C. S472 phosphorylated site was statistically significant increased in starvation conditions vs basal conditions. In particular, both nuclei and cytosol after 8 h of starvation ($p \leq 0.05$ and $p \leq 0.01$, respectively), in cytosol after 16 h ($p \leq 0.05$) and in cytosol after 24 h ($p \leq 0.05$). These data suggest that S472 is extensively phosphorylated in starvation conditions. Moreover, even more interesting is the phosphorylation trend of S199 and S200 phosphorylated sites. In cytosol, the quantitative data show a reduction of the phosphorylation till to be significant after 24h of starvation vs untreated condition ($p \leq 0.05$). While, S199 and S200 were detected in nuclei after 24h of starvation. The observations made in this multi time points starvation study could mean that the phosphorylation of S199 and S200 sites is related to NAMPT intracellular localization.

The study of these post translational modifications in transfected stable NAMPT S472A/D or S199/200A/D in B16 WT cells could elucidate their molecular significance.

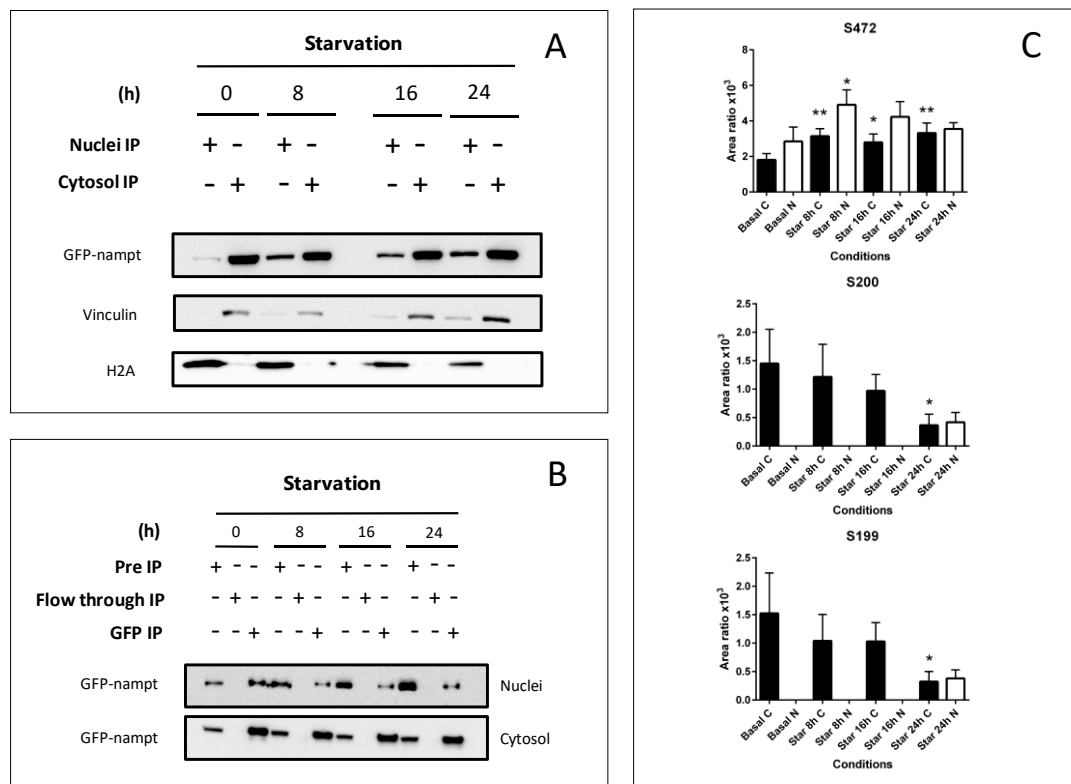


Figure 4. NAMPT Phosphorylation trends in nuclei and cytosol of B16 WT cells in basal and starvation conditions. a) Cytosol and nuclei fractionation efficiency were monitored immunoblotting the IP samples with antibody anti-Vinculin and anti-H2A, respectively. b) Immunoprecipitation was checked immunoblotting Pre IP, Flow through IP and GFP IP samples with antibody anti-GFP. Both cytosol and nuclei samples were evaluated. c) The proteins collected from GFP IP samples were precipitated, in solution trypsin digested, desalted and analysed by LC-MS in PRM acquisition mode for phosphorylated peptides containing S472, S199 and S200 Phosphorylated sites. In the graphs are reported the area ratio $\times 10^3$ of phosphorylated peptides against the average of the area values of three NAMPT unmodified peptides collected using the label free quantitative approach. Statistical analysis of area values was carried out by applying t-test analysis. P value ≤ 0.05 was considered as significant and indicated in figure with one asterisk (*). P value ≤ 0.01 was considered as significant and indicated in figure with two asterisks (**).

The experiment was performed in biological replicates and analytical duplicate each

2.3 Preliminary studies of NAMPT mutants in mouse B16 WT stable cells and as recombinant proteins

Given the LC-MS results we decided to proceed performing the site specific mutagenesis of the S472, S199 and S200 sites replacing serine with alanine to mimic the absence of phosphorylation or with aspartic acid to mimic the presence of

phosphorylation³³. All of these mutations were performed in two different vectors: pLV-GFPnampt and pET28A-nampt. The first one is a lentiviral vector bringing a GFP N-terminal fused NAMPT sequence useful for transfecting HEK293 and then infecting B16 WT cells to make stable NAMPT mutants cells. The second one was used for inducing the NAMPT mutants expression in BL-21 bacteria with the aim to purify recombinant NAMPT mutant proteins.

The data reported subsequently could be considered as preliminary data. Currently, only S472A, S199/200A mutants have been investigated. At the beginning, we opted to mutate in the same vector both S199/200A to assess whether any differences between the mutant and the WT, with the aim to study each mutation individually in case of promising results.

2.3.1 Intracellular localization of NAMPT mutants in mouse B16 WT stable cells

We studied NAMPT localization of NAMPT WT, NAMPT S199/200A and NAMPT S472A in mouse B16 WT cells in basal condition without treatments. Images took by laser confocal scanning microscopy analysis and the number of cells counted for NAMPT localization are reported in Figure 5. As confirmation, NAMPT WT is localized mainly in cytosol. NAMPT S472A is localized predominantly in cytosol with an overlapping behavior of NAMPT WT, as demonstrated by the cells counts. NAMPT S199/200A is localized in nuclei.

The residue S472 is exposed on the surface of NAMPT, and it does not seem affecting NAMPT intracellular localization. While S199 and S200 residues are in the area of dimerization of NAMPT (Figure 6).

The absence of phosphorylation in NAMPT S199/200A mutant or the absence of serine hydroxyl free moiety could be responsible of nuclear localization of the protein.

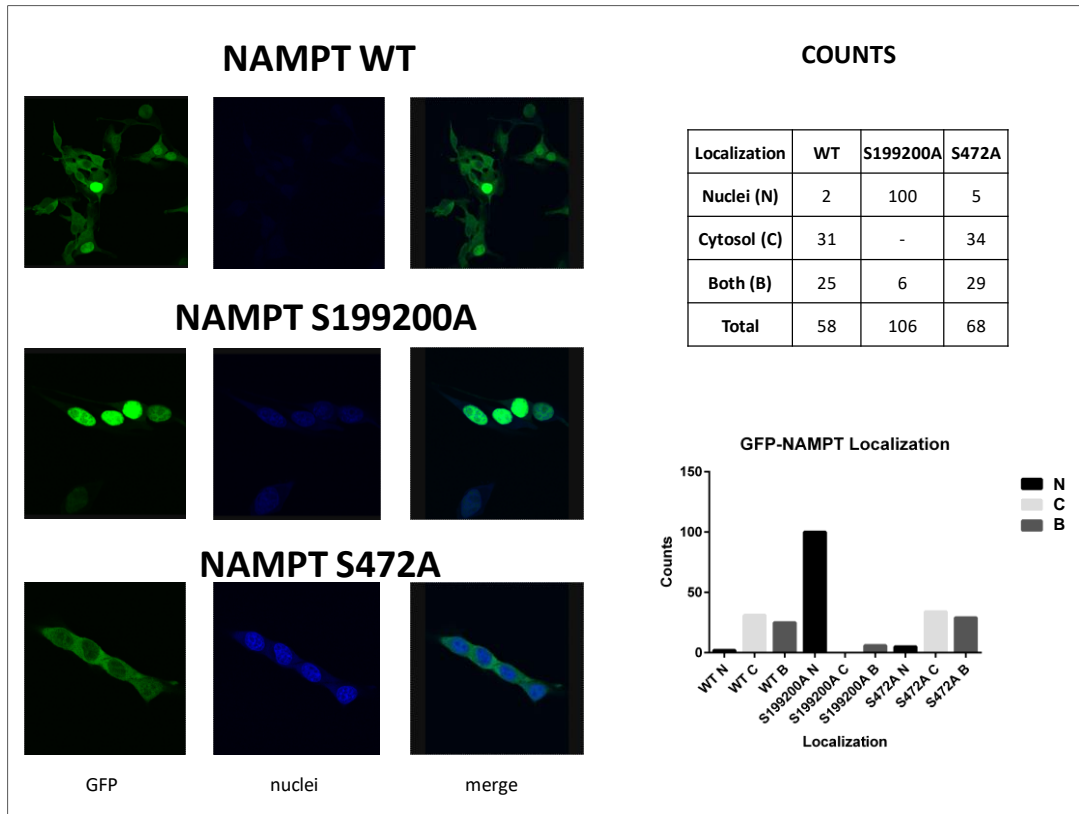


Figure 5. NAMPT WT, NAMPT S199200A and NAMPT S472A intracellular localization in B16 WT cells in basal condition. NAMPT mutant localization were evaluated in three stable cells lines: B16 GFP-nampt WT, B16 GFP-nampt S199200A and GFP-nampt S472A. Intracellular NAMPT localization was described as nuclear, cytosolic or both for unspecific localization

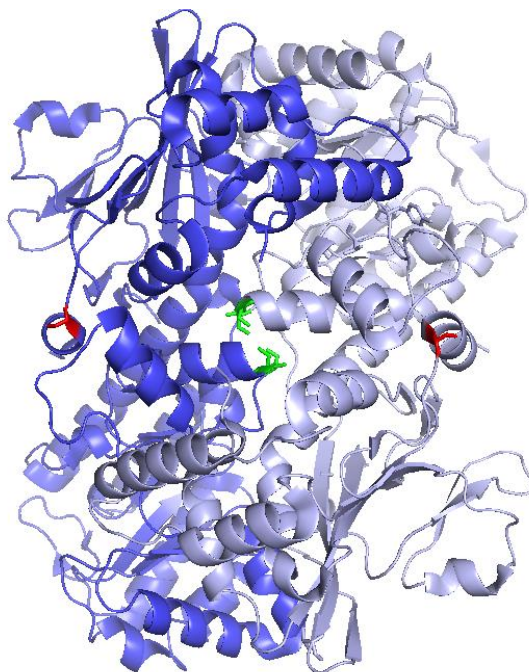


Figure 6. NAMPT dimer quaternary structure. In red is highlighted S472 amino acid and in green are highlighted S199 and S200 amino acids on both NAMPT monomers

2.3.2 Enzymatic activity of NAMPT mutant recombinant proteins

We investigated also the enzymatic activity of NAMPT WT, NAMPT S472A and NAMPT S199/200A recombinant proteins. To perform this analysis, we reproduced the *in vitro* NAMPT enzymatic assay.²⁹ For each recombinant protein, we tested their enzymatic activities at five concentrations, maintaining fixed the substrates amounts. Results are plotted in graphs in Figure 7A and 7B. The data shown that the enzymatic activity of NAMPT S472A is similar to the one of NAMPT WT. While NAMPT S199/200A is complete inactive, also at very high concentration.

The results collected indicate that the mutation S472A is not influencing the intrinsic activity of the enzyme in producing nicotinamide mononucleotide (NMN). While, it is clear that S199/200A double mutations is affecting heavily the enzymatic

production of NMN. Probably, it could be due to the unfolding of the NAMPT dimer structure, that again could be missing for this mutant.

It is important to highlight that we have not evaluated the kinetic of the reactions, so far. We can suppose that by performing a kinetic experiment altering the substrates concentration, we could better shed light on this aspect.

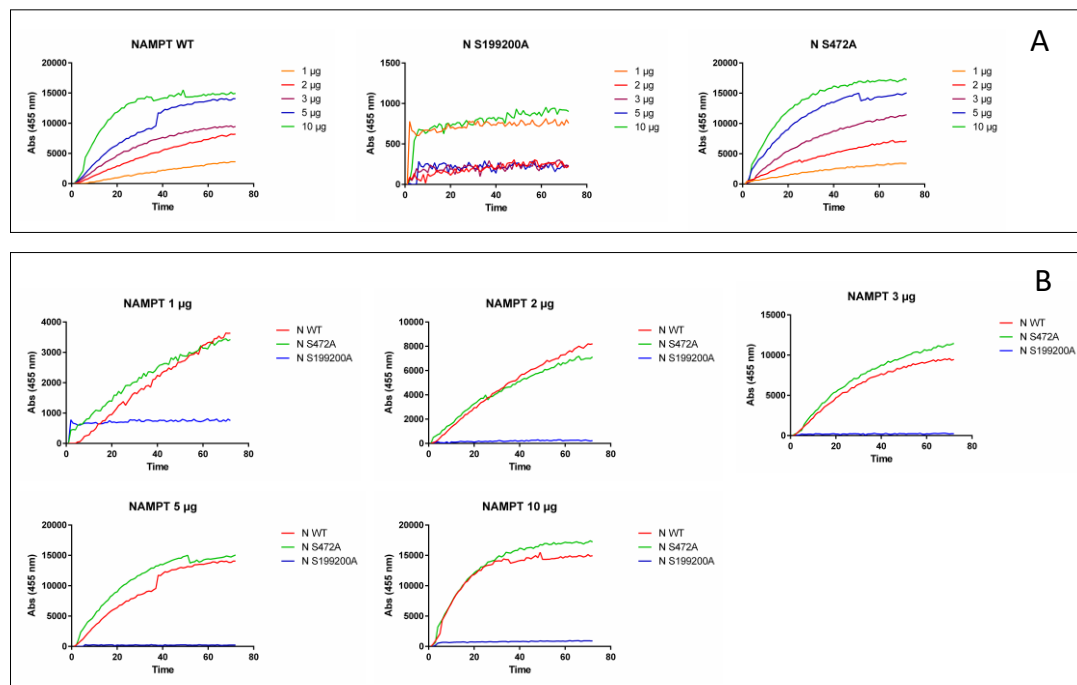


Figure 7. Enzymatic activity of mouse NAMPT WT, NAMPT S199200A and NAMPT S472A recombinant proteins. The enzymatic assay is performed at five different enzyme concentrations (1µg, 2µg, 3µg, 5µg, 10µg) in biological replicate and the averages absorbance were used. Absorbance values were revealed at 455nm wavelength each 2.5 minutes. a) Absorbance values are plotted per each NAMPT mutant. b) Absorbance values are plotted per each enzyme concentration. The experiment was performed in biological replicate

2.3.3 Investigation of NAMPT dimer formation of NAMPT mutants recombinant proteins

Considering the results obtained about the intracellular localization of NAMPT mutants and their enzymatic activity, we next tested the NAMPT dimer formation of NAMPT recombinant mutants since its dimerization is essential to guarantee its

enzymatic efficiency.²⁹ To evaluate this aspect, NAMPT WT, NAMPT S472A and NAMPT S199/200A recombinant proteins were incubated with bisulfosuccinimidyl suberate (BS3), a well-known crosslinker with the ability to cross-link lysine at 20-30 Å of distance, or with DMSO as blank. Samples were loaded on a SDS-page gel and it was stained with silver staining to detect protein gel bands (Figure 8). In agreement with gel results, NAMPT WT dimerized as expected. Also, NAMPT S472A dimerized properly in a similar way to the WT protein. While, NAMPT S199/200A seems to be less cross-linked than NAMPT S472A and WT. Furthermore, the NAMPT S199/200A monomer band is more intensive than the S472A monomer band, further index of a less dimerization of S199/200A mutant. Our data suggest that S472A mutant can dimerize, in fact the mutations from serine 472 to alanine is far from the interaction area between two NAMPT monomers. While S199/200A mutants cannot dimerize properly as expected, probably because we are replacing two amino acids in the dimerization area of NAMPT, making the dimerization of the dimer complex tough. All of these data find agreement with the results collected from the starvation localization experiment and the enzymatic assay performed.

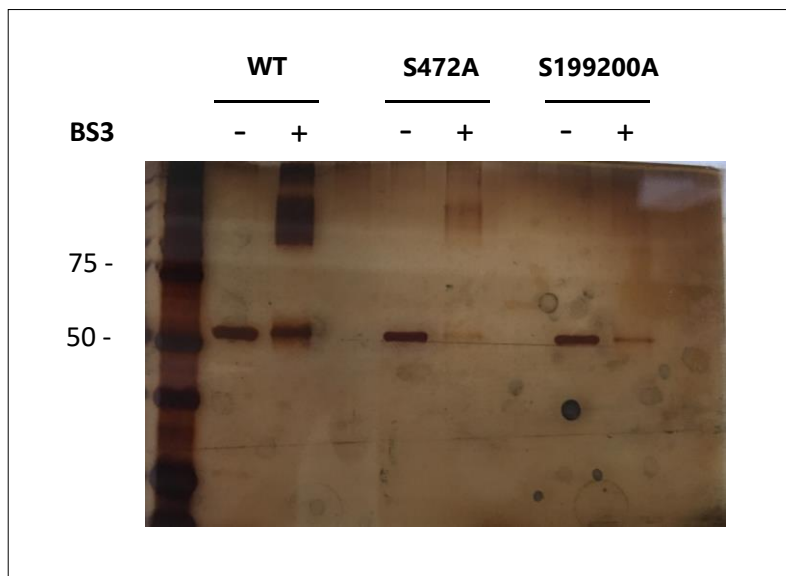


Figure 8. Cross-linking data of NAMPT WT, NAMPT S199/200A and NAMPT S472A recombinant proteins. Each recombinant protein was incubated with BS3 cross-linker or DMSO. Proteins were detected by silver staining

3. Significance:

This work described novel NAMPT phosphorylated sites in mouse B16 WT cells. All the modified sites identified were quantified under different stimuli by LC-MS based proteomics. In according with the evidences proposed, the most promising sites were selected to be S472, S199 and S200. All of these residues were mutated in alanine the study the absence of phosphorylation in stable cells lines and in NAMPT recombinant proteins. The most outstanding finding is the S199/200A NAMPT mutant to be localized in nucleus, enzymatically inactive and not able to dimerize. Taken together, it could be hypnotized that an inactive NAMPT form is storage in nuclei as monomer with some still “unknown” role that has to be elucidated.

At the same time, different mutations are object of this on-going project (*e.g.* S472D, S199A, S200A, S199D and S200D in first instance), with the aim to deeply understand the factors which regulate NAMPT functions and intracellular activities.

4. Material and Methods:

Sample preparation for mass spectrometry analyses

B16 cells were engineered to stably express NAMPT as an N-terminal GFP fusion protein. All B16 cells were normally cultured in DMEM supplemented with 10 % fetal bovine serum (FBS), 2 mg/mL glutamine, 10 U/mL penicillin and 100 lg/mL streptomycin. Typically, 1.5×10^6 cells were seeded and detached after 24 hours by trypsinization. When required, B16 cells were treated as following: (1) starvation condition: cells were grown for 8, 16 or 24 hours after adhesion in DMEM without FBS. (2) starvation condition +FBS: cells were grown for 24 hours after adhesion in DMEM without FBS, and then cells were grown for 2 hours after adhesion in DMEM with 10 % FBS. (3) Low glucose condition: cells were grown for 24 hours after adhesion in MEM with FBS. (4) UV condition: cells were treated for 20 seconds with UV light (254 nm) and were grown for 3 hours after adhesion in DMEM with FBS. (5) Kinase activators conditions: cells were treated for 1 hour with 20 μ M phorbol-12-myristate-13-acetate (PMA) and 200 μ M Forskolin. (6) Phosphatase inhibitors conditions: cells were treated for 2 hours with 100 μ M NAF and 100 μ M Na_3VO_4 .

After treatments, cells were harvested and lysed in lysing buffer 1 (10 mM Tris-HCl pH 7.5, 150 mM NaCl, 0.5 mM EDTA, 0.5 % NP-40, 0.1 mM PMSF and an appropriate aliquots of the Calbiochem Protease Inhibitor Cocktail Set V) or lysis buffer 2 (100 mM Tris HCl pH 8.00, 150mM NaCl, 5mM EDTA, 5% glycerol (60%), 0.1% NP40 (20%), 1mM DTT, 1 μ g/ml Leupeptin, 1 μ M Pepsidin, 1 mM ABESF, Phosphatase Inhibitors cocktail (BioGold), 250 U benzonase and 1 mM MgCl_2 1M). After centrifuging at 13,000 g for 10 min at 4 °C, the supernatant was mixed with GFP-trap agarose beads (gta-100, Chromotek) and rotated at 4 °C O.N. Then, beads were pelleted and washed four times with ice-cold IP buffer (without phosphatase and protease inhibitors). The bound proteins were eluted in 0.2 M glycine pH 2.5. Protein samples were treated as following: an aliquot (~30%) was treated with SDS-

PAGE sample buffer by heating at 95 °C for 8 min. Protein samples were fractionated by 10% SDS–PAGE and stained with Colloidal Blue Staining. After dehydration, proteins in the gel slice were reduced by 10 mM Dithiothreitol and alkylated by 55 mM 2-Iodoacetamide. After washing and dehydration with acetonitrile, the proteins were digested with trypsin and subjected to MS analyses. A second aliquot (~70%) was treated with TCA and acetone performing several cycles of washing and centrifugations for precipitating proteins. Protein pellets were washed with acetone and digested with trypsin. Dried pellets were dissolved in 8 M urea / 100 mM Tris-HCl, pH 8.5. Proteins were reduced with 5mM tris(2-carboxyethyl)phosphine hydrochloride (TCEP, Sigma-Aldrich) and alkylated with 10mM iodoacetamide (Sigma-Aldrich). Proteins were digested overnight at 37 °C in 2 M urea / 100 mM Tris-HCl, pH 8.5, 1 mM CaCl₂ with trypsin (Promega) in a ratio of 1:100 (enzyme:protein). Digestion was stopped with formic acid, 5% final concentration. Debris was removed by centrifugation. Digests were desalted with Thermo Scientific C18 pipette tips prior injection in the LC-MS system.

When required, samples were fractionated in nuclei and cytosol as following.

After treatments, cells were harvested in trypsin and collected in ice. For 1×10^7 cells, 200 μ l of Buffer A (300mM Sucrose, 10mM Hepes, 10mM KCl, and 2mM MgCl₂ and 0.1 mM PMSF and an appropriate aliquots of the Calbiochem Protease Inhibitor Cocktail Set V) were added to the cells precipitate. Subsequently, 0.15% NP-40 was added. The resulting solution was centrifuged at 13,000g for 15 min at 4 °C. The supernatant was collected as cytosol fraction.

The pellet was washed with 500 μ l of Buffer B (50mM Hepes, 400mM NaCl, 1mM EDTA and 1mM EGTA and 0.1 mM PMSF and an appropriate aliquots of the Calbiochem Protease Inhibitor Cocktail Set V). Pellet was resuspended in 360 μ l buffer B and sonication cycles were repeated until the lysis of nuclear membranes. The intracellular content was maintained at 4°C for 45 min and shaken for 10 sec each 5 minutes. Centrifuge samples at 13,000g for 15 min at 4 °C. The supernatant

was collected as nuclei fraction. Then, the sample preparation continues with GFP-NAMPT immunoprecipitation as reported previously. Afterwards, the protein pellets were collected as described early in 8 M urea / 100 mM Tris-HCl, pH 8.5 and digested, desalted, and LC-MS analysed.

LC-MS/MS analysis

Phosphorylated peptides were subjected to LC-MS/MS analysis using an Dionex ultimate 3000 ultra-high pressure liquid chromatography system (Thermo Scientific) connected to an Orbitrap-Fusion-Tribrid mass spectrometer (Thermo Scientific) with a Phoenix Nimbus (Phoenix S&T) ion source. Data dependent acquisition (DDA) and parallel reaction monitoring (PRM) approaches were chosen for peptides identification and label free quantitation.

For DDA, peptides were eluted on a reversed phase C18 column (250 mm × 75 mm i.d., 3 μm p.d.) by a gradient mode constituted of solvent A (0.1% formic acid, 3% DMSO in water) and B (0.1% formic acid, 3% DMSO in ACN) at a flow rate of 200 nl min⁻¹: 1–5.5% solvent B in 5 min; 5.5–27.5% solvent B in 123 min; 27.5–35% solvent B in 7 min; 35–80% solvent B in 1 min and kept 2 min before the re-conditioning of the column. The total analysis time for each sample was 140 min. In survey scans, full-scan MS spectra were acquired by the Orbitrap analyser at a resolution of 120,000, scanning from m/z 400 to m/z 1600. AGC target was 2e5 and maximum injection time was 100 ms. MS2 quadrupole selection isolation window was m/z 1.6. The top speed mode was selected. MS/MS spectra were detected using Orbitrap analyser at the resolution of 15,000. AGC target was 5.0e4 and the maximum injection time was 35 ms. The normalized HCD energy was set at 35%. For PRM, the mass spectrometry system and the chromatography gradient are described as for DDA. The resolution of MS1 full scan was set to 50,000, scanning from m/z 100 to m/z 2000; AGC target was 5e4 and the maximum injection time is

set to 100 ms. Precursors are selected by the quadrupole mass analyser using an isolation window set to 1.6 Da. The normalized HCD energy was set at 35%.

MS data processing

For the identification of phosphorylated peptides, Raw DDA MS files were processed using MS-GF+ search algorithm³⁴. NAMPT phosphorylated peptides were identified using a target-decoy approach by searching all MS/MS spectra against a forward/reversed mouse database and filtered by using a percolator derived q value of 0.01 at peptide spectral level. Carbamidomethylation of cysteines was selected as the fixed modification and the phosphorylation (STY) as the variable modification. The database search was performed with an initial precursor ion tolerance of 15 p.p.m., MS/MS tolerance at 0.02 Da, and two missed cleavages are allowed. Phosphosite localization was assessed using PhosphoRS algorithm³⁵ and the phosphopeptide containing the residues with phosphor-probability greater than 0.95 were used for further quantification. Label free quantitation was performed with skyline (version 3.7). The quantification was performed using PRM data at the MS2 level³⁶, which is widely used for phosphopeptide quantification^{37,38,39}. The intensity of phosphopeptide was derived from the peak area of specific daughter ion, and all Skyline integrated PRM data analysis were manually checked to validate peak Selection. The intensity of the phosphopeptide detected was normalized against the daughter ion peak area of NAMPT unphosphorylated peptides, chosen as control to correct sample variations.

Production of NAMPT recombinant proteins

Wild-type murine full-length NAMPT (ORF GenBank BC018358) was cloned in pET28a (NdeI/EcoRI). Mutants NAMPT S472A and S199200A were obtained by mutagenesis (QuikChange Lightning Site-Directed Mutagenesis Kit, Agilent Technologies) from NAMPT WT by using the following primers: 5'-

TTTTTCTGACTTCATCAAATGCGTAGCTTTTTGTACCTTCCC (fw) and 5'-GGGAAGGTGACAAAAAGCTACGCATTTGATGAAGTCAGAAAAA (rev) for S472A mutant and 5'-CCAGCAGTCTCTTGCGCAGCGACTCCTCTGTAACCA (fw) and 3'-TGGTTACAGAGGAGTCGCTGCGCAAGAGACTGCTGG (rev) for S199200A mutant.

All recombinant NAMPTs were expressed in *E. Coli* BL21(D3) (induction with IPTG 0.5 mM for 3 h at 25°C) and purified by His-tag affinity chromatography with NiNTA Superflow resin (Qiagen). Human recombinant NAMPT was commercially available (AG-40A-0018AA-C500, AdipoGen Inc; Seoul Korea). Correct insertion and sequence were confirmed by sequencing.

Creation of stable mouse B16 GFP-nampt cell lines

Wild-type murine full-length NAMPT (ORF GenBank BC018358) was cloned in pLV-GFP-NAMPT-IRES-GFP (Bicistronic vector). Mutants NAMPT S472A and S199200A were obtained by mutagenesis (QuikChange Lightning Site-Directed Mutagenesis Kit, Agilent Technologies) from NAMPT WT by using the following primers: 5'-TTTTTCTGACTTCATCAAATGCGTAGCTTTTTGTACCTTCCC (fw) and 5'-GGGAAGGTGACAAAAAGCTACGCATTTGATGAAGTCAGAAAAA (rev) for S472A mutant and 5'-CCAGCAGTCTCTTGCGCAGCGACTCCTCTGTAACCA (fw) and 3'-TGGTTACAGAGGAGTCGCTGCGCAAGAGACTGCTGG (rev) for S199200A mutant.

B16 GFP-NAMPT cell line was cloned in the pLV-IRES-GFP bicistronic vector. Correct insertion and sequence were confirmed by sequencing. The lentiviral particles were produced as described elsewhere⁴⁰ in HEK293T cells transfected with pMDLg/pRRE, pMD2.VSVG, pRSV-Rev and pLV-GFP-NAMPT-IRES-GFP. Briefly, after 48 h, cell medium was collected, filtrated and centrifuged for 1 h 30

min at 100000 x g. The viral particles, corresponding to the pellet fraction, were resuspended and used to infect B16 cells, after virus titration.

Stable B16 GFP-NAMPT S472A and S199/200A cell lines were created, and GFP-NAMPT expression was monitored with immunocytochemistry and Western blot.

Immunocytochemistry experiment

For immunocytochemistry experiment, cells were fixed after treatments in 4% formaldehyde. Subsequently, nuclei were stained with DRAQ5 (Thermo Fisher Scientific). Fluorescence images were acquired using a Leica (Leica Microsystems, Wetzlar, Germany) epifluorescent microscope equipped with S Fluor 40x/1.3 objective using METAMORPH (Molecular Devices, Sunnyvale, CA, USA) software.

Coupled enzymatic assay for NAMPT activity

Wild type *Mus musculus* NAMPT was recombinantly expressed in bacteria and purified to homogeneity following established procedures⁴¹. Assay was conducted as described previously²⁹, with some modifications. The reactions were run at 37 °C, with 1µg, 2µg, 3µg, 5µg or 10µg of NAMPT, reacted in a 200 µL sample containing 30 mM HEPES pH 7.5, 1 mM NAM, 0.2 mM PRPP, 1 mM ATP, 25 mM MgCl₂, 1 mM DTT, 75 mM ethanol, 30 mM semicarbazide, 5 mU mNMNAT-3 (2 µg), 2.5 U ADH (11 µg), and 110 µg BSA. NADH formation was monitored over a period of 3 hours (each 2.5 min) by emission of fluorescence at 455 nm upon excitation at 340 nm.

NAMPT dimer cross-linking experiment

Recombinant NAMPT WT, S472A or S199200A purified proteins were mixed in reconstitution buffer (50 mM NaH₂PO₄ pH 7.5, 250 mM NaCl, 0.25 mM Dithiothreitol) and maintained in ice for 20 min. Afterwards, bis(sulfosuccinimidyl)suberate (BS3) was added to the sample to a final

concentration of 100 μ M. Sample was kept in ice for two hours. Cross-linking reaction was quenched with 50 mM Tris- HCl pH 7.5 and left 15 min at 25°C in agitation. The resulting sample was treated with SDS-PAGE sample buffer by heating at 95 °C for 8 min. Protein samples were fractionated by 10% SDS–PAGE and stained with Silver Staining (Thermo Fisher Scientific).

Western Blotting

Proteins extracted were quantified by Bradford Protein Assay, separated on SDS-PAGE, blotted onto a nitrocellulose membrane, and stained with monoclonal antibodies specific for GFP, Vinculin and H2A.

Statistical analysis

All data represent the mean and SD of at least 2 biological independent experiments. T test statistical analysis was carried out by PRISM program. A p value ≤ 0.05 was considered as significant and indicated in figures with asterisks (*).

Cell culture

All B16 cells were normally cultured in DMEM supplemented with 10 % fetal bovine serum (FBS), 2 mg/mL glutamine, 10 U/mL penicillin and 100 lg/mL streptomycin. Typically, 1.5×10^6 cells were seeded and detached after 24 hours by trypsinization.

References:

1. Marletta, A. S. *et al.* Crystal structure of human nicotinic acid phosphoribosyltransferase. *FEBS Open Bio* **5**, 419–428 (2015).
2. Wang, T. *et al.* Structure of Nampt/PBEF/visfatin, a mammalian NAD⁺ biosynthetic enzyme. *Nat. Struct. Mol. Biol.* **13**, 661–662 (2006).
3. Travelli, C., Colombo, G., Mola, S., Genazzani, A. A. & Porta, C. NAMPT: A pleiotropic modulator of monocytes and macrophages. *Pharmacol. Res.* **135**, 25–36 (2018).
4. Pittelli, M. *et al.* Inhibition of nicotinamide phosphoribosyltransferase: Cellular bioenergetics reveals a mitochondrial insensitive NAD pool. *J. Biol. Chem.* **285**, 34106–34114 (2010).
5. Yang, H. *et al.* Nutrient-Sensitive Mitochondrial NAD⁺ Levels Dictate Cell Survival. *Cell* **130**, 1095–1107 (2007).
6. Samal, B. *et al.* Cloning and characterization of the cDNA encoding a novel human pre-B-cell colony-enhancing factor. *Mol. Cell. Biol.* **14**, 1431–1437 (1994).
7. Shackelford, R. E., Mayhall, K., Maxwell, N. M., Kandil, E. & Coppola, D. Nicotinamide Phosphoribosyltransferase in Malignancy: A Review. *Genes and Cancer* **4**, 447–456 (2013).
8. Grolla, A. A., Travelli, C., Genazzani, A. A. & Sethi, J. K. Extracellular nicotinamide phosphoribosyltransferase, a new cancer metabokine. *Br. J. Pharmacol.* 2182–2194 (2016). doi:10.1111/bph.13505
9. Fukuhara, A. Visfatin : A Protein Secreted by Visceral Fat That Mimics the Effects of Insulin. *Diabetes* **56**, 426–431 (2007).
10. Revollo, J. R., Grimm, A. A. & Imai, S. I. The NAD biosynthesis pathway mediated by nicotinamide phosphoribosyltransferase regulates Sir2 activity in mammalian cells. *J. Biol. Chem.* **279**, 50754–50763 (2004).

11. Pucchio, T. Di, Danese, S., Cristofaro, R. De & Rutella, S. Inhibitors of indoleamine 2,3-dioxygenase: a review of novel patented lead compounds. *Expert Opin. Ther. Pat.* **20**, 229–250 (2010).
12. Galli, U. *et al.* Medicinal chemistry of nicotinamide phosphoribosyltransferase (NAMPT) inhibitors. *J. Med. Chem.* **56**, 6279–6296 (2013).
13. Magni, G., Amici, A., Emanuelli, M., Raffaelli, N. & Ruggieri, S. Enzymology of NAD⁺ synthesis. *Adv. Enzymol. Relat. Areas Mol. Biol.* **3**, 135–182 (1999).
14. Burgos, E. S., Veticatt, M. J. & Schramm, V. L. Recycling nicotinamide. the transition-state structure of human nicotinamide phosphoribosyltransferase. *J. Am. Chem. Soc.* **135**, 3485–3493 (2013).
15. Amici, A. *et al.* Synthesis and Degradation of Adenosine 5'-Tetraphosphate by Nicotinamide and Nicotinate Phosphoribosyltransferases. *Cell Chem. Biol.* **24**, 553–564.e4 (2017).
16. Bi, T. Q. & Che, X. M. Nampt/PBEF/visfatin and cancer. *Cancer Biol. Ther.* **10**, 119–125 (2010).
17. Grolla, A. A. *et al.* Nicotinamide phosphoribosyltransferase (NAMPT/PBEF/visfatin) is a tumoural cytokine released from melanoma. *Pigment Cell Melanoma Res.* **28**, 718–729 (2015).
18. Maldi, E. *et al.* Nicotinamide phosphoribosyltransferase (NAMPT) is over-expressed in melanoma lesions. *Pigment Cell Melanoma Res.* **26**, 144–146 (2013).
19. Audrito, V. *et al.* Extracellular nicotinamide phosphoribosyltransferase (eNAMPT) is a novel marker for patients with BRAF-mutated metastatic melanoma. *Oncotarget* **9**, 18997–19005 (2018).
20. Lee, Y.-C. *et al.* High Visfatin Expression in Breast Cancer Tissue Is Associated with Poor Survival. *Cancer Epidemiol. Biomarkers Prev.* **20**,

- 1892–1901 (2011).
21. Shackelford, R. E., Bui, M. M., Coppola, D. & Hakam, A. Over-expression of nicotinamide phosphoribosyltransferase in ovarian cancers. *Int. J. Clin. Exp. Pathol.* **3**, 522–527 (2010).
 22. Olesen, U. H., Hastrup, N. & Sehested, M. Expression patterns of nicotinamide phosphoribosyltransferase and nicotinic acid phosphoribosyltransferase in human malignant lymphomas. *Apmis* **119**, 296–303 (2011).
 23. Rosti, V. *et al.* Increased plasma nicotinamide phosphoribosyltransferase is associated with a hyperproliferative phenotype and restrains disease progression in MPN-associated myelofibrosis. *Am. J. Hematol.* **91**, 709–713 (2016).
 24. Patel, S. T. *et al.* A novel role for the adipokine visfatin/pre-B cell colony-enhancing factor 1 in prostate carcinogenesis. *Peptides* **31**, 51–57 (2010).
 25. Nakajima, T. E. *et al.* Adipocytokine levels in gastric cancer patients: Resistin and visfatin as biomarkers of gastric cancer. *J. Gastroenterol.* **44**, 685–690 (2009).
 26. Nakajima, T. E. *et al.* Adipocytokines as new promising markers of colorectal tumors: Adiponectin for colorectal adenoma, and resistin and visfatin for colorectal cancer. *Cancer Sci.* **101**, 1286–1291 (2010).
 27. Pan, J. *et al.* Nicotinamide phosphoribosyl transferase regulates cell growth via the Sirt1/P53 signaling pathway and is a prognosis marker in colorectal cancer. *J. Cell. Physiol.* 1–11 (2018).
 28. Hasmann, M., Schemainda, I., Hasmann, M. & Schemainda, I. FK866 , a Highly Specific Noncompetitive Inhibitor of Nicotinamide Phosphoribosyltransferase , Represents a Novel Mechanism for Induction of Tumor Cell Apoptosis FK866 , a Highly Specific Noncompetitive Inhibitor of Nicotinamide Phosphoribosyltransferase . 7436–7442 (2003).

29. Burgos, E. S. & Schramm, V. L. Weak Coupling of ATP Hydrolysis to the Chemical Equilibrium of Human Nicotinamide Phosphoribosyltransferase. *Biochemistry* **1**, 11086–11096 (2008).
30. Yoon, M. J. *et al.* SIRT1-Mediated eNAMPT Secretion from Adipose Tissue Regulates Hypothalamic NAD⁺ and Function in Mice. *Cell Metab.* **21**, 706–717 (2015).
31. Caslavka Zempel, K. E., Vashisht, A. A., Barshop, W. D., Wohlschlegel, J. A. & Clarke, S. G. Determining the Mitochondrial Methyl Proteome in *Saccharomyces cerevisiae* using Heavy Methyl SILAC. *J. Proteome Res.* **15**, 4436–4451 (2016).
32. Liu, Q. *et al.* Molecular basis for blue light-dependent phosphorylation of *Arabidopsis* cryptochrome 2. *Nat. Commun.* **8**, 1–12 (2017).
33. Dasgupta, S. *et al.* Metabolic enzyme PFKFB4 activates transcriptional coactivator SRC-3 to drive breast cancer. *Nature* **556**, 249–254 (2018).
34. Kim, S. & Pevzner, P. A. MS-GF+ makes progress towards a universal database search tool for proteomics. *Nat. Commun.* **5**, 1–10 (2014).
35. Taus, T. *et al.* Universal and confident phosphorylation site localization using phosphoRS. *J. Proteome Res.* **10**, 5354–5362 (2011).
36. Maclean, B. *et al.* Skyline : an open source document editor for creating and analyzing targeted proteomics experiments. **26**, 966–968 (2010).
37. Guise, A. J., Mathias, R. A., Rowland, E. A., Yu, F. & Cristea, I. M. Probing phosphorylation-dependent protein interactions within functional domains of histone deacetylase 5 (HDAC5). *Proteomics* **14**, 2156–2166 (2014).
38. Bauer, M. *et al.* Evaluation of data-dependent and -independent mass spectrometric workflows for sensitive quantification of proteins and phosphorylation sites. *J. Proteome Res.* **13**, 5973–5988 (2014).
39. Lawrence, R. T., Searle, B. C., Llovet, A. & Villén, J. Plug-and-play analysis of the human phosphoproteome by targeted high-resolution mass

- spectrometry. *Nat. Methods* **13**, 431–434 (2016).
40. Revell, A. D. *et al.* The development of an expert system to predict virological response to HIV therapy as part of an online treatment support tool. *Aids* **25**, 1855–1863 (2011).
 41. Orsomando, G. *et al.* Simultaneous Single-Sample Determination of NMNAT Isozyme Activities in Mouse Tissues. *PLoS One* **7**, (2012).

Chapter 7

7. Discussion

Discussion:

Liquid chromatography tandem mass spectrometry has been a revolutionary technique since the development of an ionization interface between the liquid chromatography and the mass spectrometry in the 80s. In the last decades, novel instruments with outstanding performance and new updates made the LC-MS an essential tool with a multidisciplinary attitude in the scientific research.

As claimed by this thesis, a lot of research fields were positively affected by the impact of the LC-MS. Not only chemistry, composed by all its branches (*e.g.* the analytical, organic and medicinal chemistry) but also biology (*e.g. in vitro* and *in vivo* metabolism and post translational modifications in proteins studies). Assembling different liquid chromatography apparatus with various MS analyzers through a discrete choice of ionization sources, it is possible to build up instruments able to perform qualitative or quantitative analysis. Nowadays, hybrids LC-MS equipped with at least two MS analysers are the recent trend. They confer to the scientist the possibility to overcome a tricky situation with only one instrument exploiting all of its functions.

Against this backdrop, I focused my PhD project mainly on the developing of LC-MS methods useful to carry out targeted and untargeted analysis.

The first project was about the identification and characterization of degradation compounds of Troxerutin. Starting from Troxerutin mixture, the three mains hydroxyethyl derivates were purified and underwent to stability studies following the ICH guidelines. The main achievement was to identify and characterize three degradation products (D1, D2 and D3), and to confer to D1 the role of stability indicator compound of Troxerutin.

Subsequently, the LC-MS method used for screening all of the degradation conditions, was transferred on a LC-UV instrument. It was firstly adapted and

optimized for developing and afterwards to validate a stability-indicating method for Troxerutin pharmaceutical dosage forms (ampoules, capsules and coated tablets). In these studies, the LC-ESI-MS was constituted by an HPLC operating at micro-flows and an ion trap mass spectrometer. The LC component of the method was constituted by a basic elution on a C18 column functionalized to maintain its integrity in a wide range of pH till basic values. Indeed, the ion trap as MS analyzer could be considered one of the first choices to run these experiments. The MS operated in full MS, MS2 and MS3 for the identification and to characterize hydroxyethylrutosides purified products and its degradation compounds.

Secondly, we applied the LC-MS techniques for quantitative analysis of endogenous small molecules in biological matrices (*e.g.* cells, plasma and extracellular cells culture media).

The first bioanalytical project raised from the serendipity finding of an unpredicted reaction product formed *in vitro* by NAMPT. The product was identified by cross analysis, among which even the mass spectrometry was involved, to be adenosine 5'-tetrphosphate (Ap4). Ap4 is formed from two molecules of ATP by a new and unpredicted NAMPT phosphor-transfer reaction. This reaction was deeply studied and characterized through *in vitro* experiments.

Nevertheless, in order to evaluate a correlation between NAMPT and Ap4 production *in vivo*, the intracellular content of mammalian cells was analyzed by LC-MS. Four engineered B16 WT cells types were studied for intracellular levels of Ap4, ATP, ADP, Nam, NMN and NAD.

Quantitative results showed that NAMPT is an intracellular source of Ap4, even if we cannot rule out the possibility that other enzymes could contribute with its synthesis. Also, relevant information about ATP intracellular levels, ATP/ADP ratio and phosphoribosyltransferase reaction data were collected for each cell line.

Moreover, Ap4 and NMN intracellular levels under metabolic perturbation conditions (oxidative, low-glucose and serum-free) were described confirming and integrating the data already collected and discussed.

Finally, we measured Ap4, NMN (by LC-MS) and NAMPT (via ELISA assay) extracellular levels in mouse plasma. Not surprisingly, quantitative data reported a correlation between Ap4 and NAMPT levels and Ap4 and ATP concentrations.

Taken together these data we confirmed the activity of NAMPT phospho-transfer reaction in mouse plasma.

All of these results were obtained by collecting intracellular contents and mouse plasma samples and performing a sample preparation based on the protein precipitation with organic solvents. Two sample preparation methods were developed, one for each matrix. In fact, the matrices involved in this project have different chemical compositions in term of proteins, lipids, salts and other small molecules. We could also add that each sample preparation method was optimized to find a compromise between obtaining a satisfactory average recovery value per each analyte and a simple, rapid and easy to scale up sample preparation protocol to huge batches.

Then, we injected concentrated samples in the LC-MS. The LC component of the method was carried out using a Luna HILIC stationary phase, essential for increasing the retention of polar small molecules. An isocratic elution was developed to avoid the increment or suppression of the ionization signal during the LC-MS run, due probably to the components still present in the matrix after treatments (*e.g.* amino acids, sugars, lipids and other small molecules).

The MS system operated in both positive and negative ionization mode, according to the chemical features of each compound. Each analyte was monitored in SRM or MRM mode except for Nam that was monitored in MS2 mode cause its low molecular weight which causes the impracticability to monitor a stable MS/MS fragmentation reaction.

The quantitative data were obtained using an external calibration method due to presence of the analytes of interest in all the biological matrices in physiological conditions. In fact, it was not possible to have both matrices free of Ap4 and other analytes.

The second bioanalytical project was part of a huge study about the evaluation of the ability of trazodone to promote adult neural differentiation of murine and human Neural Progenitor Cells (NPC). The LC-MS found application in order to assess whether proneurogenic effect of TZD correlates with an increase of serotonin extracellular levels. Data showed that there are not statistically significant differences between serotonin extracellular levels in cells treated with trazodone vs untreated. Nevertheless, thanks to the LC-MS analysis, we demonstrated that ahNPCs cells does express 5-HTT receptor.

The LC-MS method developed consisted in a targeted method aimed to the quantification of serotonin in extracellular culture media.

The sample preparation consisted in protein precipitation approach of the media collected after cell treatments. In this case, it was important to have satisfactory recovery results to avoid analyte lost during this step, because serotonin levels are in general low in the samples available.

For this method, the LC component was optimized in an isocratic elution on a C18 HILIC column, really useful for polar compounds. We did not observe matrix effect during the serotonin detection. Moreover, the combination of stationary and mobile phase developed, allowed the best response in terms of retention time stability and peak shape of our compound of interest.

While, the MS worked in positive ionization, monitoring serotonin in SRM mode, one of the golden standard acquisition mode for quantitative LC-MS studies.

The third application of liquid chromatography tandem mass spectrometry technique described in this thesis is the LC-MS based proteomics. The project born from a quite surprisingly gap of knowledge regarding Nicotinamide Phosphoribosyltransferase (NAMPT). NAMPT is well described as a rate-limiting enzyme in NAD synthesis, which its high levels are related to prognosis and overall survival.

However, it has never been reported in literature studies related to NAMPT and its phosphorylation, one of the most common post translational modifications.

We identified and label free quantified thirteen phosphorylated sites on NAMPT in murine B16 WT cells treated in four conditions.

The identification and label-free quantitation of STY phosphorylated sites was performed starting from the development of an immunoprecipitation protocol suitable for LC-MS analysis. A nano-UHPLC coupled with an Orbitrap Fusion Lumos Tribrid MS was used in DDA (for qualitative analysis) or in PRM mode (for quantitative analysis). Data analysis was performed to identify, filter the false positive identifications and label-free quantify each site modified.

Based on quantitative proteomics analysis, S199, S200 and S472 NAMPT phosphorylated sites resulted the most abundant and by mutagenesis we are studying at biological level the contribution of each phosphorylation.

Different experiments were performed and as preliminary data, the double mutation of S199/200A showed the most interesting results vs NAMPT WT. It seems that this NAMPT mutant cannot dimerize, so it is not enzymatically active and localize in nuclei of B16 cells.

The investigation of individual S199A and S200A is on-going. Moreover, the characterization at biological level of phospho-mimic mutants of S472, S199 and S200 and other phosphorylation sites (*e.g.* T406) is planned in the next future.

In conclusion, in these three years of PhD program, the versatility, reproducibility and robustness of LC-MS analysis has been described and demonstrated through chemical and biological projects:

- (1) Troxerutin degradation pathway was elucidated through the identification and characterization of troxerutin degradation products.
- (2) Ap4 and NAMPT related analytes were quantified in B16 WT cells and mouse plasma.
- (3) Serotonin was quantified in extracellular culture media of murine neural progenitor cells.
- (4) Thirteen NAMPT phosphorylated sites were identified and label free quantified in murine B16 WT cells. Preliminary data about the biological characterization of NAMPT modified sites were proposed.

Chapter 8

8. List of Publications

List of Publications:

Aprile S., Canavesi R., **Bianchi M.**, Grosa G. and Del Grosso E., Development of a stability-indicating HPLC-UV method for the determination of Thiocolchicoside and its degradation products, *Journal of Pharmaceutical and Biomedical Analysis* (2017), 132, 66-71.

Amici A., Grolla A. A., Del Grosso E., Bellini R., **Bianchi M.**, Travelli C., Garavaglia S., Sorci L., Raffaelli N., Ruggieri S., Genazzani A. A., Orsomando G. Synthesis and degradation of adenosine 5'-tetrphosphate by nicotinamide and nicotinate phosphoribosyltransferases, *Cell Chemical Biology* (2017), 24 (5), 553-564.

Bortolotto V., Mancini F., Mangano G., Salem R., Xia E., Del Grosso E., **Bianchi M.**, Canonico P. L., Polenzani L. and Grilli M. Proneurogenic effects of trazodone in murine and human neural progenitors, *ACS Chemical Neuroscience* (2017), 8 (9), 2027–2038.

Bianchi M., Canavesi R., Aprile S., Grosa G. and Del Grosso E., Troxerutin, a mixture of O-hydroxyethyl derivatives of the natural flavonoid Rutin: chemical stability and analytical aspects, *Journal of Pharmaceutical and Biomedical Analysis* (2018), 150, 248-257.

Acknowledgements

First of all, I would like to thank Professor Erika Del Grosso for being my mentor in these years and for her passion in teaching me everything I know about mass spectrometry.

Thanks to Prof. James Wohlschlegel and Prof. Armando Genazzani for hosting me in their laboratories for several months for learning and performing exciting experiments. I appreciate their enthusiasm and all the opportunities given, gifting me unforgettable experiences.

A special thank goes to Prof. Giorgio Grosa and Prof. Mariagrazia Grilli, for the constructive talks, suggestions and collaborations.

Last but not least, a huge thank to all the guys I worked with side by side in all the laboratories I joined. In particular, thanks to Cristina, Ambra, Silvio, Rossana, Martina, Adarsh, William, Xiaorui, Weixian, Shima, Vijaya, Giorgia, Silvia, Valeria and Beatrice, for being more than colleagues.